



**A Late Holocene Record of sediment dynamics and a major mass movement  
obtained from Lake Altaussee (Styria, Austria)**

**MASTER THESIS**

Institute of Geology  
Faculty of Geo- and Atmospheric Sciences  
Leopold – Franzens University of Innsbruck

Supervisor: Assoc. Prof. Dr. Jasper Moernaut  
Co-Supervisor: Ass. Prof. Dipl.-Ing. Dr. techn. Erwin Heine

Julia Rechenmacher  
01516473

Innsbruck, 2025



*"So, remember to look up at the stars and not down at your feet. Try to make sense of what you see and wonder about what makes the universe exist. Be curious. And however difficult life may seem, there is always something you can do and succeed at. It matters that you don't just give up. Unleash your imagination. Shape the future."*

— Stephen Hawking

## Declaration of Originality

I hereby declare that this thesis and the work reported herein was composed by and originated entirely from me. Information derived from the published and unpublished work of others (including internet resources) has been acknowledged in the text and references are given in the list of sources.

Place and date: \_\_\_\_\_

Matriculation number: \_\_\_\_\_

First name, surname: \_\_\_\_\_

Signature \_\_\_\_\_

## Acknowledgements

I would like to thank the Walter Munk Foundation for the Oceans (WMFO) and the University of Natural Resources and Applied Life Sciences (BOKU) Vienna for supporting this project and giving me the chance to conduct research on Lake Altaussee.

A big thank you to my supervisor, Jasper Moernaut, and my co-supervisor, Erwin Heine, for their guidance and support throughout my master's thesis.

I also want to thank the Sedimentology Working Group and the Austrian Core Facility for always being there to help. A special thanks to the office crew for their availability and motivation.

I would like to give special thanks to Marcel Ortler for his help with the coring process, his contribution to the project, and for sharing his data with me. I am very grateful for that!

Finally, I want to thank my family and friends for their constant support and belief in me. You are the best!

## Abstract

Inner alpine lakes show complex sediment dynamics, influenced by both natural hazards and human impact. Lake sediments serve as a natural archive, as they can preserve sediment layers over thousands of years, providing insight into the past. By combining historical records and sediment archive data, we gain a better understanding of lake evolution. In collaboration with the 'Walter Munk Foundation for the Oceans' (WMFO) and the 'University of Natural Resources and Applied Life Sciences' (BOKU) in Vienna, a study is being conducted to investigate Lake Altaussee in detail.

Lake Altaussee is a moderately sized lake located between the carbonate platforms of the Northern Calcareous Alps in the Austrian Salzkammergut. The lake is primarily fed by subaqueous karst funnels, which are part of the karst system of the 'Totes Gebirge.' The lake has a surface outflow and a plateau in the west and a central basin in which the craters are located at the northern part. In the east, the lake runs shallowly toward the shore, and the north-eastern area is covered by blocks.

By using 22 short cores taken from Lake Altaussee, along with reflection seismics, sedimentological analysis, grain size analysis, CT scans, and  $^{14}\text{C}$  dating, a chronological sequence of sediments has been established, making it possible to interpret and discuss various processes. The cores were taken from all areas of the lake (plateau, central basin, craters, between blocks and on top of the blocks). The oldest sediments found in the short cores were dated to ~14,000 cal BP. These dense, finely laminated sediments which contain drop stones represent post-glacial deposits. There is evidence of a hiatus between this layer and the overlying sediment. Above this layer is a turbidite, up to 240 cm thick, with mass flow deposits at the base. The turbidite shows a fining-upward sequence, from pebble-sized material at the base to a mud cap at the top. Based on sedimentological and morphological data, it can be concluded that this event was caused by one or more subaerial mass movements into the lake around 1195-959 cal BP (755-991 cal CE). There is further evidence in the sediment linking the blocks in the eastern area to this event. In the western part evidence can be found for a back wash deposit, caused by the impact wave, resulting in oscillating water (seiching).

The overlying homogeneous, dark, organic-rich layers represent the background sediment. This background sediment is interrupted between ~769-581 ( $\pm 60$ ) cal BP or ~1181-1369 ( $\pm 60$ ) cal CE by a dense, light-colored, laminated sediment containing almost no organic material. By analysing the sediment unit distribution, morphology, and historical literature, it was determined that this represents a temporary redirection of the Augstbach river into Lake Altaussee. Historical documents confirm that the river was redirected out of the lake in 1319 CE due to work on the salt mine. However, there is no record of the river's initial introduction.

By analysing the lake sediments, it was possible to determine that a gravitational mass movement occurred during the Late Holocene, entering Lake Altaussee from at least two directions

simultaneously. Furthermore, a detailed reconstruction of the event chronology of the mass movement deposition and the influence of organic particles on the grain size analysis was achieved.

# Content

Acknowledgements .....	IV
Abstract .....	V
1. Introduction.....	1
1.1. Sediment dynamics and Sediment archives in Alpine lakes.....	1
1.2. Lake Altaussee and Project.....	5
1.3. Research questions and objectives .....	6
1.4. Core campaign.....	7
2. Study Area .....	8
2.1. Geographic Overview .....	8
2.2. Geological Setting.....	10
2.2.1. Quaternary .....	12
2.3. Lake Altaussee and Previous research .....	13
3. Methods .....	15
3.1. Seismic and bathymetric acquisition.....	15
3.2. Sediment core analysis.....	16
3.2.1. Multi Sensor Core Logger (MSCL).....	16
3.2.2. X CT Scanning .....	16
3.2.3. Macro- and microscopic lithological description .....	17
3.2.4. Grain Size Analysis.....	17
3.2.5. Radiocarbon Dating.....	18
3.2.6. Organic Content Measurement.....	19
4. Results .....	20
4.1. Bathymetric analysis & Seismic stratigraphic analysis .....	20
4.2. Sediment core data .....	22
4.2.1. Lithologies and Event Deposit .....	22
4.2.2. Sediment Core Correlation.....	27
4.2.3. Core to Seismic Correlation.....	28

4.3.	Grain size analysis of Event Deposit .....	32
4.4.	Organic Content .....	38
4.5.	Spatial distribution of sedimentary Units.....	40
4.6.	Dating and Age Model.....	44
5.	Discussion .....	47
5.1.	Overall evolution of sediment lithofacies .....	47
5.2.	Evolution of the Megaturbidite .....	49
5.3.	Was the megaturbidite caused by one or more terrestrial mass movements that propagated into the lake? .....	54
5.4.	Was the megaturbidite caused by a strong earthquake? .....	56
5.5.	Comparison of Lake Altaussee with Other Alpine Lake Studies .....	58
6.	Conclusion and Outlook .....	61
7.	References.....	63
8.	Appendix / Supplementary Data .....	71



# 1. Introduction

## 1.1. Sediment dynamics and Sediment archives in Alpine lakes

Sensitive alpine systems are vulnerable to various changes, including the effects of global warming. As Arias et al. (2021) describe, this can trigger cascading events such as landslides, floods, and lake outbursts due to increased precipitation. To understand a complex natural system and predict its future, it's essential to understand its past (Costanza, 2007; Sabatier et al., 2022). However, because historical records often don't go back far enough, long-term archives are needed. A widely recognized and natural geological archive system is the sedimentary records found in lakes (Strasser et al., 2013; Beck, 2009). These archives can continuously preserve high-resolution data for millennia (Beck, 2009; Sabatier et al., 2022; Gilli et al., 2013; Strasser et al., 2013). As a result, alpine lakes provide a well-protected archive for environmental changes (like climate variability and human impacts) as well as natural hazards such as floods, avalanches, earthquakes, tsunamis, and volcanic eruptions (Sabatier et al., 2022; Strasser et al., 2013), as shown in Figure 1. The use of alpine lakes to study natural hazards is becoming more important as the population grows, tourism increases, and infrastructure needs to be protected from such risks. This issue is especially relevant in mountain regions (Gilli et al., 2013). In the densely populated European Alps, natural hazards are a growing concern, especially as climate change may make them happen more often, causing serious damage (Wilhelm et al., 2022). This is already happening, as Blöschl et al. (2020) point out that the frequency and severity of flooding have increased over the past 50 years.

Analyzing past natural hazards helps answer important questions: How often do certain events happen? How severe were they, and where did they occur? What processes are involved in each type of natural hazard, and how do they change over time? By understanding these patterns, we can get a clearer picture of the future and develop better strategies to reduce risks (Gilli et al., 2013; Costanza et al., 2007).

Events such as floods, earthquakes, avalanches, and volcanic eruptions are recorded in the sediment as event layers. These layers can form in various ways, such as turbidites, debrites, slumps, or mass transport deposits, each with its own unique sedimentological signature (Sabatier et al., 2022). However, identifying the specific trigger for an event is challenging, as different processes can lead to similar deposition patterns (e.g., turbidites) (Sabatier et al., 2022). Event layers are distinct from continuous deposition, or background sediment, which accumulates steadily on the lake floor throughout the year, although it may show some fluctuations. When an event occurs, a large amount of sediment is deposited in a very short time, often within hours or days (Sabatier et al., 2022; Rubensdotter & Rosqvist, 2009). Event layers can be distinguished visually (e.g., by color or smear slides) and through physical or chemical parameters (e.g., density, magnetic susceptibility, XRF

scanning data) from the background sediment (Sabatier et al., 2022). A crucial first step is to recognize and classify these event layers to draw conclusions about their origin (Sabatier et al., 2022). Equally important is dating the event layers to establish a chronology, which helps answer questions about their frequency, as described by Sabatier et al. (2022) and Gilli et al. (2013). Many researchers (Strasser et al., 2013; Lauterbach et al., 2011; Bauer et al., 1999) have studied lake sediments to gain a better understanding of the lakes. This work aims to investigate and describe the sediments of Lake Altaussee. Studying the archive of Lake Altaussee and the surrounding UNESCO World Heritage region of Hallstatt/Dachstein-Salzkammergut is particularly significant, as salt mining has been practiced in the Salzkammergut since the Bronze Age, providing early human records from this region (Festi et al., 2020). Both climate archives and human records are essential for the continuous reconstruction of past events and system changes, providing important information that allows for the comparison of historical records with environmental archives.

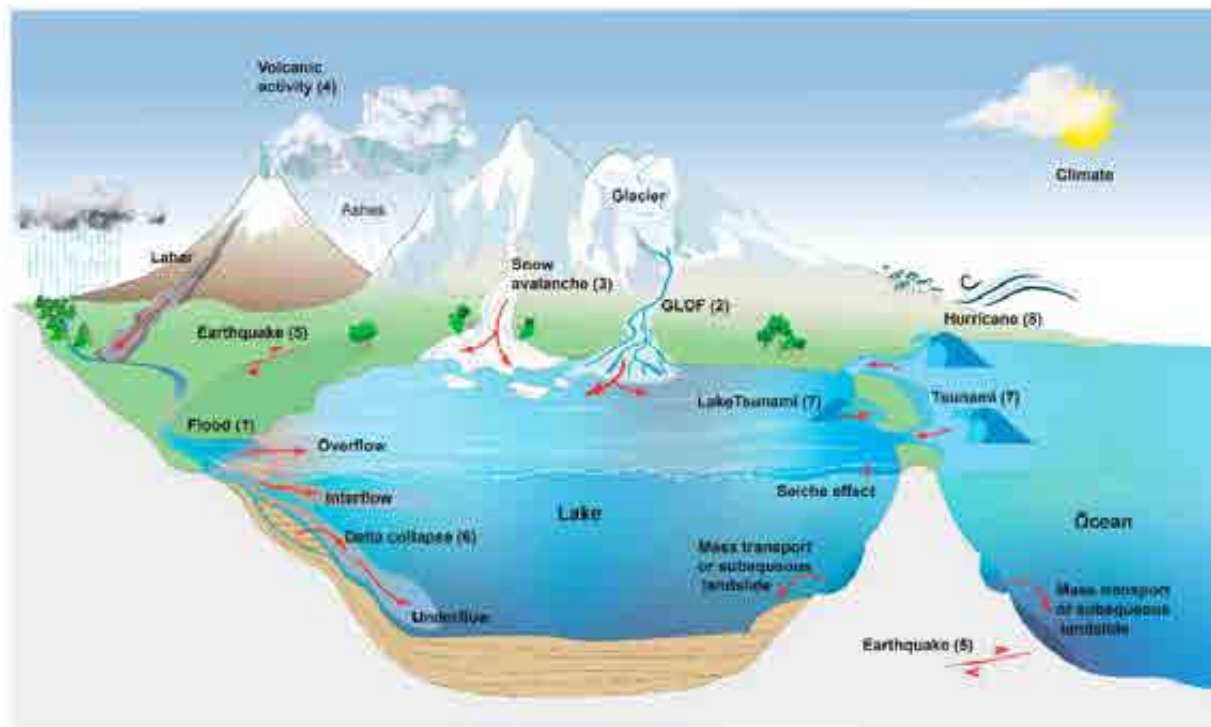


Figure 1: Schematic representation of natural events that can be stored in lake sediment archives. 1) floods, (2) glacial-lake outburst floods (GLOFs), (3) snow avalanches, (4) volcanic eruptions, (5) earthquakes, (6) delta collapses, (7) marine or lacustrine tsunamis, and (8) hurricanes - taken from Sabatier et al., (2022).

Firstly, a brief introduction to turbidites and their definition is provided, as this term is central to the study and has been referenced multiple times in the previous section. A central aspect of this thesis is the analysis of a turbidite.

The word turbidite is information about the transport process (Fig. 1.2.), i.e. a gravity flow loaded with particles that are brought into suspension by the turbulence of the water (Meiburg & Kneller, 2010). Due to differences in density and gravity, particles settle and deposit in layers. Initially, high-density

particles are deposited, leaving behind a low-density turbidity current that settles more slowly (Lowe, 1982). This process results in turbiditic deposition, commonly referred to as a turbidite (Meiburg & Kneller, 2010). Turbiditic deposits typically form a sequence that becomes finer toward the top, reflecting the decay of flow or energy after an event (Gilli et al., 2013). Bouma (1962) described gravity-driven currents in his reference work and established that conclusions could be drawn about transport and deposition processes by analysing their facies. To this end, he established a connection between flow conditions, sediment structures and grain size variations. Bouma (1962) divided the turbidites into sections Ta, Tb, Tc, Td and Te. Turbiditic deposits, however, do not always have to contain all sections of the Bouma sequences, but can also exhibit only partial sequences (Shanmugam, 1997).

The depositional characteristics of turbidites can vary depending on factors such as grain size of the source area, transport distance, and flow discharge velocity, which is influenced by grain size (Gilli et al., 2013). Another key factor in the preservation of sediment sequences is the steepness of the subsurface where the sediment is deposited. On steeper slopes, sediment is less likely to settle properly and is more easily remobilised.

Bouma (1962) was the first to propose a structural scheme for turbidites, primarily focusing on coarse-grained, sandy turbidites. However, this classification is often insufficient for all turbidites, as they can vary in appearance depending on the environment, remobilization process, and density of the turbidity current (Stow & Shanmugam, 1980). Therefore, the work by Stow & Shanmugam (1980) further structures and describes fine-grained turbidites and low-density currents in detail, as these finer deposits would all be classified under the Unit name "Te" by Bouma (1962).

A tsunami wave or a seiche (standing wave) in the lake can be caused by mass movements into the lake (which can create an impact wave), submarine slope failures or seismic tremors. When such processes occur, they are typically visible in the sediments (Sabatier et al., 2022). The term "megaturbidite" is also used in this work. A megaturbidite refers to an exceptionally thick turbidite that covers large areas of the lake floor, extends laterally, and lacks a fan structure (Bouma, 1987).

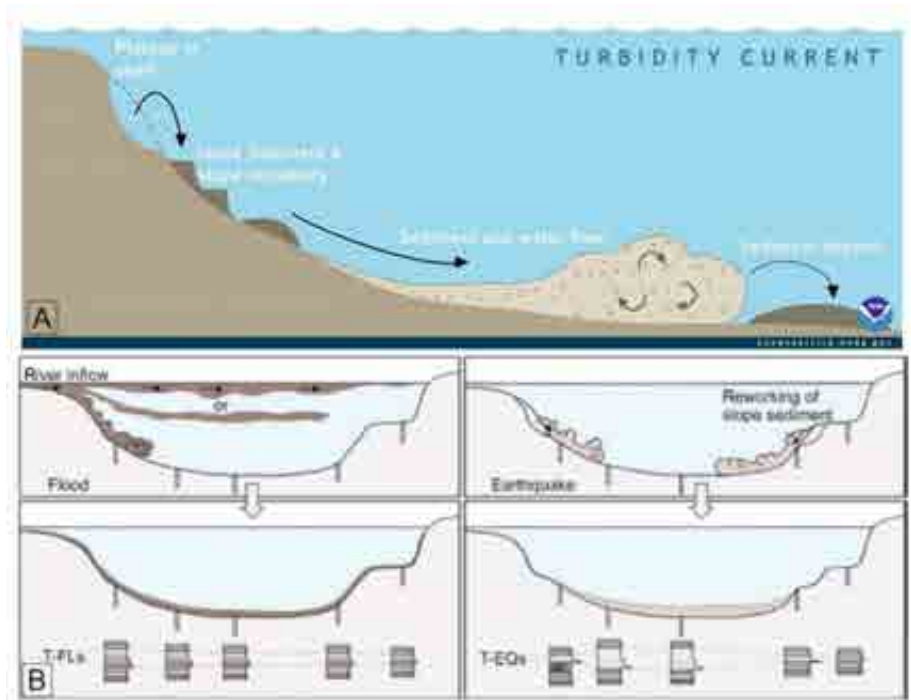


Figure 1.2: A: Schematic representation of how a turbidity current works (Oceanservice.noaa.gov). B: The differences between two differently initiated turbidity currents. Both end in a turbidite. Modified from Vandekerkhove et al., 2020).

As explained by Sabatier et al. (2022), the most effective way to identify and differentiate event deposits is through grain size analysis and examining their spatial distribution in the lake. For instance, debris flow or heavy rain deposits spread differently from turbidity currents caused by mass movements. According to Vandekerkhove et al. (2020), the trigger for an earthquake or mass movement is short-lived, typically lasting only a few minutes. In this case, the resulting turbidite would be concentrated in the deep basin, where it would be thickest, with a generally upward-fining grain size distribution.

Flood sediments, on the other hand, also show upward fining but are more evenly distributed across the lake, as flood discharge can last from several hours to days. During a flood-induced turbidite, fluctuations in current strength can bring in coarser material, leading to grain size variations throughout the event (Fig. 1.2).

## 1.2. Lake Altaussee and Project

The project was carried out in collaboration with the University of Natural Resources and Applied Life Sciences in Vienna, as part of the Lake Altaussee Project of the Walter Munk Foundation for the Oceans (WMFO). The idea for the detailed study of the lake came from Walter Munk in 2018, who spent part of his childhood there (Heine, 2021). Born in Vienna, Austria, in 1917, Walter Munk spent almost all his school vacations at his family's weekend house in Altaussee. Though his parents sent him to the USA to train as a banker, Walter chose to study physics at the California Institute of Technology instead (Heine, 2021).

Walter began working at the Scripps Institution of Oceanography (SIO), where he became its first graduate student. He later became a professor of geophysics at SIO and played a key role in the founding of University California San Diego. Throughout his career, Walter received many awards and honours, including the Crafoord Prize from Sweden for his "pioneering and fundamental contributions to our understanding of ocean circulation, tides, waves, and their role in Earth's dynamics" (Burstein Hewitt, 2017). Walter Munk was often called "The Einstein of the Oceans" and is considered "the world's greatest oceanographer" (Burstein Hewitt, 2017).

The 'Altaussee 3D' project was launched in 2019, with numerous universities, schools and other research institutes involved in the project. The first field work was carried out in 2019 by Erwin Heine from BOKU University of Natural Resources and Applied Life Sciences Vienna, in which a three-dimensional bathymetric model of the lake was created and the lake bottom was examined with the Innomar Sub Bottom Profiler. In 2020, the Institute of Geology at the University of Innsbruck joined the research team. In September 2020, the sedimentology group worked at Lake Altaussee, where we took sediment cores and subbottom profiles. Other limnogeological field data (such as long cores and additional Innomar subbottom profiles) were collected later, but were not included in this MSc thesis. Every year, the WMFO organizes a science meeting in Altaussee, bringing together all those who research and work in connection with this project, and to organize public outreach activities. Marry Munk, Walter Munk's widow and president of the WMFO, also takes part and leads this project.

### 1.3. Research questions and objectives

The focus of this work is to study the sediment dynamics and geohazards recorded in the late Holocene sedimentary infill of Lake Altaussee. With a focus on gaining a better understanding of the turbidite deposit.

This thesis seeks to clarify the following questions:

- Was the identified megaturbidite caused by one or more terrestrial mass movements that propagated into the lake?
  - Obj. 1: Conduct a detailed sedimentological analysis of the turbidite to investigate if multiple pulses can be found.
  - Obj 2: Map and interpret the distribution of blocks in the Eastern part of the basin and how it relates to onshore morphology. Can the distribution and lithology of the blocks give answers on their source location?
- Was the megaturbidite (and potentially onshore mass movements) caused by strong earthquake shaking?
  - Obj 3: Compare other lakes from this area -can we find a turbidite with a similar age?
  - Obj 4: Literature research - can we find any documentation of a strong earthquake at the time the turbidite was formed (1000-1200 cal yr BP)?
- How did sediment dynamics in this lake evolve over time?
  - Obj 5: Identification of lithofacies through a multi-proxy approach involving direct comparison of sedimentological and organo-geochemical data.
  - Obj 6: Create a continuous age-depth model and date the lithological unit boundaries by optical correlation of marker layers in multiple cores to this age-depth model.
- What is the role of Alpine geohazards or human influence for changes in sediment dynamics?
  - Obj. 7: Compare sediment types before and after the megaturbidite event to determine differences or similarities.
  - Obj. 8: Trace the sediment signature of river inflow in the lake and possibly date its onset and end. Compare this with historical documentation on human influence in the area.

## 1.4. Core campaign

The core campaign took place in September 2020, during this time, short cores were taken from Lake Altaussee (see Fig. 2.). In total 22 short cores were taken with the hammer-driven Bob Corer, the cores having a diameter of 6.3cm and a maximum length of 170cm (A.2.1.). A PVC liner is fixed in a hammer system holder mounted on a cable winch. The winch runs over a pyramidal structure. This structure is placed on an air-cushioned catamaran that we can attach to a boat and move across the lake.

The PVC liner in the mount is released in free fall and only braked when it hits the lake bottom. The momentum causes the PVC tube to pierce vertically into the soft lake sediment. Then, by pulling on the rope, the hammer system can be operated. A 7.5kg weight is hammered onto the PVC liner, allowing it to go deeper into the sediment. The core system can be pulled out of the sediment with the help of a cable winch. When it is pulled out, a lid in the coring system closes, creating underpressure and the sediment remains in the tube until it comes to the surface and is removed from the water.

Furthermore, seven Surface-cores were taken with another system, these cores have a wider diameter of 9 cm and have a maximum length of 50cm. These cores cover only the upper young sediment, but well preserved the sediment-water interface as no hammering is involved. They are used for the microplastic analysis, which is performed by BOKU in Vienna and the Scripps Institution of Oceanography at UC San Diego. As part of the ongoing work at Lake Altaussee, more cores are being taken. In the summer of 2021, long cores were taken for a PhD thesis, which provide more information. The objective is to obtain a detailed study of extreme event deposits from the Late Glacial to the Holocene through a long and continuous sediment record. And how these events could have influenced the Dachstein-Salzkammergut system and the human-environment system. In summer of 2023, a peat bog core was taken, and further short cores were taken by the University Boku in Vienna near some submerged trees.

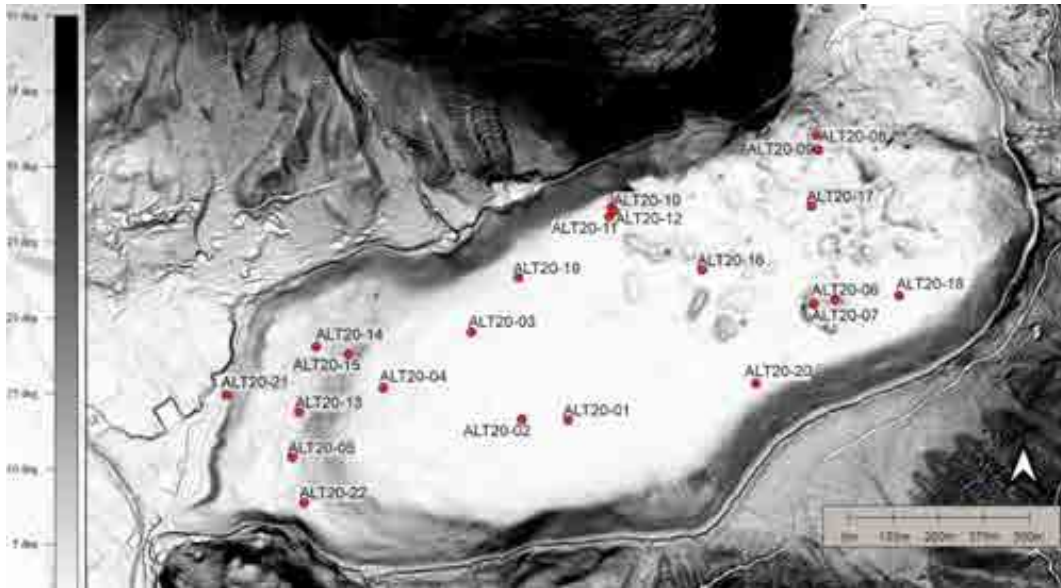


Figure 2: Hillshade map of Lake Altaussee (combined bathymetry and topography; red dots show the sampling points of the 22 short cores taken with the Bob Corer in September 2020 at Lake Altaussee).

## 2. Study Area

### 2.1. Geographic Overview

Lake Altaussee is located east of the village of Altaussee in Styria, Austria (47°38'23.3"N, 13°47'06.5"E). It is an alpine lake in the Styrian part of the Salzkammergut, situated at the base of the Totes Gebirge (Fig. 3). The lake sits at an altitude of 712 m a.s.l. and covers an area of 2.1 km<sup>2</sup> (Riedl et al., 2008). The Lake is surrounded by the Loser (1837 m) to the north, the Trisselwand (1754 m) to the east, and the Tressenstein (1201 m) to the south (Riedl et al., 2008). Towards the northeast there is a small Dead ice hole which is filled with water, it is often referred as Ostersee or Astersee, which is connected to the Altausseer See (Lobitzer, 2011). Lake Altaussee has a catchment area of 54,5 km<sup>2</sup>, but the lake has no major surface inflows and is almost entirely fed by subaqueous karst springs (Riedl et al., 2008; Zötl, 1961). Some of the channels that feed the lake become active only during periods of increased rainfall or snowmelt in spring. The catchment area consists entirely of carbonate rock from the Northern Calcareous Alps. The lake's outflow is located at its southwestern end, draining through the Altausseer Traun with an average discharge of 3.8 m<sup>3</sup>/s (Riedl et al., 2008; Aigner, 2019).

Lake Altaussee serves as a year-round recreational area, attracting visitors for various leisure activities both on and around the water. In addition to recreation, the lake has a long-standing tradition of fishing, which continues today. As in other lakes in the region, fishing is still practiced using nets. The primary fish species in the lake are char and trout (Riedl et al., 2008).



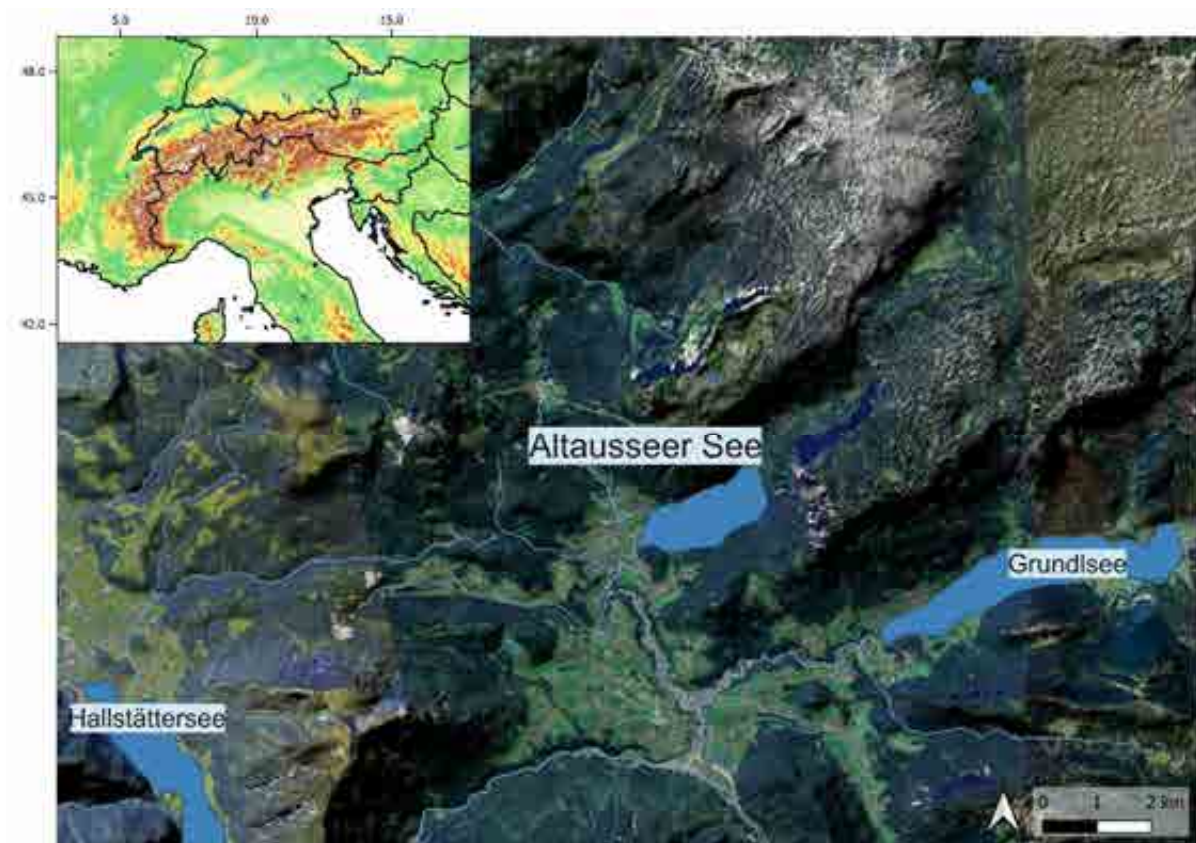


Figure 3: The top left of the figure displays the location of Lake Altaussee within Europe. Below this, the lake is shown in its local setting in north-western Styria. Adapted from Marcel Ortler, 2024.

In the western part of the lake there is a plateau which leads through a steep slope into the central basin of the lake. The lake basin reaches its deepest point in the western centre of the basin, with a maximum of 53m. The north-eastern part of the lake is covered by large blocks, which are visible in the lake's bathymetric maps - shown later in Figures 7 and 8. Also noticeable are some funnel-shaped depressions at the lake bottom, which are in the northern part of the lake. These are the subaqueous karst springs that supply the lake with water. The biggest karst spring is ~25m deep and reaches a total water depth of ~77m at their deepest point.

The mountain range directly to the north of Lake Altaussee is rugged and is intersected by tunnels, on the one hand due to the large number of karst caves that form a large network (Spötl et al. 2016) and on the other hand, due to the tunnels driven by man to mine the salt in the mountain (Lamer, 1998). It has been documented that salt mining was carried out there since at least 1147 (Pelzl & Pelzl 2005; Lamer, 1998). As in the other places in the Salzkammergut where salt was mined, the mine has had a great impact on the surrounding area (Lamer, 1998). Several tons of salt were mined, boiled and sold during the years of mining, which gave the community a good reputation and financial prosperity. The environment was also affected, for example in the 14<sup>th</sup> century almost all the trees in the region were felled in order to obtain enough wood for the brewing pans (Lamer, 1998).

Altaussee was one of the earliest settlements in the region, as evidenced by late Roman settlement traces in the Leisling area, and the salt deposits may have been crucial to early settlement. Salt is still mined there. About half of Austria's total salt production comes from here (Lobitzer, 2012). Salt mining used to be the most important economic sector in the region, but today it is tourism. The Hallstatt-Dachstein-Salzkammergut region is a UNESCO World Heritage Site and attracts many tourists every year for hiking around the lakes or as a winter sports destination. (Mandl, 2012 a).

## 2.2. Geological Setting

The Altaussee area is located in the northern limestone Alps, a region shaped by glacial and river activity and surrounded by mountain and limestone plateaus (Mandl and Van Husen, 2012). The lake and its catchment area lie within the karst of the Totes Gebirge. The Tote Gebirge area is the largest contiguous karst area to be found in Austria with a total area of 1057km<sup>2</sup> (Geyer et. al., 2016). A significant geological feature of this region is the Schwarzmooskogel cave system, a branched cave system northeast of Lake Altaussee. Almost all of the cave system's development extends in a south-west direction towards Lake Altaussee, which is predominantly fed by subaquatic karst springs. The lake exhibits typical water level fluctuations consistent with a karst-fed system (Geyer et al., 2016). This subaquatic spring has an average discharge of 3.75 m<sup>3</sup>/s, with only 20 l/s originating from small springs along the lake's shore. This indicates that the biggest amount of water entering the lake comes from underground karst springs (Schubert, 2012). Geologically, the area primarily consists of Upper Triassic Dachstein limestone, supplemented by Upper Jurassic Plassen and Tressenstein limestones (Riedl et al., 2008; Mandl & Van Husen, 2012). To the southwest lies the Dachstein massif, dominated by thick limestone beds, which are characteristic for the Dachstein formation (Behm et al., 2019).

The geological evolution of the Altaussee area spans several time periods. During the Triassic, the Dachstein limestone north of the lake was deposited, followed by Jurassic carbonates from the Allgäu and Oberalm formations. South of the lake are some Jurassic carbonates, while in some isolated places Hallstatt Triassic limestones are exposed in the southwestern parts of the region (Mandl, 2012c; Mandl & Van Husen, 2012) - this can be seen in Figure 4.

The salt deposits of Altaussee, located within the Hallstatt zone, belong to the Haselgebirge, often referred to as "salt rock" due to its unique composition of salt minerals, clay, and sandstone (Lobitzer, 2012; Mandl & Lobitzer, 2012). These deposits date back to the Upper Permian 299 to 251 million years ago, as climatic changes and warming initiated the evaporation of Tethys Ocean water in lagoons and basins. This led to the formation of evaporites along the continental margin of Pangaea (Mandl & Van Husen, 2012). These were subsequently deposited along with clay and sand (Mandl, 2012c).

During the Triassic, carbonate platforms, such as Wettersteinkalk, began forming. Sea-level fluctuations led to the deposition of Hauptdolomit, Plattenkalk, and Dachstein limestones atop these platforms, as well as the Hallstatt facies distinctive to the Dachstein region. In the Jurassic, the

supercontinent Pangaea began to fragment, creating the Central Atlantic Ocean basin and causing subsidence of the sedimentary layers. By the Cretaceous, parts of the area that now include Bad Ischl had been eroded and exposed. During the Paleogene, the sediments forming the Eastern Alps were thrust onto the European continental shelf (Mandl & Van Husen, 2012). At the beginning of the Neogene, the movement of the Adriatic plate led to a strong north-south compression of the Eastern Alps by over 100 km. This significantly characterized the appearance of the Eastern Alps today. This process led to the compression and thickening of the Alpine units (Mandl, 2012c). Afterwards, erosion, glaciers and rivers, which are responsible for the valleys and lakes, shaped the terrain as it is today.

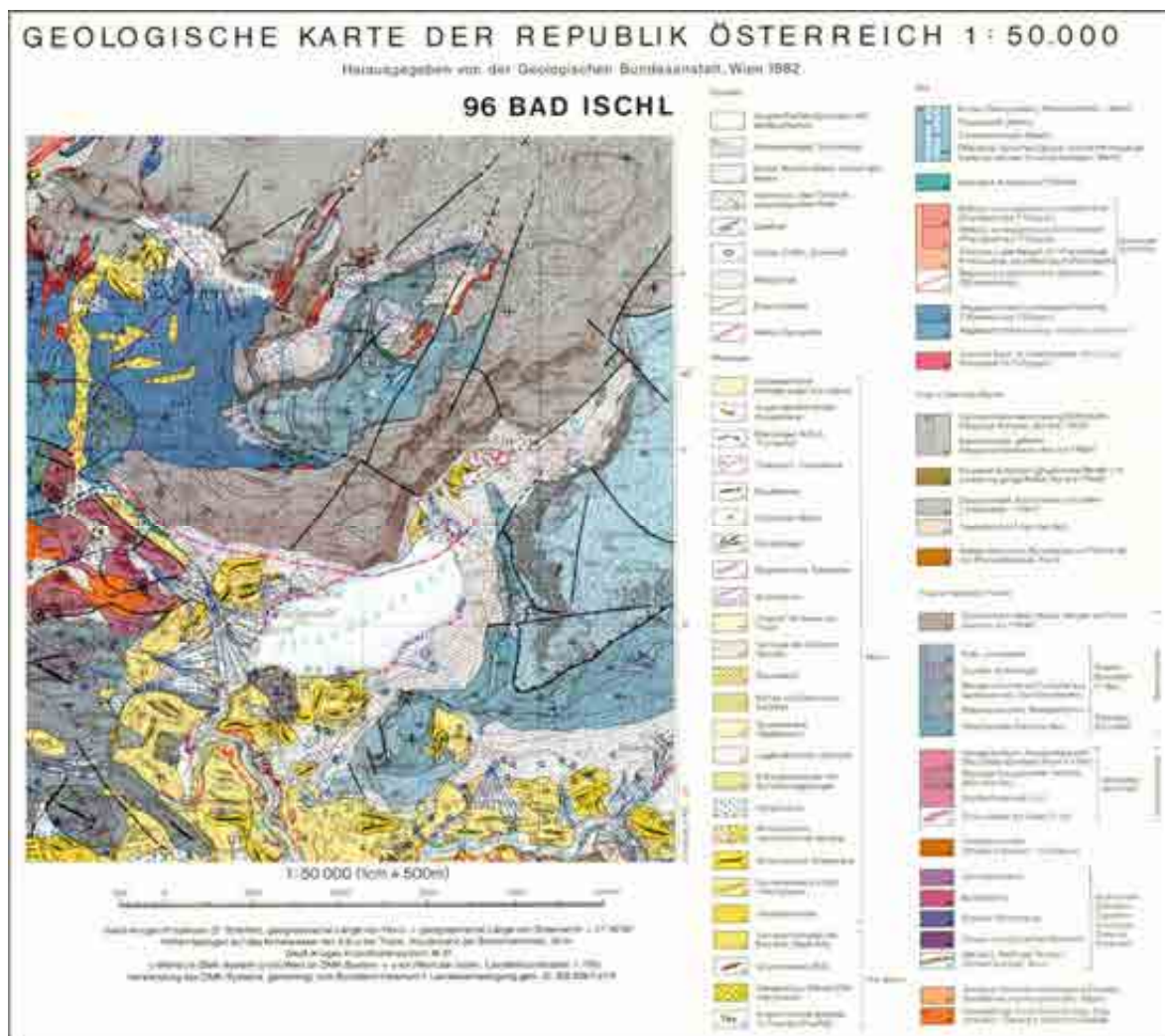


Figure 4: The figure shows a section of the map sheet '96 Bad Ischl' of the Austrian Geological Survey. The map shows the Lake Altaussee, the surrounding geological units and the Quaternary deposits in the lake and its catchment area. Figure modified from "Geologische Bundesanstalt, Vienna 1982".

The area around Altaussee is mildly seismically active and classified as Zone 1 on the earthquake hazard map for Austria (Lehnhardt, 2012; see Figure in Appendix). Weak earthquakes, with a magnitude of approximately 3, occur every two years on average. Stronger earthquakes, with magnitudes around 4, occur approximately every 12 years. Historically, significant seismic events with higher magnitudes have occurred roughly every 50 years. According to Lehnhardt (2012), these stronger earthquakes often

originate from more distant epicenters and are associated with the ongoing north-south compression of the Alps. One notable geological feature near Lake Altaussee is the "Toplitz fault" or "Toplitz lineament," as described by Schwingenschlögl (1986). This fault runs beneath Lake Toplitz and Lake Grundlsee. However, it is only marked as "suspected" on the "Geologische Karte der Republik Österreich Blatt 96" by Mandl et al. (2012) and has not been definitively confirmed. Around Lake Altaussee, several small faults are also suspected, as illustrated in the geological map by Mandl (2012), included in the Geologischen Bundesanstalt and referenced in the Appendix (A.1.3.). These faults run in a west-east direction along the northern and southern shores of the lake. Confirmed smaller faults can be found on the Trisselwand, located along the lake's eastern shore.

### 2.2.1. Quaternary

The region around Lake Altaussee underwent significant transformations during the Quaternary period, with former glaciers playing a crucial role in shaping the landscape (Riedl et al., 2008). The area is characterized by alluvial fans, moraine landscapes, and limestone plateaus (Mandl and Van Husen, 2012). The bedrock in this region was extensively eroded by the movement of the Traun Glacier, leading to the formation of overdeepened basins. This phenomenon has been described by Van Husen (2012) and Schmalfluss et al. (2022). Evidence for such glacial erosion was confirmed through an exploratory borehole that reached a depth of 880 meters without reaching bedrock. This suggests that the overdeepened basin is almost 880 meters deep and subsequently filled with sediments. Similar processes resulted in the formation of lakes in such valleys (Van Husen, 2012).

During the repeated retreat and advance of the glaciers in the different glaciation periods, several structures were formed that are still preserved today, such as terminal and ground moraines (Van Husen, 2012). The yellow regions on the map, labelled with the number 33, represent lateral and terminal moraines as well as ground moraines, most of which are concentrated in the western part of the lake. Another example of geological deposits from the Quaternary period are alluvial fans observed on the western side of the lake, where several alluvial fans line the shoreline. The village of Altaussee is built on an alluvial fan. More alluvial fans can be found along the southern shore and one near the northern part of the lake, close to Ostersee—a smaller lake located directly northeast of Lake Altaussee. The remaining shoreline is primarily marked by slope debris, as indicated on the geological map (Fig. 4).

The area around Lake Altaussee frequently experiences mass movements, particularly during the Holocene. Such processes are still present to this day. One of the most notable and recent incidents took place in 1920 on the Sandling mountain (Lehmann, 1926). Several landslides and boulders are marked on the geological map. They can also be recognised in the direct vicinity of Lake Altaussee, as shown in Figure 4.

## 2.3. Lake Altaussee and Previous research

Some research has already been conducted on and around Lake Altaussee and is briefly described here. Until recently, there had been no detailed hydrogeological and geological investigation of Lake Altaussee, although the surrounding area has been studied for some time. In 1980, an aeromagnetic survey detected a gravity anomaly about 3 km south of the lake (Van Husen & Mayer, 2007). In 1998, Salinen Austria Ges.m.b.H. drilled an exploratory borehole, which reached a final depth of 880 meters. The recovered sediment was largely described as lake sediments by Van Husen and Mayer (2007). As part of the DOVE (Drilling Overdeepened Alpine Valleys) project, which is part of an ICDP drilling project, the sediments will be re-examined and described (Schmalfuss et al., 2022). Both Van Husen & Mayer (2007) and Schmalfuss et al. (2022) conclude that these are lake sediments covered by a LGM moraine. Methods such as sedimentological core description and clast petrography were used to reach this conclusion. From the data, Schmalfuss et al. (2022) interpreted that a salt body was dissolved by meltwater, forming a lake more than 800 m deep.

Lake Altaussee is constantly being analysed and monitored, but so far from a hydrological/hydrogeological perspective, as the lake is a public bathing water and is actively used for fishing.

Another discovery in the lake that is being researched are trees at the bottom of the lake. During an echosounder survey, standing trees were discovered at the lake bottom. These were already mentioned in the „IDNDR - Aktivitäten der Geologischen Bundesanstalt im Zeitraum von VII/1990 to IX/1994“ (unpublished). A master's thesis, which was also written as part of the 'Altaussee 3D' project, describes these trees that were found on the lake floor. The aim of Wagner's work (2021) was to create a detailed geomorphological mapping of the entire lake bottom using multi-beam echosounder data and photogrammetric images. Among other things, the already known upright trees in the lake were described and mapped. Wagner (2021) estimated that there are about 302 trees. In its report, the Federal Geological Survey determines the death of the trees to be between ~700 and 730 ±50 A.D.

In 2010, the big funnel shaped karst springs were discovered at the bottom of Lake Altaussee by Wolfgang Gasperl, head of the water rescue unit of the fire brigade in Altaussee (Heine, 2021). In order to better understand these karst springs, two bachelor theses have already been written on this topic at the Institute of Geology at the University of Innsbruck. One was the "Analysis of sediment dynamics in Lake Altaussee using six short cores", by Strachwitz (2021). In this thesis, the sediment of the crater cores was divided into event layers and background sediment, using various methods such as smear slides, MSCL, ITRAX - XRF scanner, CT scans and grainsize data. Four different event layers could be distinguished. These can be partially explained by regular events such as snow melting or irregular events such as heavy rainfall. From this it was possible to draw conclusions about the activity of the two craters and to show that the largest crater also has the strongest outflow. The second work on this topic is the "Analysis of sediment dynamics in the surrounding of underwater springs in Lake

Altaussee (Salzkammergut)” by Neuner (2022). Here the same methods were used to analyse long cores from this lake, looking back up to 2000 years. It was also possible to correlate periods of stronger crater activity with heavy rainfall events and the first onset of sediment expulsion by spring activity in the sedimentary record.



### 3. Methods

#### 3.1. Seismic and bathymetric acquisition

The first seismic survey of the lake was carried out in 2019 by project leader Erwin Heine. He investigated the lake using the Innomar SES 2000 system (4-15kHz), which provided information about the geometry and acoustic facies of the sediment layers. Based on the initial bathymetric map, it was possible to plan in advance the locations for coring the short cores.

In addition, further seismic lines were recorded in autumn 2020 to obtain high-resolution seismic profiles in areas of interest such as the underwater craters, the plateau and the rock blocks in the lake. The Kongsberg Geopulse Pinger was used for this purpose. The Geopulse Pinger creates subbottom profiles with a frequency of 3.5 kHz (a lower frequency than the Innomar SES2000 System). The combination of the lines from both surveys yielded approximately 50km of seismic lines, allowing very detailed investigations of the lake to be carried out even before receiving other information (Fig. 5). Later in 2023, some more seismic lines were made in the south-west of the lake to better explore the plateau. In this work, the grey (Geopulse pinger) and green (Innomar SE2000) lines in Figure 5 were mainly used, the analysis of the seismic lines was done in 2021 - 2022 before the new lines were added.

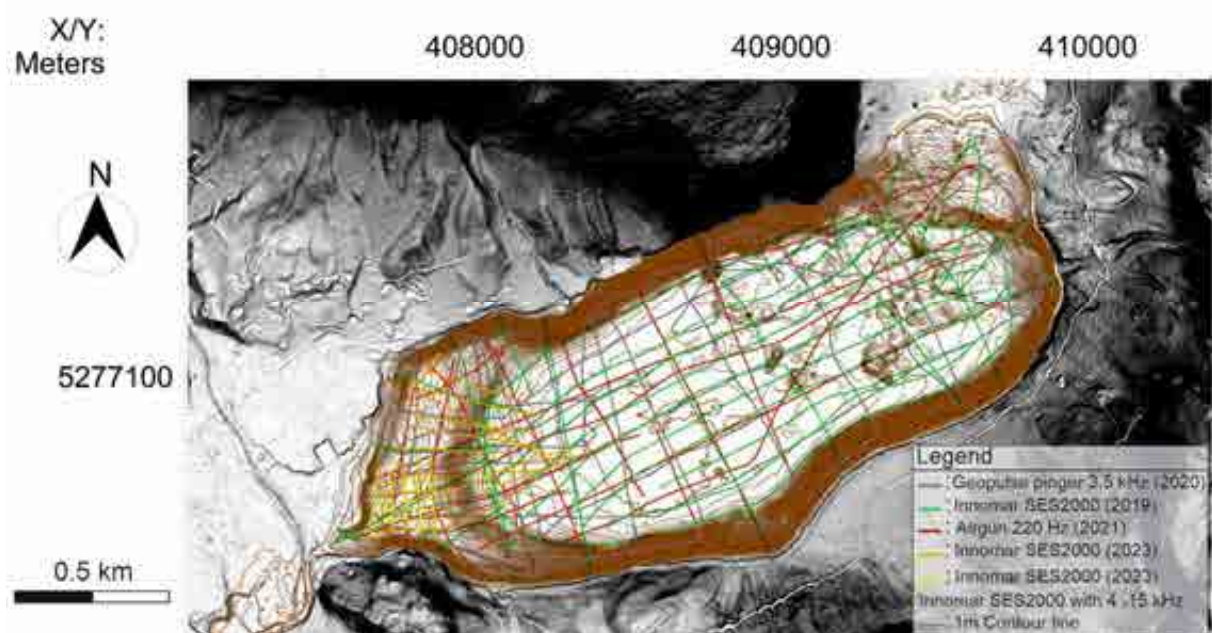


Figure 5: Map of Lake Altaussee with the different seismic lines which has been recorded over the years.

The IHS Markit Kingdom™ program was used to visualize the seismic lines. This is a program for display and interpretation of seismic and geological data. The program enables an initial analysis of the lake sediments, allowing the thickness and distribution of individual sedimentary units to be observed in the seismic data. By using Kingdom™, a bathymetric map can be created and maps with a distribution of the thickness of the different sediment units can be produced. Therefore the acoustic horizons of the

individual layers can be picked along the seismic line. Based on this information, a linear interpolation of this layer horizon can be constructed over the entire lake. This can be used to calculate the depth of a layer over the entire lake. This allows initial conclusions to be drawn.

## 3.2. Sediment core analysis

### 3.2.1. Multi Sensor Core Logger (MSCL)

The sediment core was examined with the Multi Sensor Core Logger at room temperature. The parameters of magnetic susceptibility (MS), density, and P-wave velocity were measured with a distance of 0.5 cm. Magnetic susceptibility is measured by an artificially applied magnetic field and describes the magnetizability of a material. The magnetic field is created by an oscillating coil in the sensor. The magnetizable particles in the core change the frequency of the oscillator when the magnetic field is applied. The more magnetizable a material is, the greater its influence on the frequency, allowing the strength of the magnetic susceptibility to be determined (GEOTEK Manual, Chapter: Sensors, 2021).

The density of the sediment core is measured by gamma radiation. A <sup>137</sup>Cesium source with a radiation of 0.37 GBq is used as the gamma radiation source. The emitted photons pass through the core and are detected on the opposite side. Based on the attenuation of the radiation, the detector determines the density, as denser materials allow less radiation to penetrate compared to looser materials (GEOTEK Manual, Chapter 5, 2021).

The instrument then measures the P-wave velocity. This involves sending an ultrasonic signal through the sample. The P-wave velocity depends in part on the density of the material, as well as the compressive modulus and shear modulus of a material. To determine the P-wave velocity, the instrument sends a short P-wave pulse through the core, and the travel time is detected. Afterwards, the P-wave velocity can be calculated after the calibration (GEOTEK Manual, Chapter: Sensors, 2021). In the core laboratory of the Austrian Core Facility, the cores were not only scanned with the MSCL but also with the ITRAX core scanner. Since this data was not used directly in this work, the information can be found in the appendix (A.2.2.).

### 3.2.2. X CT Scanning

The examination of sediment cores using X-ray CT is an effective method to gain initial information about the interior of the core and the sediment structures, even before the core is opened. During the process, key features in the sediment, such as inclined stratification or folds, can be made visible. If these features are to be analysed in the sediment, the X-ray CT examination indicates in which orientation the core should be opened in order to observe them in the split core. X-ray CT examinations can also be conducted on cores that have already been opened. X-ray CT scans allow sediment layers



to be distinguished based on X-ray attenuation, which depends on material composition and density (Van Daele et al., 2014). Thus, small differences in soft sediment composition can be visualized in a still-closed sediment core. For CT scanning, we measured eight cores: ALT20-01, ALT20-04, ALT20-07, ALT20-08, ALT20-11, ALT20-15, ALT20-18, and ALT20-22 (in the closed state). The medical X-ray CT scanner (Siemens, Somatom Definition Flash with a voxel size of 0.2 x 0.2 x 0.3 mm) at the University Hospital Innsbruck was used. ImageJ software was employed for further analysis and visualization of the CT data.

### 3.2.3. Macro- and microscopic lithological description

For the description of the cores the paper “Classification of lacustrine sediments based on sedimentary components” (Schnurrenberger et al., 2002) was used. In the first step it is distinguished whether the sediment is clastic, biogenic or chemical. The exact macroscopic classification of the sediments, according to Schnurrenberger et al., 2002 is divided into five parameters:

- Color and texture of the layers
- Thickness of the layers and other properties
- Sedimentary structures
- Properties of the layer boundaries
- Disturbances caused by hammer cores

The colors that are in the opened sediment core, were determined using the color chart “Munsell Soil Color Chart”. The color of the sediment core is ideally determined immediately after opening the core, since the color can change due to the oxidation process.

For microscopic description of the grains in the cores, smear slides were prepared, in which a small amount of sediment is taken, and a smear is made on a slide with water. After drying, the remaining sediment is fixed to the slide with glue and a cover slip. The resulting smear slides can be analysed with a transmitted light microscope. The full structure of the grains can be seen, since the grains are not ground as in a thin section. During the analysis, attention is paid to distribution, grain size, minerals and possibly organic components. The smear slides are used to characterize the background sediment or event layers.

### 3.2.4. Grain Size Analysis

A grain size analysis can reveal a lot about the sediment, such as how it was transported and deposited. For this purpose, some bulk samples from the cores were initially measured. To better understand the hydrodynamics of turbidite formation, sediment samples were taken again from the same core depths and treated with hydrogen peroxide to remove most of the organic matter. This treatment was done to better observe the grain size of the clastic sediment and to assess the effect of organic matter on the grain size spectrum.

For the sample preparation, between 3g and 5g of sediment were taken from the material. Hydrogen peroxide (35%) was added to the samples in 1 ml increments and heated (to 80°C) in a water bath to speed up the reactions. Between 70 and 110 ml of hydrogen peroxide was added to each sample until almost all the organic matter was removed, or until the reactions weakened. At this point, it can be assumed that most of the organic matter was dissolved, and it should no longer influence the grain size measurement.

Grain size analysis was carried out using the Malvern Mastersizer 3000. This is a Malvern Panalytical analyser for measuring particle size distributions by laser diffraction, with a detection range of 0.01–3500 µm (laser granulometric measurement). A laser beam is passed through a sample containing dispersed particles, causing scattering of the incident light. When the light hits large particles, it scatters at small angles, while small particles scatter light at large angles relative to them (Malvern Panalytical, 2015).

The optical unit is one of the main components of the Mastersizer and uses a sequential combination of red and blue light sources to measure across the entire particle size range of the dispersed sample. The scattered light creates a scattering pattern, which is recorded as angular scattering intensities by the optical unit detectors and processed and interpreted by the software to calculate the particle size (Malvern Panalytical, 2015). The scattering of electromagnetic waves on spherical particles is used for the calculation. Their radius corresponds approximately to the order of magnitude of the wavelength of the incident light beam (Mie, 1908).

Grain size analysis is an important basis for further investigations. For example, grain size is a critical factor in the analysis and classification of event layers. Passega used the D50 and D90 values to differentiate transport processes and draw conclusions about the type of depositional process, such as whether it was a turbidite deposit or a flood deposit (Passega, 1964; Arnaud et al., 2016).

### 3.2.5. Radiocarbon Dating

Radiocarbon age dating is used to determine the age of organic material found in sediment which is younger as 50.000 years (Blaauw & Christen, 2011). Radiocarbon dating is one of the most common methods for age dating in archaeology and for geoscientific investigation of the Quaternary period (Hajdas, 2009). In age dating, the content of the radioactive carbon isotope  $^{14}\text{C}$  in the sample is compared with a standard. The isotope  $^{14}\text{C}$  is formed in the atmosphere and becomes part of the biosphere. However, it should be noted that the  $^{14}\text{C}$  content did not always remain constant, but was subject to fluctuations. Living organisms continuously take up  $^{14}\text{C}$  atoms, when an organism dies the  $^{14}\text{C}$  content decreases. This can then be measured and compared to the original amount of  $^{14}\text{C}$ , providing a mean radiocarbon age and the associated measurement error (Blaauw & Christen, 2011). Macrofossils, mainly leaf fragments or needle pieces, were used as  $^{14}\text{C}$  material. Hajdas (2009) describes terrestrial organic material and macrofossils as the most commonly used for dating because

they only have a short life span and do not form a reservoir age. The age model was calculated using Bacon (in R Studio), a model for reconstructing the accumulation history using Bayesian statistics (Blaauw & Christen, 2011). Used for the age-depth-model was the IntCal20-calibrations curve (Reimer et al., 2020) see appendix (A.2.3.). Radiocarbon dating was performed at ETH Zurich in the Ion Beam Physics Laboratory with Dr. Irka Hajdas.

### 3.2.6. Organic Content Measurement

To obtain an overview of the organic content in the individual sediment layers, the Loss on Ignition (LOI) method was used. LOI is a widely used method to get a good overview of the organic content in samples (Heiri et al., 2001).

The measurements were performed at the Institute of Geography, University of Innsbruck, with the support of Prof. Clemens Geitner. A Nabertherm® muffle furnace with digital temperature display and thermostatic temperature control was used for the LOI analyses. When measuring loss on ignition, the sediment sample was first dried and crushed at 50°C. Then the sample was dried again in the oven at 105°C to evaporate the remaining liquid and weighed. Then the sample is placed in the muffle furnace where it is heated to 550 °C within 1 hour. This temperature is maintained for about 4 hours. The sample is then placed in a desiccator to cool and weighed again. The weight loss before and after heating the sample gives the weight percentage of the organic matter. At a temperature of 500-550 °C, organic matter burns (Heiri et al., 2001). If the sample were heated further to 950°C, further weight loss would occur as the carbon dioxide contained in carbonate rocks would evaporate (Heiri et al., 2001). The list of samples can be found in the Appendix (A.3.1.).

This method gives a good overview of the organic content in a sample but can also lead to somewhat inaccurate results; it should be noted that at temperatures above 550°C, gypsum and clay minerals also lose their water of crystallization (Blume et al., 2011). The organic content was calculated as follows (Blume et al., 2011):

Loss on ignition in percent by mass:

$$wV = (mb - mc) / (mb * 100);$$

- Where (mb)= The sample material was dried and cooled for 1 h (in a desiccator) and then weighed.
- Where (mc)= The sample material was cooled down to 100°C after muffling in the muffle furnace. The sample is then cooled to room temperature in the desiccator and weighed again.

## 4. Results

in the following sub-chapters 4.1 to 4.6, the data and observations obtained will be presented objectively so that these data can then be interpreted, compared and possible scenarios discussed in chapter 5.

### 4.1. Bathymetric analysis & Seismic stratigraphic analysis

The lake stretches from northeast to southwest and consists of a single basin. The bathymetric map of Wagner (2021) shows that there are steep slopes directly on the shores (Figure 7). Particularly in the north and south of the lake, the steep flanks continue directly into the deep basin. In the western part of the lake, the short flank ends on a plateau, which also continues into the deep basin after 200 meters. In the eastern part of the lake, a gentle transition from the shore to the deep basin can be observed. The deepest part of the lake (~52 meters) is in the western section of the deep basin. An analysis of the map in Figure 7 shows that the lake's outflow is directed toward the southwest, at the plateau. It also reveals that the lake has few surface inflows, with only small streams being active during heavy rainfall or snowmelt. The lake is mainly fed by subaquatic karst springs located in the northern part of the lake. One of these is still active, while others are inactive or have only a gentle water flow and have been filled or covered by sediment. The largest crater, shown in Figure 7 (top right), has a depth of 20 meters and a crater width of 70 meters (in diameter). An underwater block field can be observed in the north-eastern part of the lake on the bathymetric map of Figure 7 (bottom right). The boulders extend from the shoreline deep into the lake, with a maximum diameter of ~70 meters.

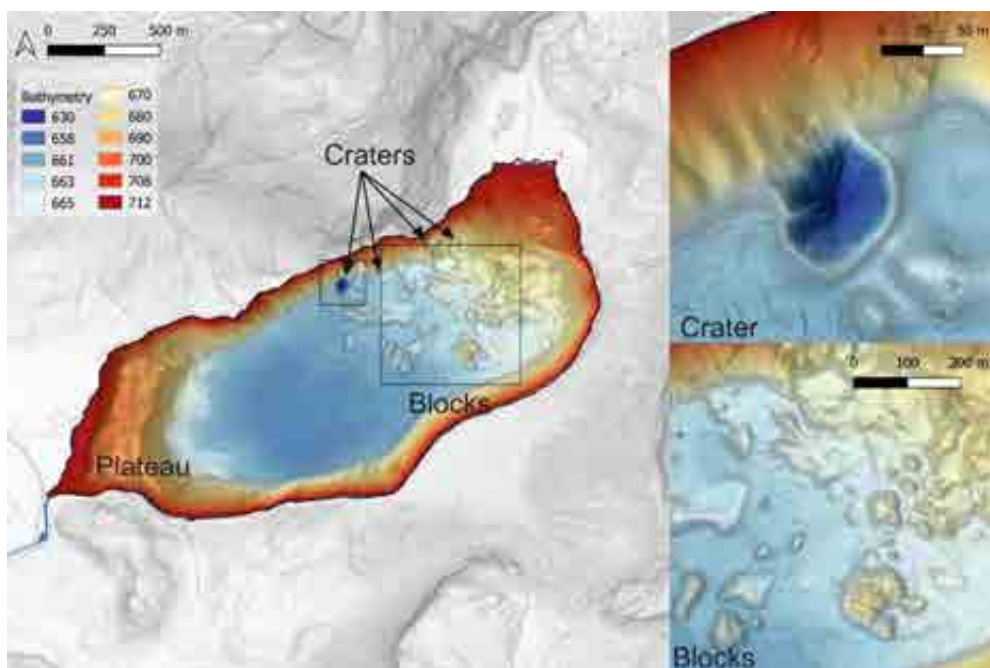


Figure 7: A bathymetric map of Lake Altaussee based on Wagner, 2021 is shown (left). It shows the outflow (blue arrow), the plateau in the west, the deep basin in the middle of the lake, the boulder field that covers the eastern lake floor and the

*subaqueous craters that can be found in the north-eastern part of the lake. top right: a larger image of the most prominent and active crater. Bottom right: representation of the block field. Figure adapted from Marcel Ortler, 2024.*

Seismic analysis can be used not only to observe the surface structure around the lake and underwater. Seismic surveys can also be used to look into the sedimentary layers. This provides initial stratigraphic information about the subsurface. As already described in the methodology, many seismic lines were recorded with different devices. The average penetration depth is 1-2m. Unfortunately, it was not possible to record deeper profiles because of gas blanking almost everywhere in the basin. This occurs when gas is trapped in the sediment, resulting in strong absorption of the sound wave energy (Tóth et al., 2014). This is illustrated in Figure 8 (left), where the gas blanking is shown as a bumpy layer below the acoustically-transparent layer.

The seismic lines clearly show the plateau, the basin, the blocks and also the craters. Different sedimentary facies can be identified, particularly in the deep basin. In total, 3 different facies can be distinguished in the seismic images.

- Seismic facies 1: This is shown as green number one in Figure 8. It's the uppermost facies and starts at the lake bottom and is around 0.6m/1.1m thick. It shows a continuous reflection with a high to a moderate amplitude. This layer is present throughout the whole lake and is noticeable in all parts of the seismic data, including the basin, slopes, plateau, blocks, and around the craters.
- Seismic facies 2: This is shown in figure 8 with an orange number two, it's located below seismic facies 1 with an approximate thickness of 1m/2m in the seismic profiles. It looks acoustically transparent (i.e., very weak amplitudes) in the seismic profile. This seismic facies is found almost exclusively in the deep basin. Interestingly, it also appears on top of the blocks, though it is thinner than in the deep basin. The sedimentary facies is slightly thicker in the western and eastern parts of the basin. The base of this facies is not sharply defined, but rather forms a wavy line
- Seismic facies 3: Begins below seismic facies two. The boundary between two and three is a very bumpy and irregular boundary (Fig. 8). The seismic data shows nothing below it.

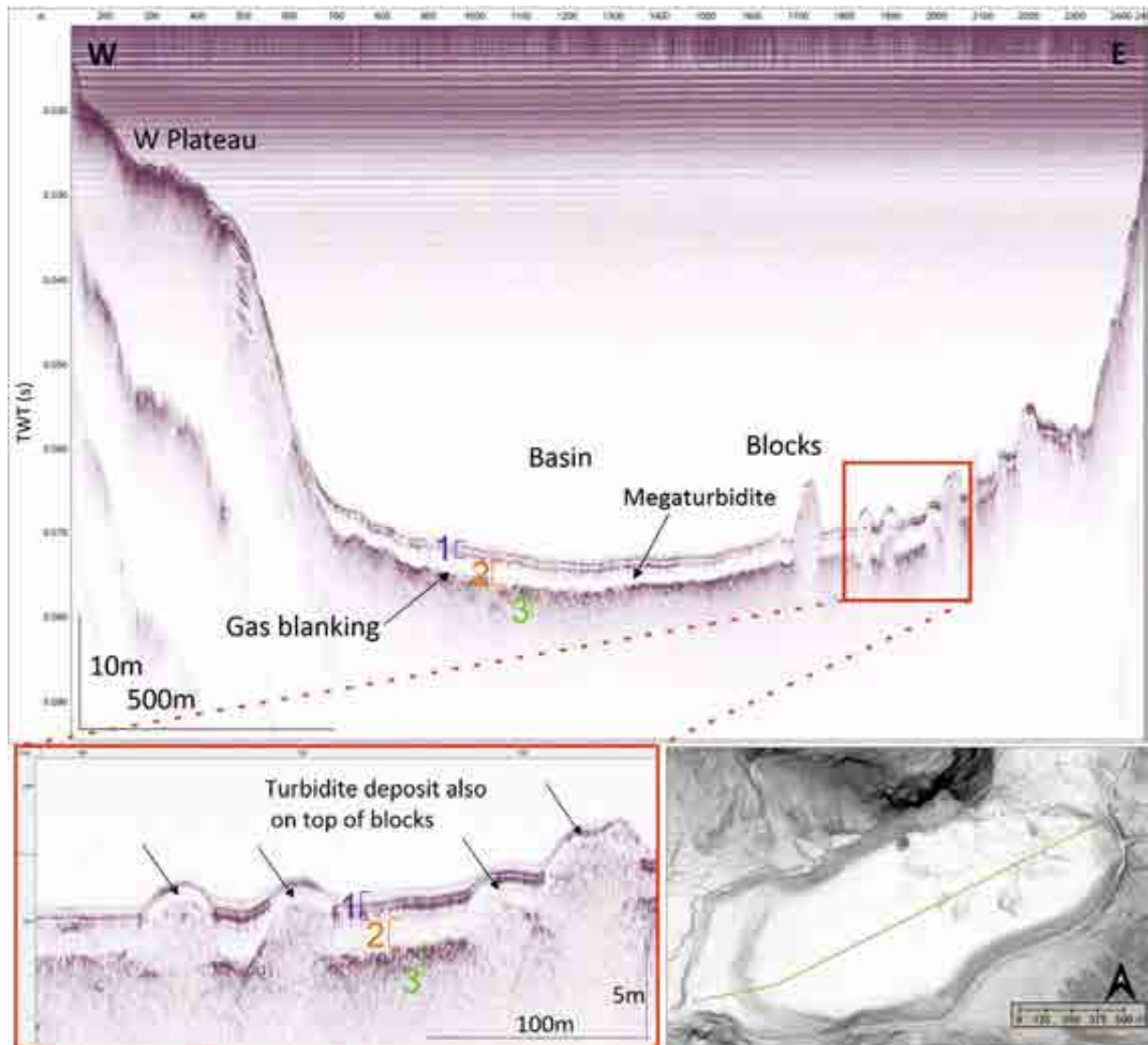


Figure 8: The upper picture shows a seismic line going from the west to the east of Lake Altaussee. Significant objects have been marked. The three seismic facies are numbered and colored. The bottom left picture provides a close-up of the blocks, revealing the deposition of seismic facies one and two on it. The bottom right picture indicates the progression of the seismic profile.

## 4.2. Sediment core data

This subchapter focuses on the different types of sediment lithofacies and the information that can be gained from them. It is important to note that the cores around and from the craters are not considered in this thesis. Two detailed bachelor theses have already been written on this topic: *"Analysis of Sediment Dynamics in Lake Altaussee Using Six Short Cores"* by Maximilian Graf von Strachwitz-Helmstatt (2021) and *"Analysis of Sediment Dynamics in the Surroundings of Underwater Springs in Lake Altaussee - Salzkammergut"* by Raphael Neuner (2022).

### 4.2.1. Lithologies and Event Deposit

Here we try to find similarities and differences in the sediment to distinguish it into lithofacies. Of course, the sediment does not always look the same, but has different characteristics. At first sight,

the cores show a quite similar sequence (especially in the basin), or at least the same units can be observed in most cores. At the plateau and at the crater cores there is a little more spatial variety in the sediment. These lithofacies have been successfully subdivided according to optical, chemical and physical parameters. They have all been collated to provide a detailed subdivision.

Depending on the location in the lake where the cores were taken, there is variation in the thickness or even the absence of certain units. Overall, the lithology of the cores can be grouped into five distinct units – with some sub units as showed in Figure 9.1. The five lithofacies are represented by two cores, ALT20-04 and ALT20-15. Core ALT20-04 contains very well exposed Units **1** to **4**. Unit **5** is only exposed and visible in core ALT20-15. This is due to the position of the core therefore it is possible to look deeper than in the other cores. Due to the inclination on the slope, less material is deposited during the sedimentation process, as it moves directly downwards into an area with less inclination, or is remobilised more quickly even with a slight influence and then moves downwards.

- Lithofacies 1: The lithological unit describes the youngest sediments at the top of the core. They clearly stand out in all cores, as they represent the darkest sediment in the core.
- Lithofacies 2: Lithofacies number two represents a homogeneous brown sediment with low density.
- Lithofacies 3: This is clastic laminated and dens sediment. This also stands out from the core due to its light color.
- Lithofacies 4: This is the thickest lithofacies. This unit is progressively finer from the bottom to the top and covers a wide range of grain sizes from gravel to fine silt and can be subdivided into several sub-units.
- Lithofacies 5: This unit can only be observed in core ALT20-15. All other cores end within or at the base of lithofacies 4. It is a very dense and finely laminated sediment with a light color. Consisting mainly of clastic materials little organic matter and as the CT images have shown, drop stones as well.

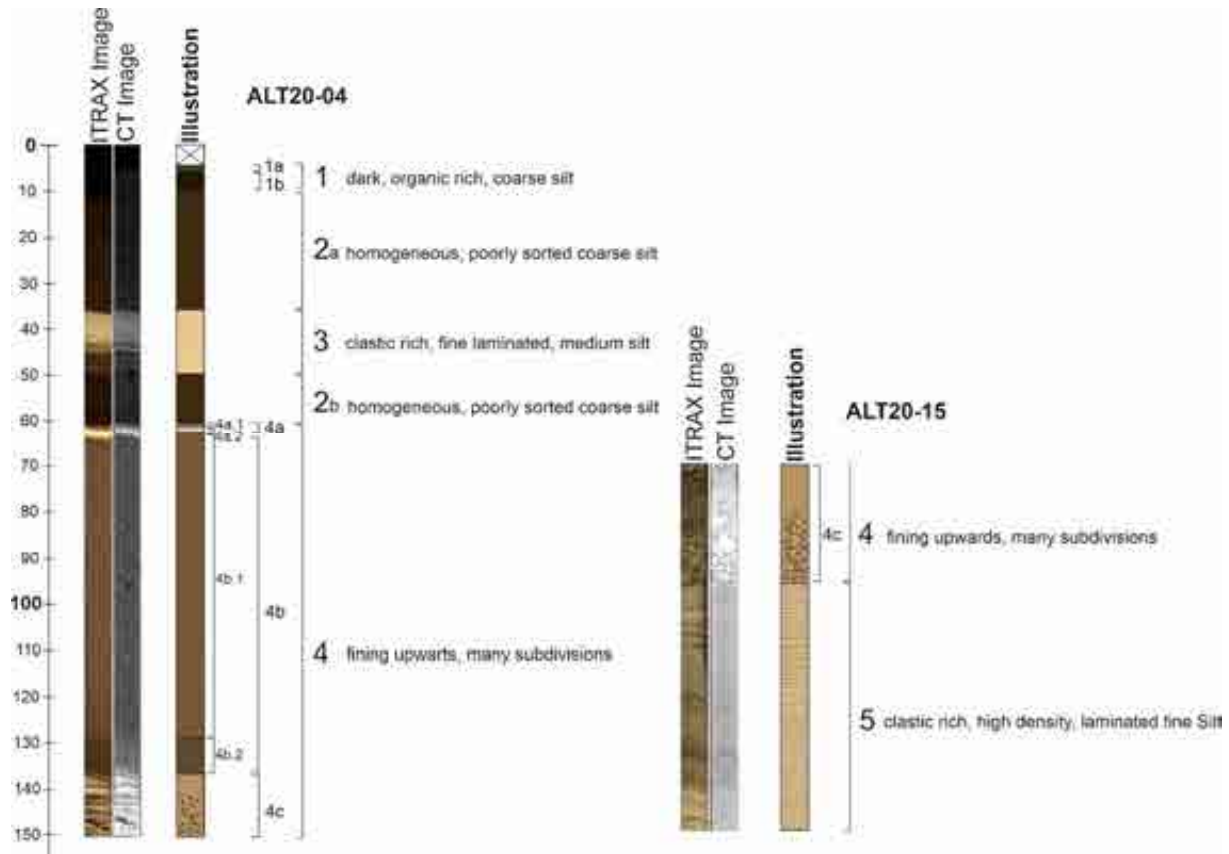


Figure 9.1: Shown are the sediment cores ALT20-04 and ALT20-15 which form the 5 lithofacies found in the short cores of Lake Altaussee. An ITRAX image, the CT image and a graphic illustration of the lithofacies are shown.

In order to better understand the differentiations of the lithofacies, they will now be described here with the help of Figure 9.2. In Figure 9.2 the lithofacies are again clearly shown independently of the core and their special characteristics, which have contributed to the differentiation.

#### 1a: Poorly sorted, organic rich coarse silt

This lithofacies comprises the recent lake bottom and the underlying dark sediments. The sediment is dark brown/grey and contains a fine orange layer. The smear slide (Fig. 9.2) shows many large pieces of organic matter. The measured organic content also shows the highest value of organic matter for Unit 1a at 24% - but more in Chapter 4.4. on the topic of organic matter content. Density is low throughout, with increasing magnetic susceptibility values. The sediment was highly saturated with water and very soft after opening the core.

#### 1b: Organic rich, very dark, poorly sorted coarse Silt

The dark brown and homogeneous sediment is characteristic. The smear slide image in Figure 9.2 also shows organic matter. It is not as large as in 1a, but it also contains a lot of organic matter (see chapter 4.4.). The density within this lithofacies is uniformly low at 1.1 g/cm<sup>3</sup>. The magnetic susceptibility increases even more, reaching a maximum for this area of 4.3 SI \* 10<sup>-5</sup> and decreasing towards the end of the lithofacies. The sediment in the core was very soft and highly saturated with water after opening.



**2a:** Homogeneous, very poorly sorted, very coarse/coarse Silt

Characteristic of this lithofacies is that it is uniformly dark brown in color (Fig. 9.2). Not only is the color homogeneous, but the density is also uniform at about  $1.2 \text{ g/cm}^3$ . The magnetic susceptibility is slightly elevated at the beginning of the unit, decreases and then remains uniform. The smear slide also contains many larger organic particles and little clastic material, which is also reflected in the color of the sediment.

**3:** Clastic rich, fine laminated, poorly sorted fine/medium Silt

Characteristic of this unit is the light color, which is immediately noticeable when looking at the sediment (Fig. 9.2). The light sediment is irregularly finely laminated. There are isolated larger organic fragments (leaf fragments or similar) up to 4 mm and isolated slightly sandy layers. Overall, the sediment is predominantly clastic-rich and poor in organic matter, as indicated by its color. The sediment is poorly sorted and consists of fine to medium silt in grain size. The base of this layer is sharply defined, but there is still intercalation of organic-rich material in the lower part, which is also found in the underlying lithofacies. The organic-rich material intercalates before the clastic material takes over. This can also be seen in the density; at the base, the material is less dense because the sediment is still intercalated with the underlying material. Once only the dense clastic and finely laminated sediment is present, the density also increases significantly to  $\sim 1.5 \text{ g/cm}^3$ . The magnetic susceptibility is lower in the denser area and increases slightly in the less dense area. It is also clear from the smear slide that little organic material is present. This sedimentary facies occurs only once in the core; it is not seen before or after.

**2b:** Homogeneous, very poorly sorted, coarse Silt

This lithofacies **2b** looks very similar to lithofacies **2a** described above. It is also a brown and very homogeneous sediment. The grain size is medium to coarse silt that is poorly sorted. The sediment contains many larger organic particles (Fig. 9.2), as can be seen in the smear slide, particles up to  $100\mu\text{m}$  are present. The color of the sediment also suggests that some organic matter must be present, more on this in chapter "4.4. Organic content". The density is constant at about  $1.2\text{g/cm}^3$  and the magnetic susceptibility is  $4.2 \text{ SI} \cdot 10^{-5}$ .

**4a.1** poorly sorted, medium Silt

This is a very narrow lithofacies, only about 1 cm to 2 cm thick. The sediment is beige in color, poorly sorted and has a grain size of medium silt. Density increases within the narrow lithofacies. Magnetic susceptibility is  $3.5 \text{ SI} \cdot 10^{-5}$ . As can be seen from the smear slide image (Fig. 9.2), there is little organic rich material here, only clastic particles.

**4a.2:** clastic rich, poorly sorted, medium Silt

This lithofacies is also a very thin layer of sediment with an average thickness of 1cm to 3cm. The sediment is very light and rich in clastic particles (Fig. 9.2), which is also visible in the smear slide. The sediment is poorly sorted and has a medium silt grain size. Density continues to increase after lithofacies **4a.1**, peaking at  $1.7 \text{ g/cm}^3$ . Magnetic susceptibility remains constant.

**4b.1:** Homogeneous, very poorly sorted, coarse Silt

This lithofacies occupies a large part of most cores and is prominent in most cores. It should be noted that the thickness varies greatly in the cores. This lithofacies is present in thicknesses of over a metre, a few centimetres or not present at all. The strongest expression would be in the deep basin with 77,2 cm- but not exposed in the short cores. This can be seen in one of the long cores taken at a later date. As can be seen in the Figure 9.2 this unit is homogeneous over its entire length.

**4b.2:** Darker, very poorly sorted, very coarse Silt/ fine Sand

Lithofacies **4b.2** is the continuation of Unit **4b.1**, but the sediment changes slightly. The sediment becomes darker and slightly coarser grained from coarse silt to very coarse silt/fine sand. The sediment becomes coarser towards the bottom, the grain size increases and the sediment structure changes, the sediment is less homogeneous. The sediment itself shows fine stratification, which can be seen particularly well in the CT images of the cores (Fig. 9.2). The density of the sediment increases. The magnetic susceptibility shows a slight increase already at the transition of the previous lithofacies. The increase in grain size can also be seen on the smear slide.

**4c:** Fining upwards, very coarse Sand up to pebbles

It is noticeable that the sediment in this lithofacies has become very coarse (Fig. 9.2). The grain size of the sediment has reached its maximum, up to a grain size of pebbles. In the upper part, the sediment is stratified with a grain size of fine to medium fine sand. Towards the bottom the grain size increases and the sediment becomes unsorted and unstructured. The smear slide shows that the sediment has little organic content and is predominantly clastic. Isolated pieces of organic matter up to a few millimetres in size can be found in the sediment. In some cores, several centimetres of wood were found at the base of this lithofacies. Density increases with grain size up to  $2.0 \text{ g/cm}^3$  and magnetic susceptibility decreases to  $1.0 \text{ SI} \cdot 10^{-5}$ .

**5:** Clastic rich, high density, laminated fine Silt

Very characteristic of this layer is the fine lamination of clastic fine silt. There is little or no organic matter in this section. The sediment is light grey/beige in color. Within the fine laminations there are a few millimetres sized grains, which can be seen well on the CT image in Figure 9.2. Note the high density (up to  $2.1 \text{ g/cm}^3$ ) and high magnetic susceptibility (up to  $7 \text{ SI} \cdot 10^{-5}$ ). After opening the core, the sediment was very dense and low in water.

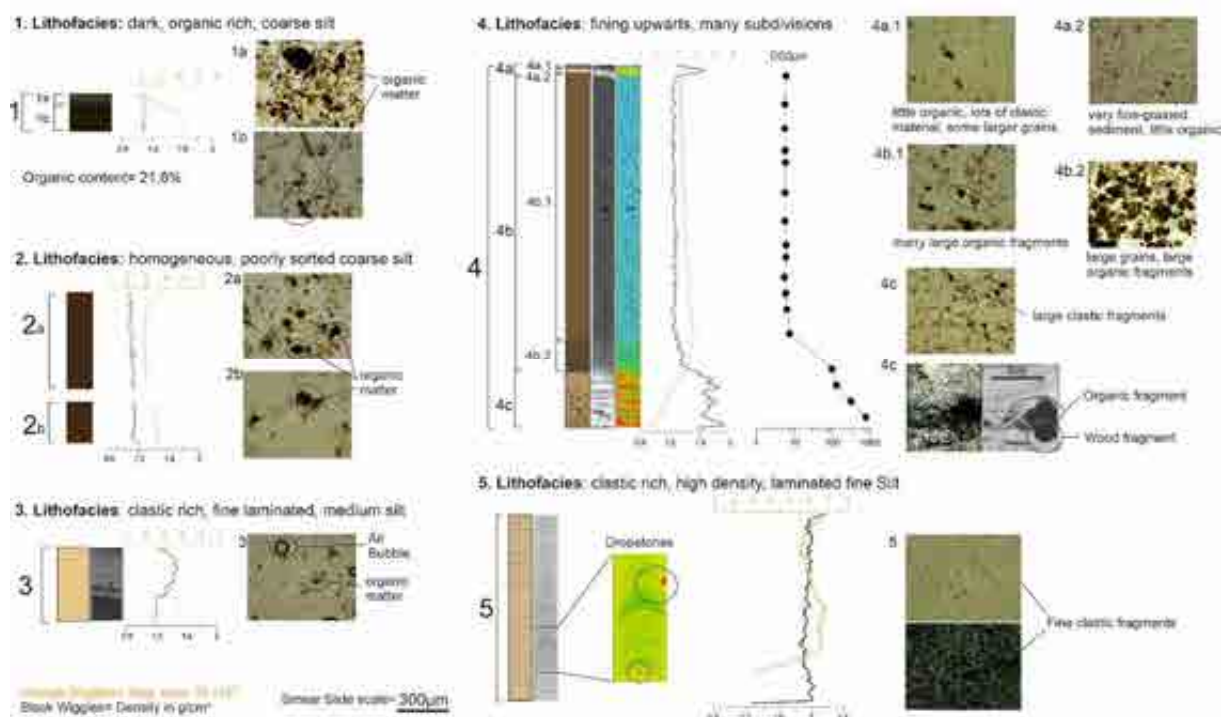


Figure 9.2: Shown are the five lithofacies that can be distinguished by different parameters. In each case the illustrated representation of the unit is shown, followed by the wiggle curves for magnetic susceptibility and density. Characteristic smear slides of each unit or subunit are also shown. For some lithologies, key elements are shown as CT images, also in different colors as for Units 3, 4 and 5, or a grain size curve for Unit 4.

#### 4.2.2. Sediment Core Correlation

All 22 short cores can be correlated with each other using both optical parameters and physical parameters, such as density and magnetic susceptibility. The sediment shows clear stratification within the cores, which can also be recognized in almost all of them. The individual lithologies differ in thickness from core to core, depending on the respective core location. Occasionally, an individual lithology may not be depicted in a core. Figure 10 shows eight sediment cores. One or two representative cores were selected from each area of the lake and visualized (Fig. 10). The cores were arranged so that they are presented from the west of the lake (plateau), across the deep basin, to the east of the lake (boulders and craters). An attempt was made to establish a correlation between the cores or a correlation of the lithofacies already identified in Chapter 4.2.1, "Lithologies and Event Deposit."

Almost all lithofacies can be found in all cores, with the exception of lithofacies 5. As already mentioned, this lithofacies type only occurs in core ALT20-15. It is also noticeable that the cores taken in the immediate vicinity of the crater contain only a few of the lithofacies. Only Lithofacies 3, 4a.1, 4a.2, 4b.1, 4b.2, and partially 4c can be recognized in the crater cores. These lithofacies are very conspicuous sediment patterns, which can also be found in the otherwise very different cores.

The sediments of the cores in the basin (ALT20-01, -02, -03, -04, -19), in the basin between the blocks (ALT20-16, -17, -18, -20), and on the blocks (ALT20-06 and -07) look particularly similar. However, the

cores in the plateau, near the slope, and near the craters differ greatly, both in terms of shape and thickness. The thicknesses vary at some locations, and the distribution of the individual lithofacies in the lake is discussed in the following chapter, 4.5 'Spatial Distribution of Sedimentary Units'. The possible reasons for the distribution are discussed in the interpretation of the data.

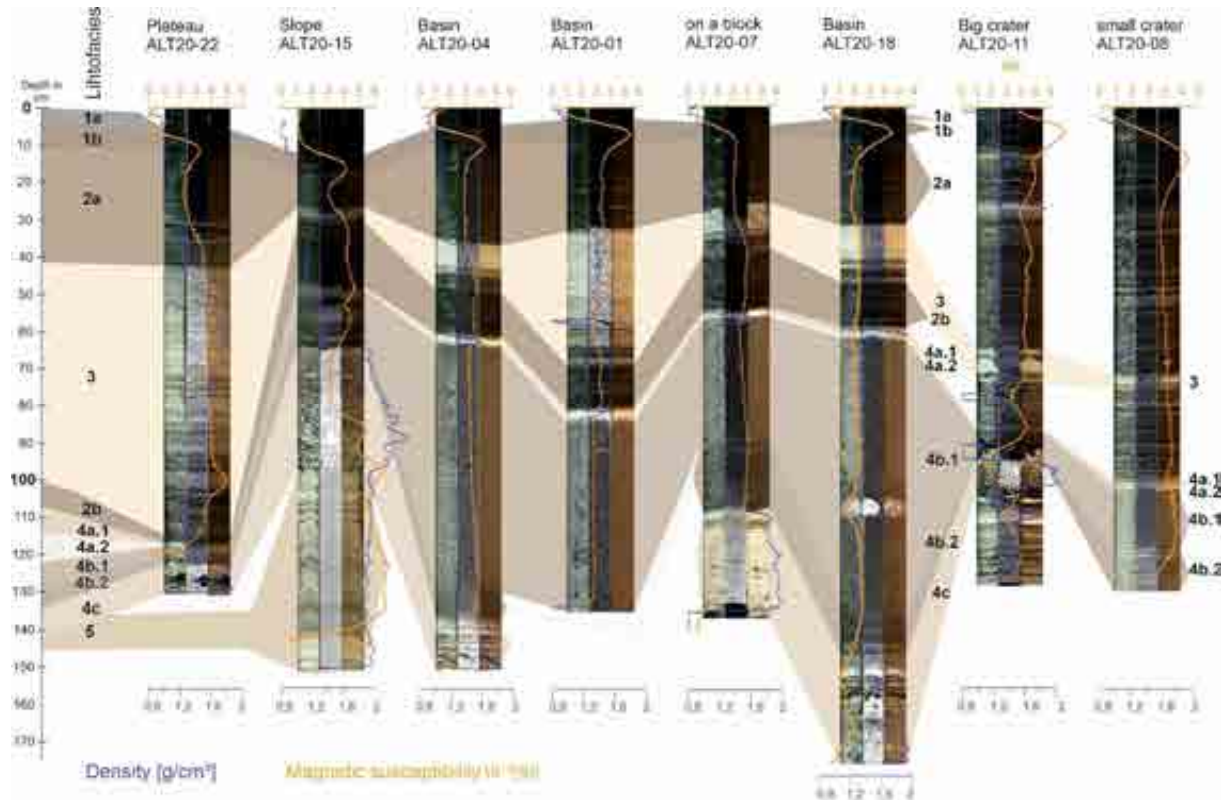


Figure 10: Lithofacies correlation for representative cores from west to east. Also shown are the magnetic susceptibility and density, which help to distinguish the lithofacies.

The cores that were taken close to the craters or within the craters (ALT20-08 to ALT20-12) are not discussed in this Thesis, as the sediment of these cores has already been extensively described and interpreted in the two bachelor theses mentioned above (Strachwitz, 2021 and Neuner, 2022).

### 4.2.3. Core to Seismic Correlation

The seismic profiles have been analysed, the sediment and its units have been described, and the cores have been correlated with each other. In this subchapter, an attempt will be made to correlate the sediment cores with the seismic data. Four seismic lines were selected, from which cores were also taken. The seismic lines and cores were chosen so that they cover the four important depositional environments of the lake: Figure 11.1 in the deep basin, Figure 11.2 on a block, Figure 11.3 on the slope, and Figure 11.4 on the plateau. The key factor in determining whether a lithofacies can be recognised or not is the difference in density/impedance and composition. Chapter 4.1 already described the seismic units, which can also be recognised here in the seismic lines.

Figure 11.1 shows a seismic line running from southwest to northeast across the lake. The core location of ALT20-02 is situated on this line, which passes through the deep basin. The lake floor is marked by the blue line, which also represents the top of the core. The section between the blue and orange lines appears light in the seismic profile, indicating a lower reflection amplitude. The sediment in this section is dark and has a low density. Lithofacies **1a**, **1b**, and **2a**, as defined earlier, are present in this section. A sharp change in both the seismic profile and the sediment core is marked by the orange line. The profile displays a more intense colored section, indicating a higher amplitude between the orange and the green lines. At this point, the sediment becomes lighter and denser, representing Lithofacies **3**. The green line indicates the next transition. The seismic profile and sediment core indicate that there is a significant change in density. There is a transition to a low amplitude section in the seismic profile. The sediment of Lithofacies **2b** corresponds to this interval and has a dark color and low density. The purple line denotes the transition from Seismic Facies 1 to Seismic Facies 2 from Chapter 4.1. The transition appears as a distinct boundary in the sediment, but in the seismic profile, it is a gradual transition to a lower amplitude. This marks the beginning of the lithofacies of Unit 4 in the sediment, which become denser and richer in gas towards the bottom.

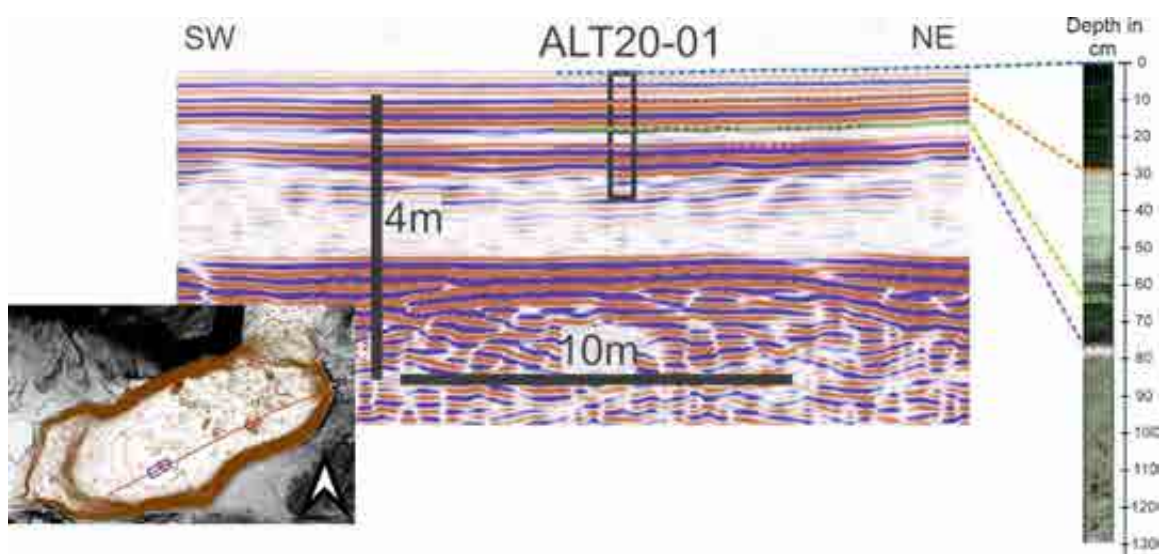


Figure 11.1: Part of a seismic profile line is compared with sediment core ALT20-01. The core is taken from the deep basin.

Figure 11.2 shows a seismic line running from south-west to north-east in the deep basin of the lake. Core ALT20-07 was taken along this seismic line, which can also be seen here in Figure 11.2. The core was taken from one of the largest blocks with sediment on it. The block is located in the eastern part of the deep basin. The blue line once again indicates the top of the core and the lake floor. The profile indicates that the area between the blue and orange lines is an area with less reflection, which would correspond to the first 22 cm of the sediment core. This is a dark sediment with low density and includes Lithofacies **1a**, **1b**, and **2a**.

Furthermore, the orange line marks the transition to an area of higher amplitude, which in the core corresponds to the transition to Lithofacies 3. The area between the green and violet lines in the profile marks a section with slightly less reflection amplitude. This could match Lithofacies **2b** in the core, as this unit is less dense and homogeneous. The violet line indicates the transition to Lithofacies **4a.1**, **4a.2**, **4b.1**, and **4b.2**, which become progressively denser towards the bottom. The fact that this area becomes lighter and lighter towards the bottom of the profile is probably due to the sediment in this area being very homogeneous and containing more gas. The black line marks the transition to Lithofacies **4c**, as the sediment is much coarser and denser.

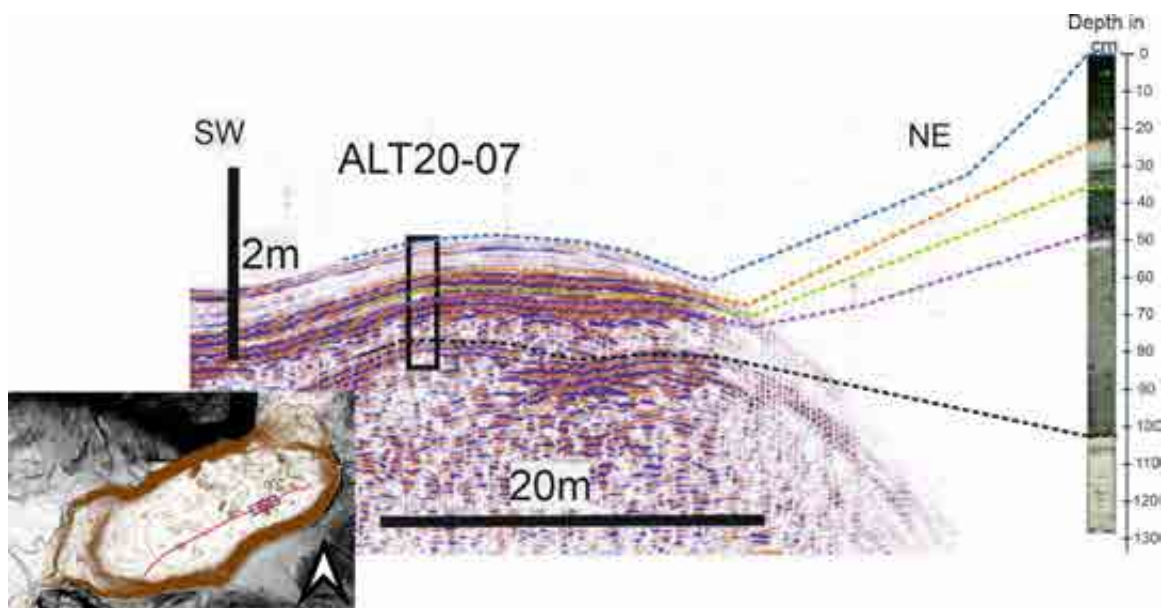


Figure 11.2: Part of a seismic profile line is compared with sediment core ALT20-07. This core was taken from sediment that was deposited on a block.

The seismic line in Figure 11.3 runs in a west-east direction and shows core ALT20-15 in the slope area. The blue line once again marks the top of the core and the lake floor in the seismic profile. The sediment core has a slightly different structure. The upper part of the core consists of dark sediment with a lower density. All units are present at the top of the structure in condensed thickness and therefore cannot be resolved in detail in the seismic survey, as an effect of topography. Thus, the area between the blue and violet lines probably contains the less dense and homogeneous units such as **1a**, **1b**, **2a**, **3** (only weakly pronounced – normally very dense and a strong reflector), and **2b**. This probably results in a brighter section in the seismic profile. The area between the violet and black lines is shown more intensively, with stronger reflection. This may correspond in essence to the section with the sub-units of Lithofacies **4**. The black line is then shown, and a layer boundary can be clearly recognised in the profile. This may correspond to the transition between Lithofacies **4c** and **5** in the sediment core, as these sediments also vary strongly in their composition and parameters.



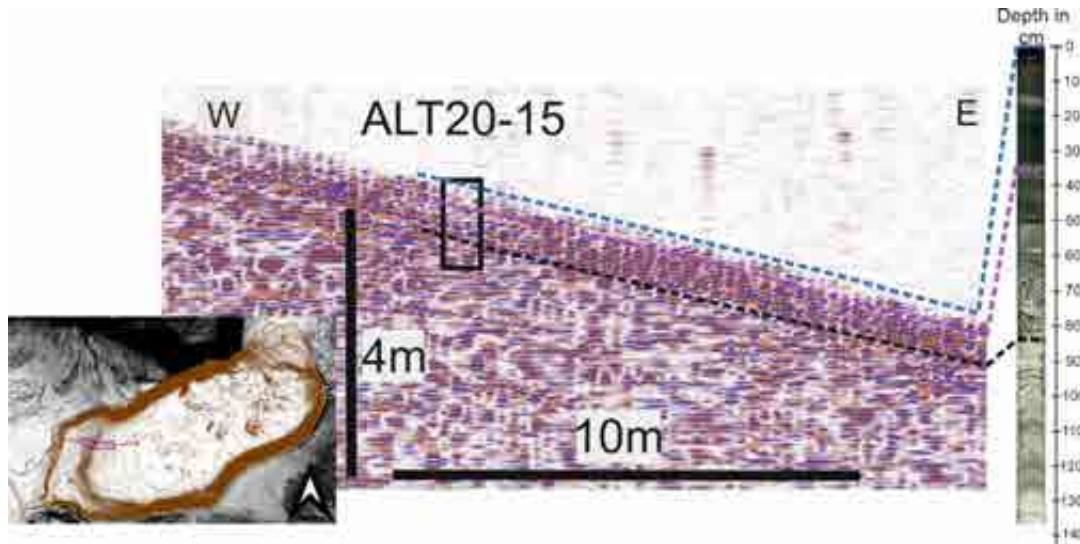


Figure 11.3: Part of a seismic profile line is compared with sediment core ALT20-15. The core was taken from a slope from the plateau to the deep basin.

Figure 11.4 shows a seismic profile in a west-east direction across the plateau in the west of the lake. The sediment core ALT20-13 was taken from this profile. The blue line once again marks the surface of the lake floor. As can be seen in the upper profiles, the area between the blue and orange lines is light-colored with low reflection. In the sediment core, this would correspond to a dark and less dense sediment unit. Lithofacies **1a**, **1b**, and **2b** are contained in this core section. Then, between the orange and green lines, there is a section of stronger reflection in the profile, which corresponds to the dense, laminated, and compressed sediment of Lithofacies **3** in the sediment core. Between the green and violet lines, there is another phase of weaker reflection, which again corresponds to the homogeneous and less dense sediment of Lithofacies **2b** in the core. Below the violet line, there is again a more intense reflection; the sub-units of Unit **4** would then follow.

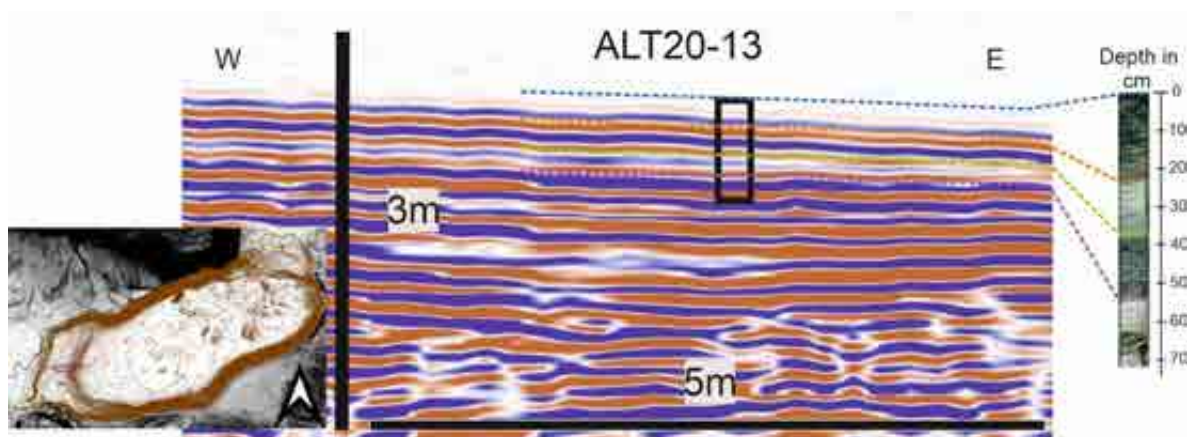


Figure 11.4: Part of a seismic profile line is compared with sediment core ALT20-13. This core was taken from the plateau in the west of the lake.

### 4.3. Grain size analysis of Event Deposit

The focus of the grain size analysis was primarily on Lithofacies **4** and its subdivisions. To briefly anticipate and make it easier to understand why the priority here is on Lithofacies **4**, we must note that this is an event layer. As described in the introduction, investigating the grain size of the event layer is an important aspect of this thesis. Lithofacies **4**, which consists of subsections **4a.1**, **4a.2**, **4b.1**, **4b.2**, and **4c**, is visualised here using three cores. The cores ALT20-07, ALT20-15, and ALT20-18 were selected as they were considered suitable for covering the entire Lithofacies **4** and recognising all sub-facies, which is not the case for all cores. Grain size analysis was conducted on these three cores.

Figure 12.1 visualises the grain size analysis of core ALT20-07, which was taken from the top of a block in the western lake area. Figure 12.1 shows a direct comparison of the sediment and the grain sizes between treated and untreated sediment. In this sediment core example, the individual fractions of Lithofacies **4** are clearly recognisable. The light-colored and dense facies **4a.1** and **4a.2** show a fine grain size spectrum in the untreated sediment. Unit **4a.2** displays the finest grain size of the sediment core and falls within the medium silt to fine silt range in the graphical representation. Treatment with  $H_2O_2$  results in a smoother peak for the fine grains. Unfortunately, there is no comparison of Lithofacies **4a.1** with the treated sediment, as this unit was deposited very thinly in the core, and there would not have been enough material for the  $H_2O_2$  treatment. Unit **4a.2** shows a slight shift into the finer grain spectrum after treatment with hydrogen peroxide. The sediment at the sample point in 59 cm core depth was classified as "medium silt" (with values  $D_{50} = 10.26 \mu m$ ;  $D_{90} = 64.77 \mu m$ ) before treatment and as "very fine silt" (with values  $D_{50} = 7.15 \mu m$ ;  $D_{90} = 38.70 \mu m$ ) after treatment with  $H_2O_2$ . This sediment classification comes from "Gradistat."

Lithofacies **4b.1** is very homogeneous and consistent in grain size, and is located in the medium silt spectrum. After treatment with hydrogen peroxide, a shift to the left is observed, indicating a somewhat finer spectrum now in the medium to fine silt range. For example, at the sample point at a core depth of 70 cm, the  $D_{50}$  value was  $23.68 \mu m$  and the  $D_{90}$  value  $233.8 \mu m$ ; after treatment with  $H_2O_2$ , the  $D_{50}$  value was  $7.47 \mu m$  and the  $D_{90}$  value  $43.97 \mu m$ . Another example is at the measuring point at 85 cm, where the values for  $D_{50} = 19.65 \mu m$  and  $D_{90} = 285.8 \mu m$ ; after treatment, the values were  $D_{50} = 7.07 \mu m$  and  $D_{90} = 34.32 \mu m$ .

The sediments in Lithofacies **4b.2** show a general increase in grain size (Fig. 12.1). Here, the line is no longer so consistent, which can be attributed to the onset of slight stratification, leading to an alternation of fine and coarser grains. This is clearly visible in the CT and ITRAX images. The grain size generally increases within this lithofacies. Sediments with grain sizes ranging from coarse silt to medium sand are found in this lithofacies. After the removal of organic material, a shift towards a finer grain size spectrum can be observed. The sediment now falls within the spectrum from fine to very coarse silt.



To give an example, at the core depth of 98 cm in Lithofacies **4b.2**, the grain size values before treatment were  $D_{50} = 65.99 \mu\text{m}$  and  $D_{90} = 495.4 \mu\text{m}$ ; after treatment, these became  $D_{50} = 12.55 \mu\text{m}$  and  $D_{90} = 98.76 \mu\text{m}$ . In the lower part of Lithofacies **4b.2**, there is a change, and the sediment spectrum shifts to a coarser range ( $D_{50} = 148.3 \mu\text{m}$  and  $D_{90} = 312.4 \mu\text{m}$  becomes  $D_{50} = 192.1 \mu\text{m}$  and  $D_{90} = 391.8 \mu\text{m}$ ). This shift is only observable in the last 2 cm.

At the transition to Lithofacies **4c**, a significant coarsening is visible. This sediment is very coarse, light-colored, and dense. This unit becomes coarser towards the base and lies in the middle sand range. The general trend that the sediment shifted to a finer spectrum after treatment ends at approximately 108 cm. Here, it can be observed that the sediment infill becomes coarser, and the treated sediments shift to a coarser spectrum. This does not mean that the sediment increases in grain size after treatment, but that the finer material has been dissolved, and the  $D_{50}$  or  $D_{90}$  line now falls within a coarser fraction on average. It was not possible to measure the entire Unit **4c**, as the grain size measurement on the Mastersizer 3000 is limited to 2 mm. Therefore, measurements were only taken up to a core depth of approximately 120 cm; anything below this would be larger than 2 mm.

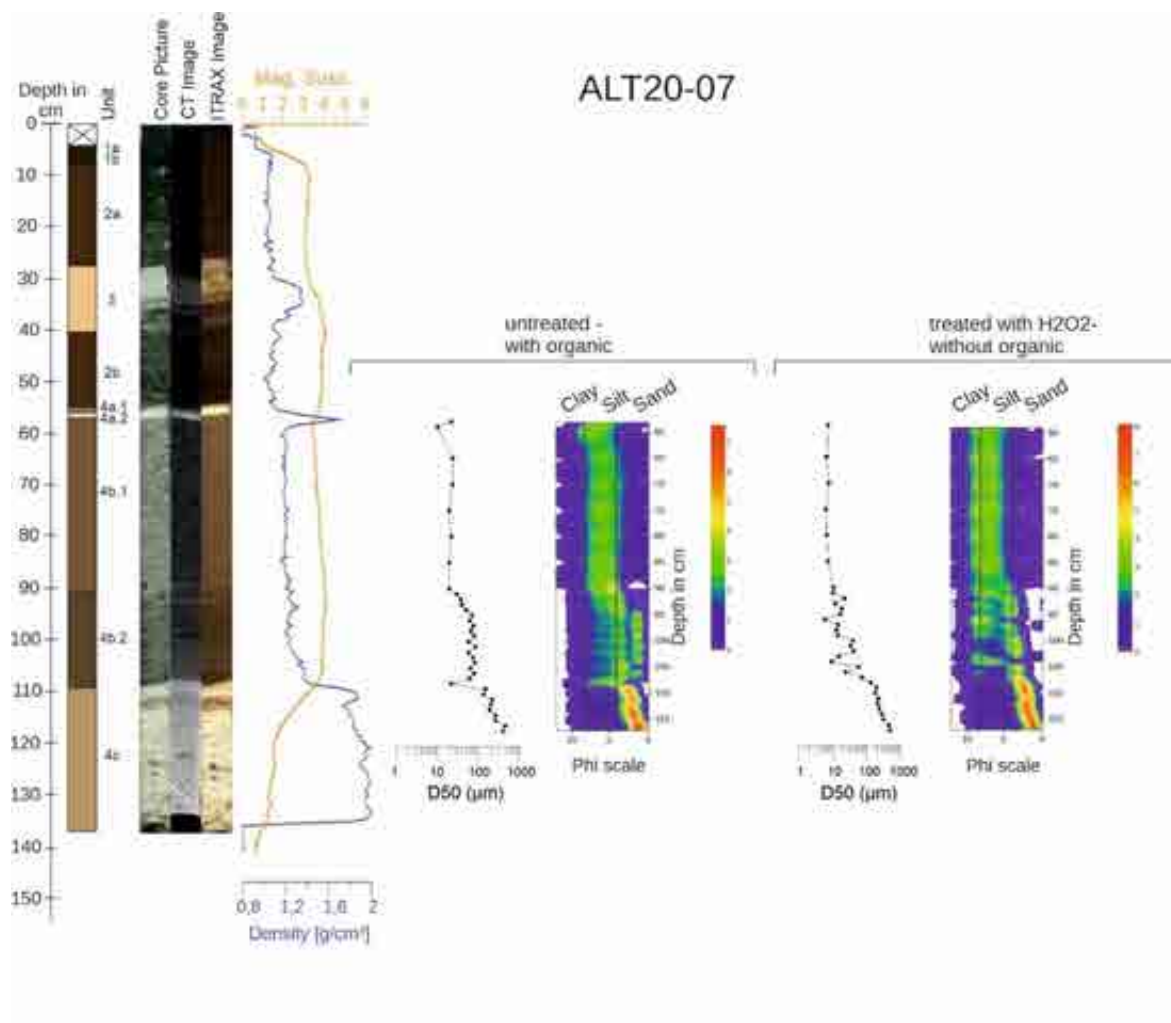


Figure 12.1: The grain size analysis of the ALT20-07 core is shown on the left: a false color image, a CT image and an ITRAX image of the core. Density and magnetic susceptibility are shown on the right. Further to the right is a grain size comparison

*between untreated and treated sediment. Core ALT20-07 was taken from the top of a block. Note that on the Phi scale, a small number (0) means a large grain size and a large number (10) means a very small grain size.*

Figure 12.2 shows the sediment core ALT20-15 visualised with the grain size distribution of Lithofacies **4**. This core was taken from the western part of the lake, on a slope between the plateau and the deep basin. The individual subdivisions of the lithofacies are not as clearly recognisable here as in cores ALT20-07 and ALT20-18. Lithofacies **4a.1** and **4a.2** are only very thinly developed in this core, which is evident in the images. Lithofacies **4a.1** is not shown in the grain size data, as it has a thickness of only 0.2 cm in this core. The first two samples in the upper part of the core are from Lithofacies **4a.2**. This unit is fine-grained and is described in the "Gradistat" programme as "fine sandy, medium silt." This designation changes to "very fine silt" after treatment. Expressed in values, for the sample taken at 48 cm, this change is as follows: Before: D50 = 17.68  $\mu\text{m}$ , D90 = 197.5  $\mu\text{m}$ ; After: D50 = 5.6  $\mu\text{m}$ , D90 = 23.8  $\mu\text{m}$ .

In Unit **4b.1**, the untreated sediment shows a sharp peak in the grain size curve. The reason for this could be that an exceptionally large fragment of material was detected during the measurement or that the laser beam measured an air bubble. The second reason is more likely, as it only occurred in one measurement. Unit **4b.1** is normally very homogeneous, but in this core, a soft, less dense, and darker sediment is present between 51 cm and 55 cm. This is followed by a fine stratification that usually only appears in Unit **4b.2**. The sediment shows a grain size that increases with depth, from medium silt to coarse silt, which can also be seen in the untreated sediment. Comparison is difficult here due to the anomaly.

In Lithofacies **4b.2**, the sediment becomes generally coarser, with grain sizes ranging from very fine sand to coarse silt. The differences between untreated and treated sediment at 60 cm are: Before: D50 = 44.59  $\mu\text{m}$  and D90 = 254.2  $\mu\text{m}$ ; After: D50 = 27.98  $\mu\text{m}$  and D90 = 108.9  $\mu\text{m}$ . The transition from Lithofacies **4b.2** to **4c** can be seen in the grain size curves (D50 in  $\mu\text{m}$ ) as a clear and steep increase. This transition is also clearly visible in the core images, as well as a sharp increase in the density curve. The grain size increases towards the bottom and moves from fine/medium sand to very coarse sand. Only a small difference between treated and untreated sediment can be recognised. For example, in the data at 70 cm, the curve shifted slightly to a finer spectrum after treatment. Before treatment, the values were: D50 = 479.4  $\mu\text{m}$  and D90 = 1002.1  $\mu\text{m}$ ; after treatment, D50 = 410  $\mu\text{m}$  and D90 = 882.2  $\mu\text{m}$ . The sediment could only be measured up to a core depth of 72 cm, where the sediment exceeds the grain size that can no longer be measured by the Mastersizer. The coarsest clasts in the sediment have a maximum size of 4.5 cm.

Even though the cores, and therefore the sediment, are very different from the previous core, it can be clearly seen that the grain size curves (D50 in  $\mu\text{m}$ ) exhibit a similar pattern.

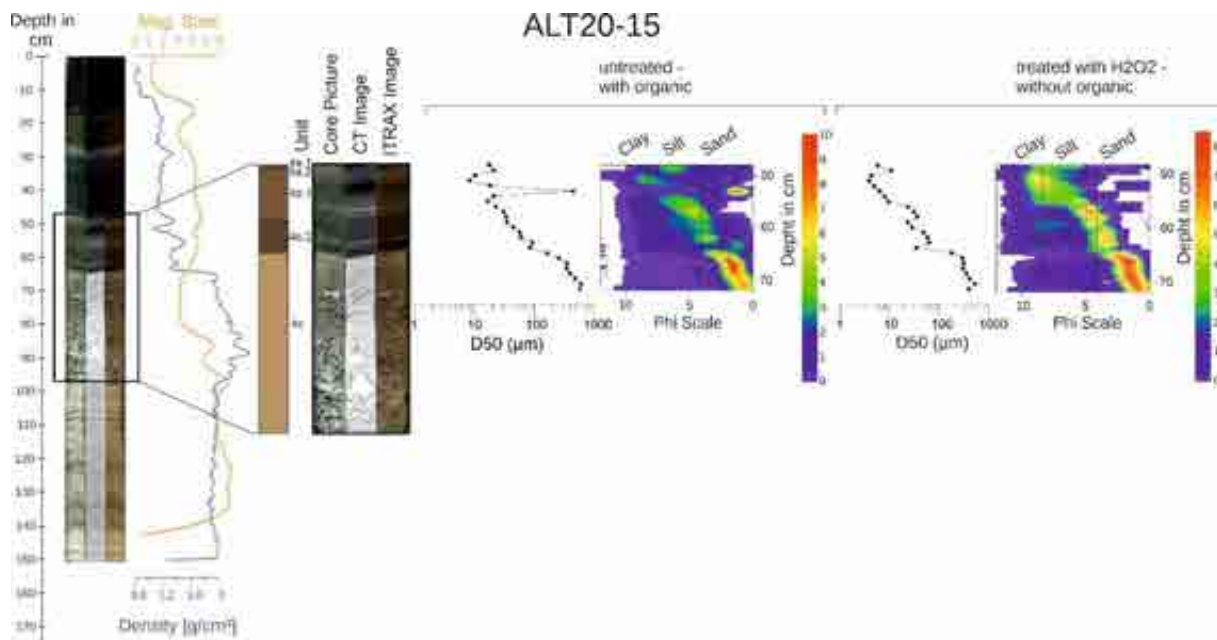


Figure 12.2: The grain size analysis of the ALT20-15 core is shown with a false color image, a CT image and an ITRAX image of the core on the left. Density and magnetic susceptibility are shown on the right. A close-up of Lithofacies 4 is shown. Further to the right is a grain size comparison between untreated and treated sediment. Core ALT20-15 was taken from the western slope. Note that on the Phi scale a small number (0) indicates a large grain size and a large number (10) indicates a very small grain size.

The sediment core ALT20-18 is visualised in Figure 12.3. A comparison of grain size between treated and untreated sediment is also shown. This sediment core was taken from the basin between the blocks in the south-eastern part of the lake. In this core, all the lithofacies units are very well exposed. As can be seen in Figure 12.3, Lithofacies **4a.1** has a grain size of coarse silt. This is the first time that it has been possible to take enough material from **4a.1** and treat it with H<sub>2</sub>O<sub>2</sub>. It was observed that the grain size curve shifted to a slightly coarser spectrum. Expressed in numbers, for Lithofacies **4a.1** before treatment: D50 = 13.53 µm and D90 = 58.94 µm, and after treatment: D50 = 19.68 µm and D90 = 92.93 µm.

Lithofacies **4a.2** is finer-grained than Lithofacies **4a.1**, which is clearly visible in the grain size spectrum of the untreated sediment. Here, the grain size is in the fine silt range. However, when the sediment is compared with the H<sub>2</sub>O<sub>2</sub>-treated sediment, it shifted to the finer spectrum after treatment. This small difference for **4a.2** is barely recognisable in the graphic illustration.

The homogeneous sediments of Lithofacies **4b.1** are all in the medium silt range of the grain size spectrum before the treatment. However, the same samples treated with hydrogen peroxide are all in the fine silt range, so they have all shifted slightly to the left. To give an example of the shift in Figures, at a core depth of 102 cm: before treatment D50 = 17.31 µm and D90 = 147.6 µm; after treatment: D50 = 5.6 µm and D90 = 24.17 µm. This difference can be clearly seen graphically.

In the middle of **4b.1**, there is a very prominent sand lens (medium sand) which has a higher density than the rest. A clear coarsening can be seen in the D50 (µm) line and also in the grain size distribution map. This observation also holds for the H<sub>2</sub>O<sub>2</sub>-treated sediment; here the data shows that it has only

become slightly finer after treatment. At a depth of approximately 136 cm, a change in the sediments can be seen. The colour becomes darker, the density increases, and the grain size becomes larger. This point also marks the transition from Lithofacies **4b.1** to **4b.2**. The sediment is laminated and shows greater fluctuations in grain size because some layers of the stratification have coarser and finer grains. Lithofacies **4b.2** shows a big difference between treated and untreated sediment, both graphically and in the data. At a depth of 140.5 cm, this lithofacies was sampled and showed a difference: before treatment: D50 = 52.73  $\mu\text{m}$  and D90 = 473.4  $\mu\text{m}$ ; after treatment: the sediment showed values of: D50 = 15.50  $\mu\text{m}$  and D90 = 92.92  $\mu\text{m}$ .

Lithofacies **4c** also shows an increase in grain size with depth. It can be seen that the sediment is finely layered at the beginning and then changes to a massive form with very large components, which tends to become coarser towards the bottom. The fine layers at the beginning of Lithofacies **4c** are very variable in grain size, which is recognisable in the grain size spectrum and in the density curve. Clasts of finer sediment can be found between the rock clasts, such as at a depth of 162 cm. This finer material can be seen in the graphical representation, in the grain size curve, and also in the density curve. The grain size range goes from medium-grained silt to very coarse sand. The bottom ~5 cm of the sediment core could not be measured with the Mastersizer as the sediment exceeds the permissible grain size (> 2 mm). The sediment of Lithofacies **4c** generally shows a slight shift in the spectrum after treatment with  $\text{H}_2\text{O}_2$ . In the graphical illustration, the differences are only slightly recognisable. The data show a change from D50 = 112.6  $\mu\text{m}$  and D90 = 610.8  $\mu\text{m}$  to D50 = 124  $\mu\text{m}$  and D90 = 289.7  $\mu\text{m}$ .

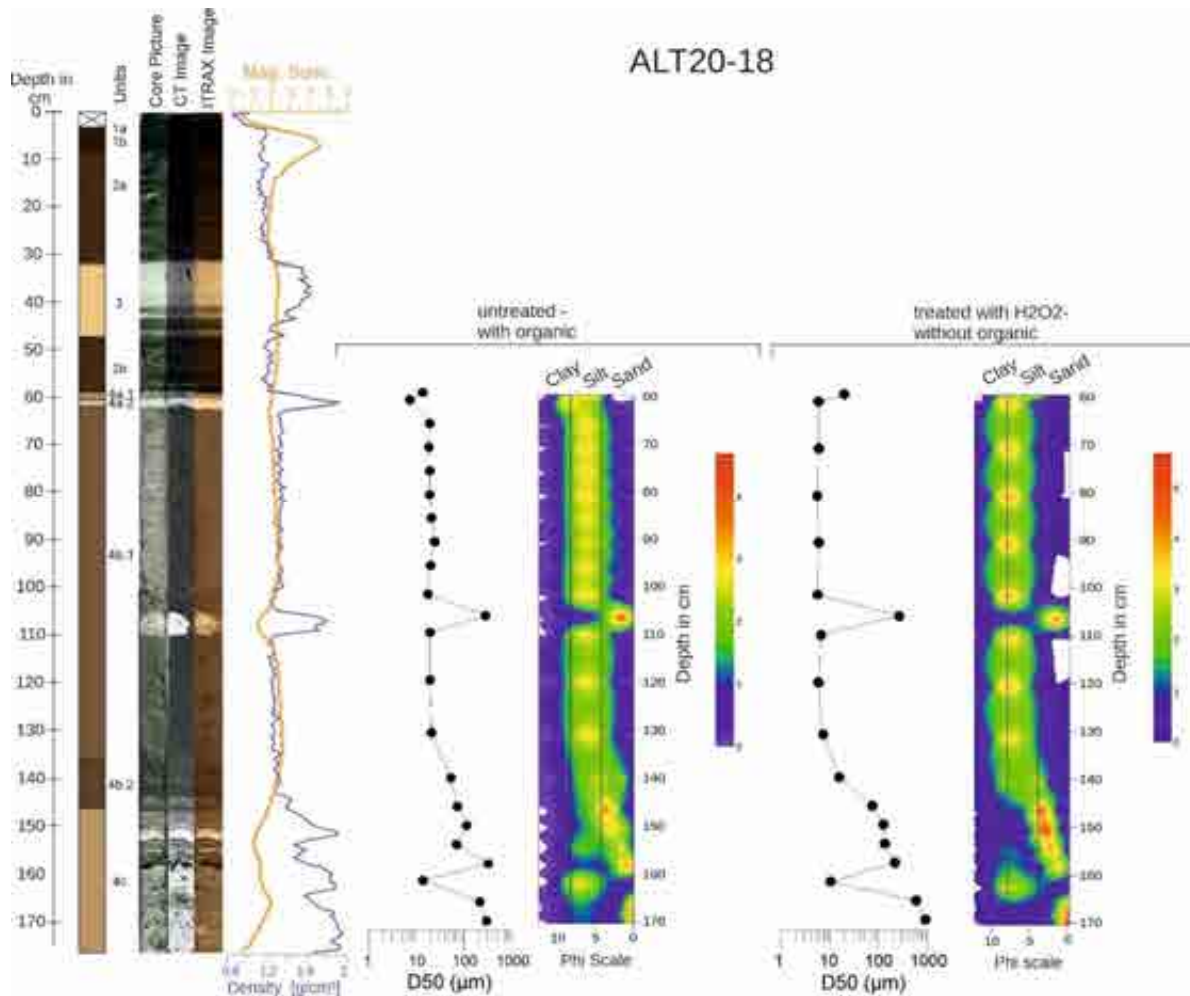


Figure 12.3: The grain size analysis of the ALT20-18 core is shown on the left: a false color image, a CT image and an ITRAX image of the core. Density and magnetic susceptibility are shown on the right. Further to the right is a grain size comparison between untreated and treated sediment. The ALT20-18 core was taken from the deep basin between the blocks. Note that on the Phi scale a small number (0) indicates a large grain size and a large number (10) indicates a very small grain size.

It can be observed that in most cases the sediment has shifted slightly to a finer grainsize spectrum after treatment with hydrogen peroxide. It can be observed that the D90 values show greater differences before and after treatment than the D50 values. However, there is also the case that the sediment shifted to a coarser spectrum after treatment. The biggest differences between treated and untreated occurred in Lithofacies **4b.1**, this also were the samples with the strongest response to H<sub>2</sub>O<sub>2</sub>. This is illustrated in Figure 13, where the D50 (μm) lines for both treated and untreated sediment overlap (A.3.4.). The influence of the H<sub>2</sub>O<sub>2</sub> becomes clear. The changes can also be seen microscopically in the sediment itself. The organic pieces became less after treatment and in some cases organic clusters were separated or large organic fragments were reduced in size. Which can influence the shift of the grain size curve. For **4b.1** in particular, a clear difference can be seen in the organic content and organic size after treatment. When looking at the images for **4c**, the reason for a coarser particle size curve can also be recognized. The organic particles are smaller than the clastic components. Once these have been removed, a larger proportion of large particles remains, resulting in a coarser spectrum.

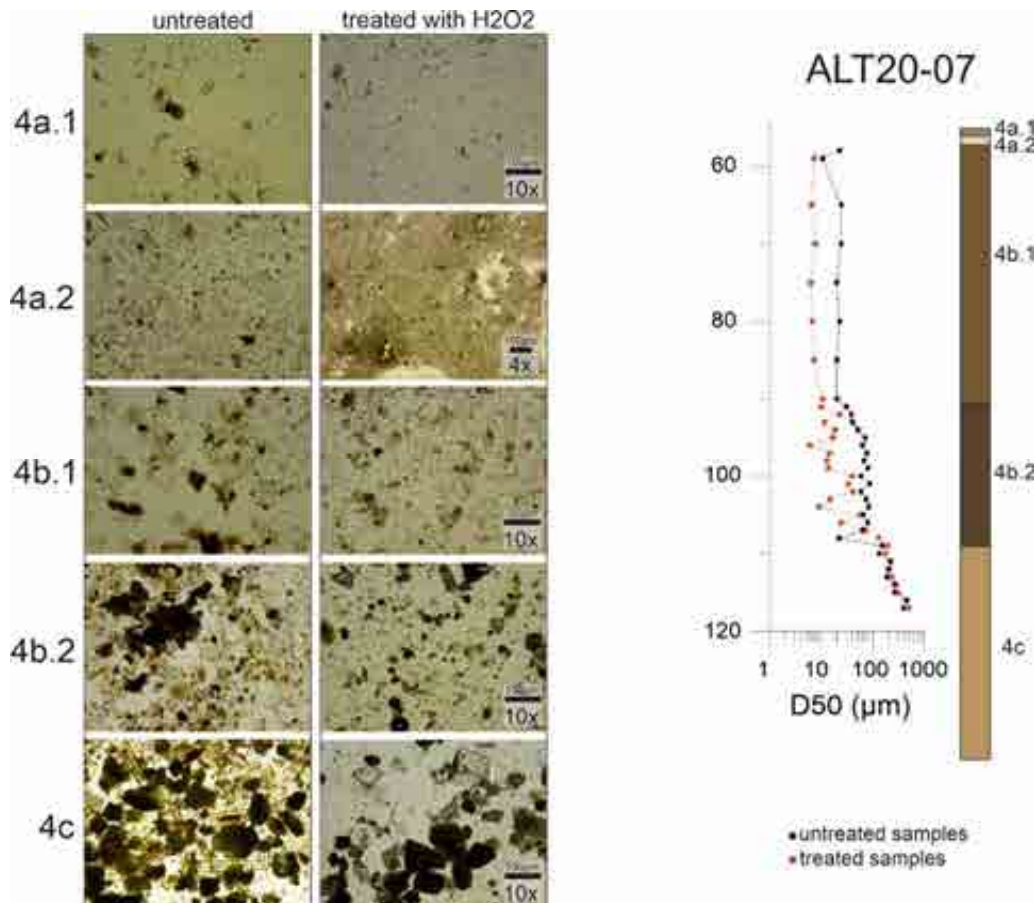


Figure 13: Smear slides from untreated and treated sediments are shown. The exact details of which core and depth the respective smear slide originates from can be found in the Appendix A.3.3. Average grain size (D50 & D90 in  $\mu\text{m}$ ) and organic content (in %) of the lithofacies from the untreated sediment.

#### 4.4. Organic Content

The organic content of the sediment is an important aspect. As described in the previous section, organic matter was removed to allow a more accurate measurement of sediment grain size. During the treatment of the sediment, it was found that some sections of the core reacted more strongly to the addition of hydrogen peroxide than others. Therefore, the question of how much organic matter is present in the sediment needed to be clarified. The percentage of organic matter was measured once for each lithofacies unit. Core ALT20-06 was used for the Loss On Ignition (LOI) measurements. This core was taken on top of a block. It was chosen because the core had not been sampled before, and the majority of the lithofacies units are present. As can be seen in Table A.3.1. the last sample in the list was taken from core ALT20-13 and comes from Lithofacies **4c**. This lithofacies is missing from core ALT20-06. The measurement was carried out using the LOI method, and the exact procedure is described in Chapter 3.2.6.

The samples were taken from core ALT20-06 (except the sample of Lithofacies **4c**, which comes from core ALT20-13), the table with the samples can be found in the Appendix A.3.1. Additionally, a



comparison is made with the neighbouring Core ALT20-07, and the core locations in the lake are marked.

As Figure 14 shows, the distribution of the organic content varies greatly within the core. The uppermost Lithofacies **1a**, also contains the largest proportion of organics with 21.64%. This unit is also the darkest unit of the core. The underlying Lithofacies **1b**, which also has a dark sediment color, contains 19.05% organic matter. The organic content then decreases to about 14% in the course of Lithofacies **2a**, which also roughly correlates with the color gradient (getting lighter). Lithofacies **3** has a very low organic content of 3-5%. The organic content increases sharply again in the underlying Lithofacies **2b**, where it ranges from 12.95% to 15.13%. Lithofacies **4a.1** could not be measured here, as its thickness would have been too thin to obtain the required sample quantity. The organic content drops sharply again in Unit **4a.2** to 3.54%. At the beginning of Lithofacies **4b.1**, the organic content is elevated at 9.95–10.49% and decreases within the unit. This decreasing trend continues continuously until the end of Unit **4b.2**. Further into Unit **4c**, the content decreases further to 3.24%.

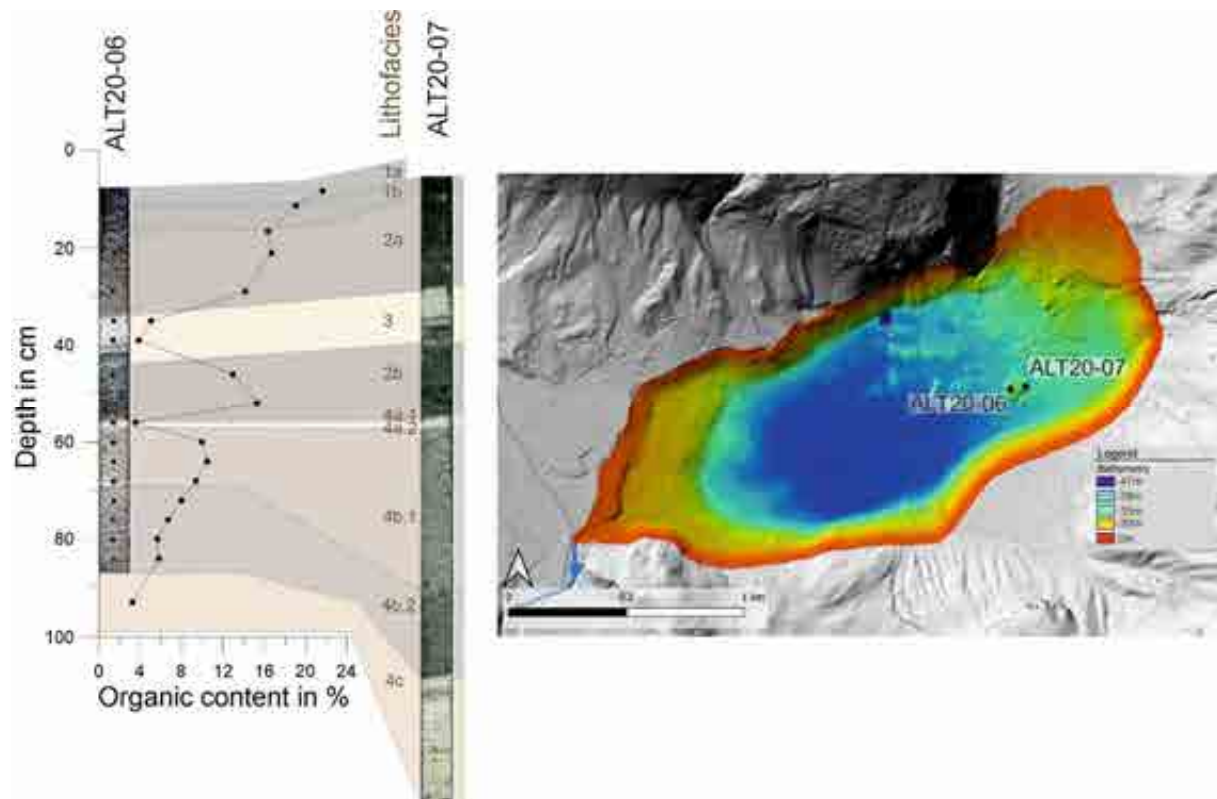


Figure 14: Core ALT20-06 is visualised with the sampling points of the material. The measurement of the Lithofacies 4c was done on core ALT20-13. The organic distribution curve of the organic content in per cent. Shown is a direct comparison with core ALT20-07, which is the neighbouring core. Also, a visualisation of these two cores in Lake Altaussee.

In summary, it can be said that the organic content is mostly correlated with the color. Dark-colored sediments have a high percentage of organic matter, whereas light-colored sediments have a lower percentage of organic content. However, there is an unexpected exception. Within Lithofacies **4b.1** and **4b.2**, the color becomes darker towards the bottom, but the organic content decreases sharply. It

was also noticeable that the sediments in Unit **4b.1** reacted most strongly when the samples were treated with hydrogen peroxide, although they do not have the highest organic content.

## 4.5. Spatial distribution of sedimentary Units

In this subchapter, the thickness distribution of the individual lithofacies across the lake is visualised and discussed. It is important to mention the following points right at the beginning for a better understanding:

- Not all cores contain all lithofacies or have preserved them.
- Not all cores extend to lithofacies 4c; this core method is limited to a length of 1.70 metres. It is possible that the last lithofacies in the core is Unit **4b.1**. However, this does not mean that only sediment up to **4b.1** was deposited. It means that this depth was not reached during coring process.
- Core ALT20-09 is a crater core that was only filled with homogeneous fine/medium grained sand; therefore, it does not show any of the lithologies and is not shown in the following maps.
- Core ALT20-21 does not appear on this map as it was not used for this study. This core was taken for testing purposes only.
- Core ALT20-05 has a question mark in the maps (Fig. 15.2.) of Lithofacies **4a.1**, **4a.2**, **4b.1**, **4b.2** and **4c**, which means that the units are present but cannot be measured in cm. As these units are damaged, this was probably caused during core removal.

Figure 15.1 visualises Lithofacies **1a** to **3** and Figure 15.2 Lithofacies **4a.1** to **4c**. These were only visualised separately for reasons of space. The size of the circles represents the thickness of the respective lithofacies at the core location.

Lithofacies 1a: In the legend of the corresponding Figure for Lithofacies **1a**, it can be seen that it is a generally thin unit. The maximum occurring thickness is 3 cm. This lithofacies occurs in almost every core, except in the crater cores ALT20-08, ALT20-09 and ALT20-10. The greatest thickness of this lithofacies is found in the cores on the plateau and on the slope. It is less thick, however, in the deep basin area.

Lithofacies 1b: This unit is also present in small thicknesses and is at its maximum 9 cm thick. As can be seen in the Figure 15.1, this lithofacies is somewhat more pronounced in the north-east of the lake. Throughout the rest of the lake this unit is relatively constant, with no major variations in distribution across the basin, slope and plateau. This lithofacies is present in nearly all cores, except again in crater cores ALT20-08, ALT20-09 and ALT20-10.



Lithofacies 2a: As can be seen in Figure 15.1, this unit can be found in almost all cores, except in core ALT20-21 and crater cores ALT20-09, ALT20-10 and ALT20-12. This lithofacies is much thicker in the basin than in the plateau or slope. This unit is particularly thick in the northern part of the basin and around the crater slope. This lithofacies reaches a maximum thickness of up to 60 cm.

Lithofacies 3: This lithofacies is clearly recognisable in every core, the light-colored sediment is prominent in all cores. The sediment of this unit has a maximum thickness of 60.5 cm. The thicker deposits lie in a line across the lake, starting in the southern plateau area and extending into the south-western area of the blocky basin (Fig. 15.1). The thickest deposits are located in the southern plateau area. In the northern part of the plateau, the sediment is only thinly developed. In the deep basin of the lake, the sediments of this lithofacies are also clearly pronounced. From here onwards, the thickness decreases more and more towards the west. Lithofacies 3 is therefore most pronounced in the south-western area of the lake.

Lithofacies 2b: In the case of this lithofacies, too, it is represented in every core, as can be seen in Figure 15.1. It is clearly pronounced on the plateau, more so in the northern area. Furthermore, in the north-eastern area of the basin. The maximum extent of this unit is 24.2 cm.

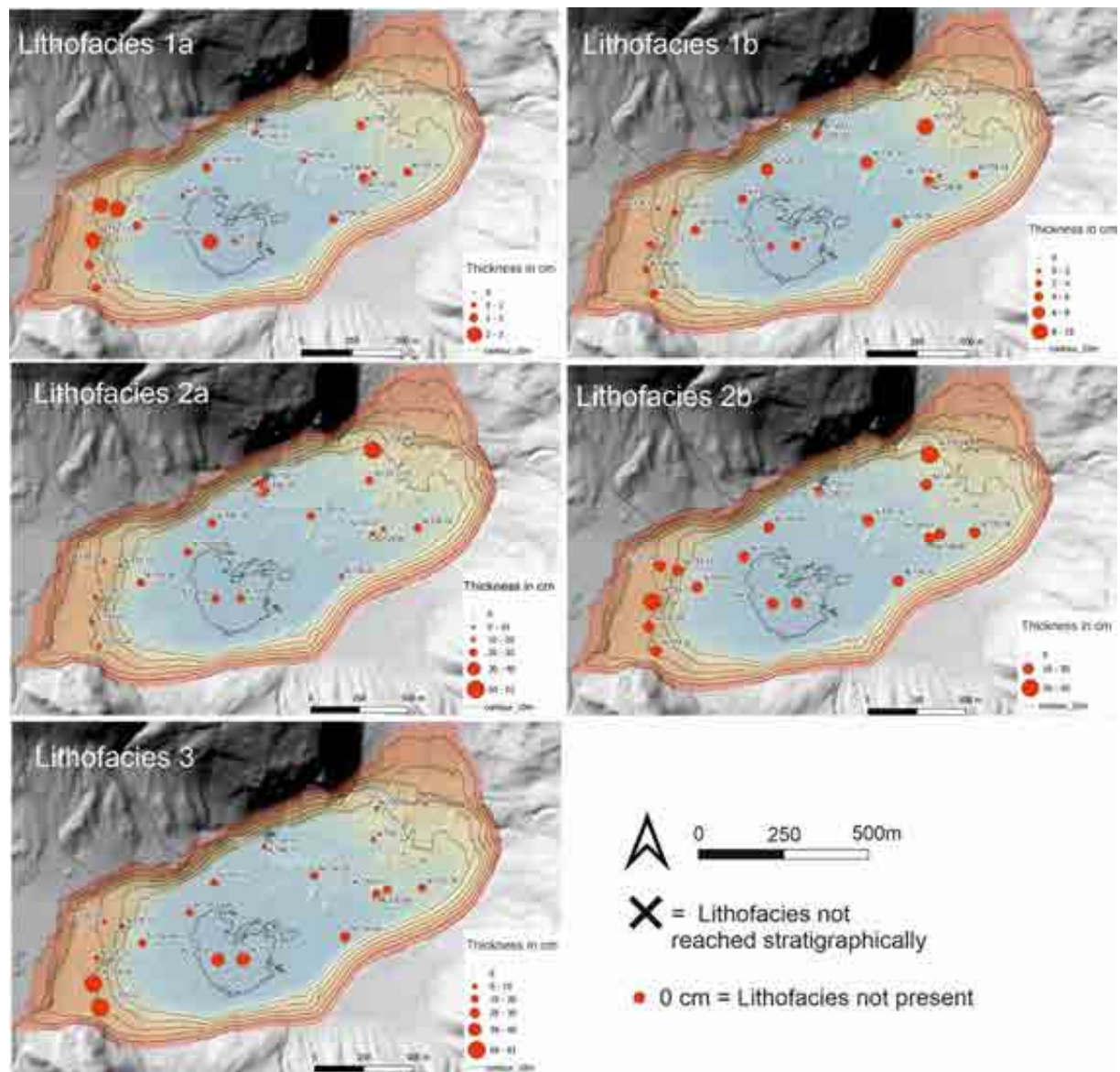


Figure 15.1: The thickness distribution of Lithofacies 1a to Lithofacies 3 across the lake is visualised. The larger the red circle at the respective core location, the thicker the respective lithofacies is at this core location in the lake. There is a separate Figure for each lithofacies. Each Figure contains a legend in which the exact thicknesses are given in cm.

**Lithofacies 4a.1:** Lithofacies **4a.1** is a very thin unit with a maximum thickness of 2.3 cm. This fine lithofacies is not preserved in every core. In particular, it is not found in the crater cores of the largest crater. At first view, there is no recognisable structure in the distribution.

**Lithofacies 4a.2:** This lithofacies is also a very thin sedimentary unit. With a maximum thickness of 3.3 cm. It can be found in almost every core, with small exceptions in craters and on the plateau. As can be seen in Figure 15.2 the thickness distribution of this lithofacies varies within the lake. Roughly two places can be recognised where the thickness is increased. This can be seen in the north-western part on the plateau of the lake and in the western part of the basin.

**Lithofacies 4b.1:** This lithofacies has a maximum thickness of 77.2c m within the short cores. The actual thickness of the lithofacies may be much thicker as the short cores do not reach the end of the

lithofacies at all points. On the basis of the short cores and their thickness distribution in Figure 15.2 it can be said that this lithofacies is thicker in the basin than on the slope or plateau. In the deepest part of the basin, the cores unfortunately do not reach the end of this unit but would be even thicker there. As already mentioned, further research is being carried out on the sediments of Lake Altaussee and long cores were taken as part of a PhD thesis. These reach a much greater depth than the short cores taken for this work. It was found that the Lithofacies **4b.1** in the deep basin, approximately at the same location of core ALT20-02 (long core 1002-1-A), has a maximum thickness of about 140 cm. Which is a big difference in thickness from what has been seen so far in the short cores.

Lithofacies 4b.2: As can be seen in the Figure 15.2 this unit can only be found in a few cores. This is not because this unit was not deposited at these locations, but because this deep-seated lithofacies was not captured during coring. It can therefore be assumed here that if the core were longer or had penetrated deeper into the sediment, this unit could be seen in the core. This mainly applies to the cores in the deep basin. The situation is different in the plateau/slope area, where this unit was probably not deposited or only so fine that it is not recognisable. Some cores end within this lithofacies, so it is not completely mapped in the core. This means that the lithofacies would be even thicker. It is therefore difficult to make a statement about the distribution, as it can only be seen in very few cores. The lithofacies in Figure 15.2 is 18 cm thick at its maximum thickness, which is located in the eastern and north-western part of the lake. Here too, as with Lithofacies **4b.1**, a look was taken at the long core 1002-1-A. There it can be seen that in the deep basin, the sediment of Lithofacies **4b.2** has a thickness of approximately 60 cm, which does not deviate greatly from that already seen in the short cores.

Lithofacies 4c: The thickness or distribution of this lithofacies cannot be described on the basis of the short cores. As the full lithofacies can only be recognised in its entirety in one core (ALT20-15). In the other cores in which it can be found, this lithofacies cannot be seen to the full end. So, there is no total thickness of this lithofacies to be seen.

Lithofacies 5: Lithofacies **5** is not shown here because it is only visible in core ALT20-15 and not all the way to the end. The core is located in the eastern part of the lake on the slope from the plateau to the deep basin. Therefore, in the case of Lithofacies **5**, no statement can be made about its distribution in the lake on the basis of short cores.

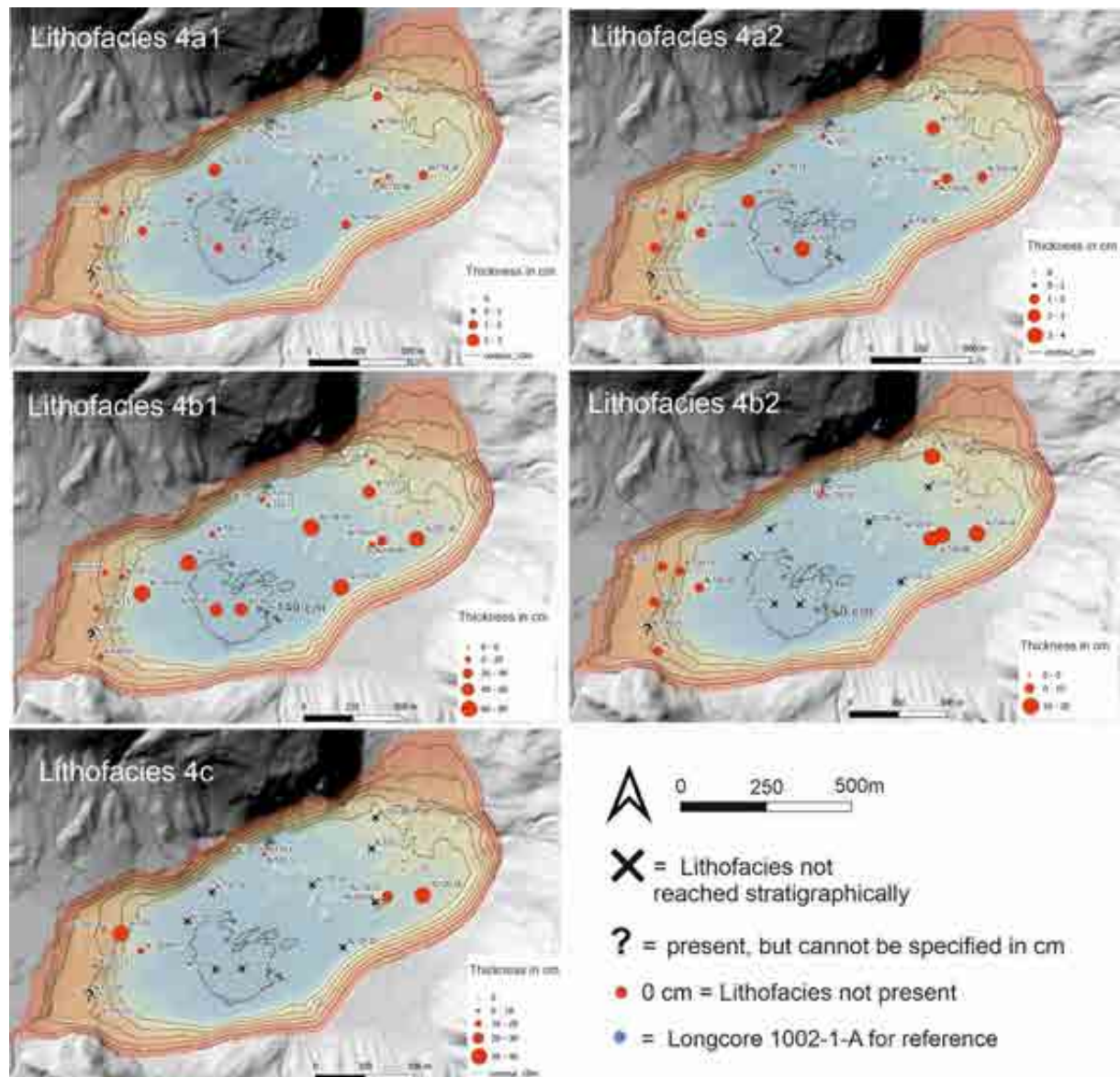


Figure 15.2: The thickness distribution of Lithofacies 4a.1 to Lithofacies 4c across the lake is visualised. The larger the red circle at the respective core location, the thicker the respective lithofacies is at this core location in the lake. There is a separate Figure for each lithofacies. Each Figure contains a legend in which the specific thicknesses are indicated in cm.

To summarise, it can be said that an analysis of the sediment distribution in the lake is only possible to a limited extent. As already mentioned at the beginning of this subchapter, not all lithofacies can always be recognised in all cores, as the cores vary in length and are limited to 1.70 m. This makes it difficult to interpret the spatial distribution of Lithofacies **4a.1**, **4a.2**, **4b.1**, **4b.2**, **4c** and **5**. It may be the case that the respective lithofacies was not deposited at the core location or that it was not captured by the end of the core liner.

#### 4.6. Dating and Age Model

The sediments were sampled and radiocarbon dated to place them in chronological order. Organic material was extracted and dated. This was taken from what is known as 'background' sediment, which is continuously deposited sediment. It is important not to sample sediment that has been deposited

as an event layer. Such sediment could give a false age, as the sediment could be mixed. Sediment that has already been deposited could be resuspended and redeposited, or organic remains that have been outside the lake for some time could be transported into the lake by an event. This considerably limits the choice of possible sampling sites. Three sites were therefore selected for sampling and found to be appropriate. These are in core ALT20-02 at 26.5-27 cm, 66.5-67 cm, and at 80-82 cm (Table 1).

The dated age of the sediment can be entered into the Bacon program along with other information, such as event locations or other anomalies that may influence the age. A sedimentary/section boundary was entered at 28 cm, and an event boundary at 67 cm. A boundary is defined where there are clear changes in the sediment, which likely indicate a shift in sediment dynamics. This provides additional information that the program itself cannot detect but which can enhance the age model. This results in the age curve shown in Figure 16. This age-depth model provides a high-resolution age for the core. The calculated curve provides information about the sedimentation rate and its changes. The steeper the calculated curve, the higher the sedimentation rate. The three samples are shown in blue in the figure. The wider the blue line, the greater the potential error in the measurement. The following ages are given for the samples:

*Table 1: The table with the ages of the three samples used for the age model of the ALT20-02 core is shown. Used for the age-depth-model was the IntCal20-calibrations curve (Reimer et al., 2020).*

Lab number	Sample ID	C14 age BP	$\pm 1\sigma$	min. age BP	max. age BP
111039	ALT20-02_26,5-27cm	591	22	645	543
111038	ALT20-02_66,5-67cm	842	22	783	689
111037	ALT20-02_80cm-82cm	1178	60	1267	957

In Figure 16, it can be observed that there are four different sections of sedimentation. The first section, which starts at 0 cm and goes up to 24 cm, contains Lithofacies **1a**, **1b**, and **2a**. The calculated age of this section is between (mean) -70 ( $\pm 3$  years) cal BP and 581 ( $\pm 65$  years) cal BP. The average sedimentation rate in this section is about 0.0365 cm/year.

The second section, ranging from 24 cm to 64 cm, contains Lithofacies **3**. In time, this section spans from (mean age) 581 ( $\pm 65$  years) cal BP to 769 ( $\pm 60$  years) cal BP. The sedimentation rate within this time span is approximately 0.322 cm/year. This is almost ten times the sedimentation rate in the previous section.

In the section below, from 64 cm to 80 cm, is Lithofacies **2b**. It is dated (mean age) from 769 ( $\pm 60$  years) cal BP to 1129 ( $\pm 99$  years) cal BP. The approximate sedimentation rate in this section is 0.0387 cm/year. This is again similar to the sedimentation rate in the first section. This is also consistent with the steepness of the two sedimentation curves.



The fourth and lowest section in this core ranges from 80 cm to 130 cm. It contains Lithofacies **4a.1**, **4a.2**, and **4b.1**. If Lithofacies 4b.2 and 4c were present in this core, they would also be included here. This section contains the mean age from 1129 ( $\pm 99$  years) cal BP. As the program was first instructed that the section covering Lithofacies **4c** to **4a.1** is an assumed event deposit, Bacon calculates a vertical line for the sedimentation rate inside the event. This demonstrates that the material from this section was deposited in a very short period of time, probably within hours or a few days.

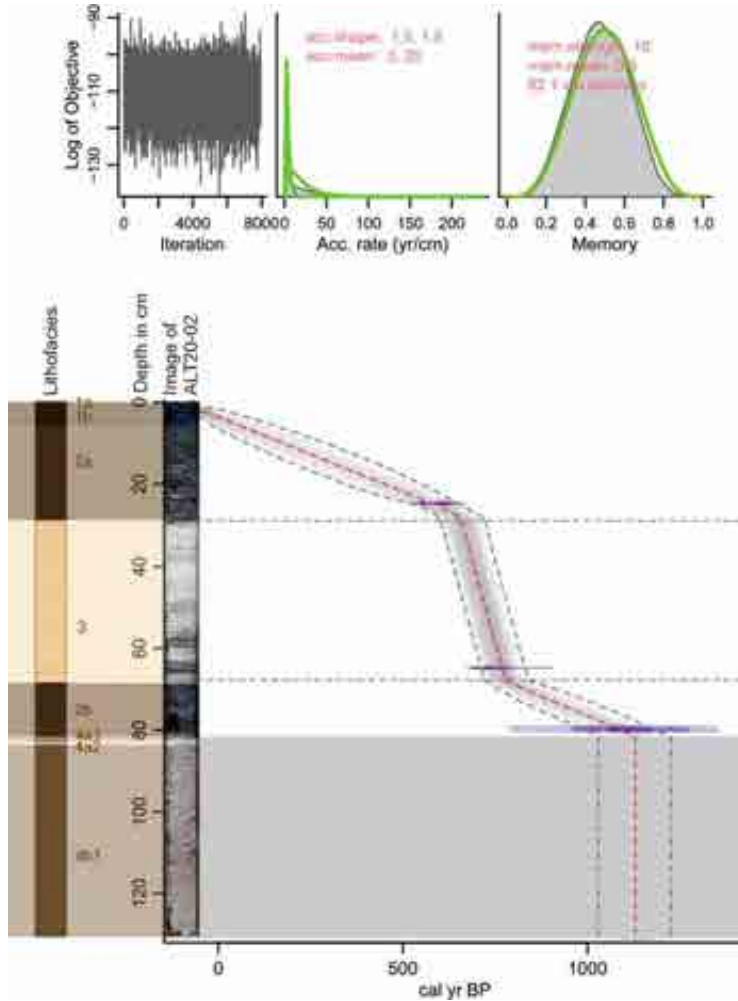


Figure 16: The age model generated by “Bacon” from the  $^{14}\text{C}$  dated ages is visualised. The core ALT20-02 is visualised on the left with a depth scale. To the right, the generated age curve is visualised in red. The blue markers indicate where the age sample was taken. The horizontal grey markers (dashed line and banks) indicate a change in sedimentation rate.

## 5. Discussion

"By using different devices and methods, a lot of information can be taken from the sediment. By looking at this data and comparing it with what we already know, we can learn more about the lake and its past. Bringing all of this together will help answer the questions set at the beginning of this thesis.

### 5.1. Overall evolution of sediment lithofacies

#### Unit 5 – Late Glacial

The deepest and oldest layer found in the short cores consists of late-glacial sediments. These were formed after the Ice Age, during a period of warming, when the large glaciers melted in the early stages after the lake formed. This is evident in the sediment, which is very fine-grained, contains almost no organic matter and contains drop stones. The sediment has a very high density and shows significant compaction. All these characteristics point to late glacial deposition, as interpreted by Deheyn et al. (in review). This lithofacies was only found in the short core ALT20-15, the slope core. In one of the long cores (1002-2-A), which reached deeper into the sediment, late glacial sediments with similar characteristics were identified. In the long core, a sample of Unit 5 was dated by  $^{14}\text{C}$  to an age of 14,253-14,878 cal BP (Deheyn et al., in review). The following lithofacies (**4c**) was dated to 959 - 1195 cal BP (Fig. 17). This indicates that a large period is missing from the sedimentary record at this particular location, i.e., the western plateau. In addition, the event deposit has an erosive base. It can therefore be assumed that there is a hiatus between lithofacies 5 and **4c**.

#### Unit 4 – Megaturbidite

The sediments from Unit 4 were interpreted as a megaturbidite from a significant event that occurred in the lake, during which a large amount of material was deposited in a short period of time. Sediments from this event were dated to an average age of  $1,129 \pm 99$  cal BP (755-991 cal CE).

The sediment becomes progressively finer towards the top, with some sedimentary structures that providing information about depositional processes. Unit 4 can be divided into several subunits, which are discussed in more detail in Chapter 5.2, 'Evolution of the Megaturbidite'.

#### Unit 3 – Augstbach sediment

Lithofacies 3 shows a significant lithological transition both at the beginning and at the end of the unit. The sediment is distinctly different: it is very light-colored, dense, rich in clastic particles, with low organic content and laminated. The sedimentation rate increases significantly in this unit and reaches 0.322 cm/year (measured at core location ALT20-02). This unit was deposited between  $769 \pm 60$  cal BP

and  $581 \pm 65$  cal BP. The clastic nature of the sediment and its low organic particle content suggest that it was transported by the nearby Augstbach. Since the temporary inflow of the river was in the western part of the lake, the highest concentration of clastic sediment is found in this area, as shown in Figure 16.1. The figure shows that the thickness of Lithofacies **3** is greatest near the inflow in the western part of the lake and decreases towards the east. Historical records confirm that the Augstbach was redirected (diverted away from the lake) by human intervention. Lamer (1998) and Geiswinkler (2014) describe this redirection as being related to the salt mine. Increased salt production led to frequent unintentional salt leaks, some of which ended up in Lake Altaussee. To prevent this, the Augstbach was diverted away from the lake around  $\sim 1319$  CE/ $631$  cal BP (Geiswinkler, 2014). This age corresponds well with the calculated end of this lithofacies at  $581 \pm 65$  cal BP.

However, no precise records have been found to indicate whether the Augstbach was originally directed into the lake by humans or a natural process on the alluvial fan, but it starts around  $769 \pm 60$  cal BP ( $1,181 \pm 60$  CE). The mine is first mentioned in historical records in 1147 CE (Lamer, 1998; Geiswinkler, 2014), indicating that mining activities were already taking place at the onset of the Augstbach unit. In most sediment cores, the introduction of the Augstbach sediments appears to be gradual, without forming a sharp boundary, and is occasionally interrupted by background sediments. This could indicate a natural or temporary human diversion.

#### Unit 2 - background sediment

Lithofacies **2a** and **2b** represent the background sediment, which is continuously deposited over the annual period. Unit **2b** was dated (mean age) from  $769 \pm 60$  cal BP to  $1129 \pm 99$  cal BP. Lithofacies **2a** was deposited between  $581 \pm 65$  cal BP and  $100 \pm 92$  cal BP. The sediment is less dense, homogeneous and has a higher organic content. The organic content for **2b** is  $\sim 13$ - $15\%$ , for **2a** the organic content is  $14$ - $17.7\%$  (Fig. 14). During the period of background sedimentation, Lake Altaussee has very few surface inflows and is mainly fed by the karst funnels. Therefore, the sedimentation rate of  $\sim 0.037$  cm/year (ALT20-02) is lower than in the Augstbach unit.

Two thin flood layers can be documented in almost all cores. One flood layer with an average age of  $\sim 361$  ( $\pm 100$  years) cal BP and one with an age of  $\sim 526$  ( $\pm 80$  years) cal BP. For the more recent event, a local flood event can be found in the literature (Hübl & Pürstinger, 2003). In 1594 CE ( $356$  cal BP) the "Göß Höh" flood occurred in the area of Lake Traunsee, where the water level increased by three metres (Hübl & Pürstinger, 2003). As Lake Altaussee is located in the hydrological catchment area of Lake Traunsee, there may be a connection between this event and the flood layer.

#### Unit 1 - recent sediments



The upper units of the core cover the period from -70 ( $\pm 3$  years) BP to 100 ( $\pm 92$  years) cal BP. Lithofacies **1a** and **1b** are also background sediments but differ in color and magnetic susceptibility. In this area the sediment has been strongly influenced by anthropogenic activity. The sediment in this area spans 100 years BP to -70 (2020 CE) - the year of core sampling. Lakes around the world show the influence of nuclear weapons testing between 1953 CE and 1963 CE, the Chernobyl nuclear disaster in 1986 CE (Appleby, 2001) and the influence of leaded car fuel. Villages and hotels have been built around the lake. This change in land use around the lake also led to water pollution, such as wastewater pollution into the lake (Riedl et al., 2008). This, together with increased fertilisation in the catchment, has resulted in an increase in organic content of up to ~21% (Fig. 14).

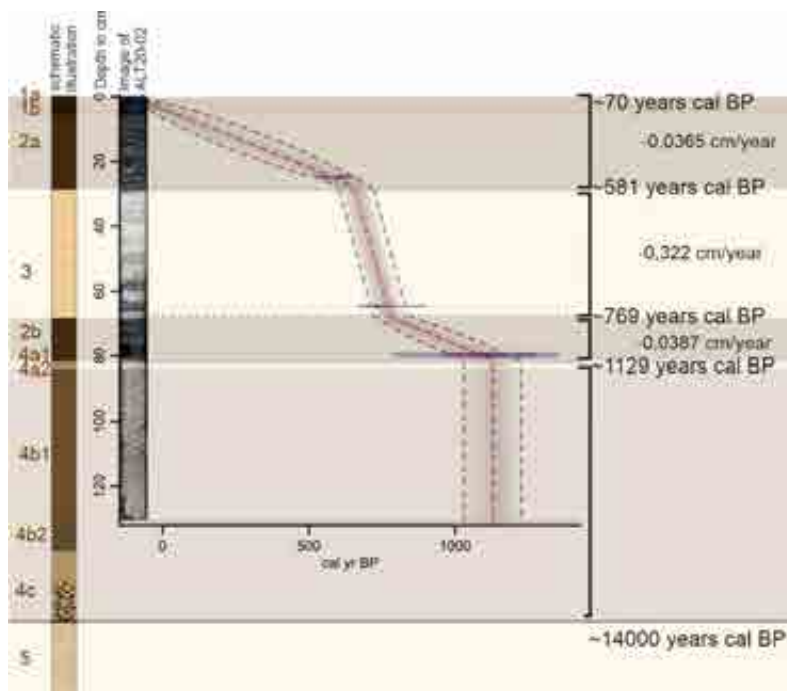


Figure 17: Shown is an age-depth model created by Bacon in R. To the left of the age model is a schematic core image of all lithofacies types and a core photo. To the right of the age model is the sedimentation rate distribution.

## 5.2. Evolution of the Megaturbidite

This event layer is found in most of the cores and is the main focus of this thesis. This unit covers the entire lake bed and is found almost everywhere. It spans the deep basin, rests on blocks, extends across the plateau, and even deposits are found on the slope faces. It has a maximum thickness of up to 240 cm (measured in long core 1002-1-A) in the deep basin. The spatial distribution of the lithofacies in the lake, and especially the thickness of the homogeneous part of the turbidite, allows it to be described as a megaturbidite (Sabatier et al., 2022; Schnellmann et al., 2002).

Another indicator supporting the megaturbidite interpretation is the semi-transparent unit and the ponding geometry visible in the seismic profiles. Similar deposit characteristics have been described in seismic profiles from Lake Lucerne and classified as megaturbidites by Schnellmann et al. (2002).

As the focus is on the turbidite, it is compared with other existing classifications. As shown in Figure 18.1, the turbidite sequence from Lake Altaussee can be compared with the Bouma (1962) classification. Some lithofacies match well, such as the general fining-upward trend of the event deposit, the coarse base, the subsequent parallel lamination and the homogeneous section. However, the Bouma sequence does not correlate with all parts of the sequence.

For example, the "Ta" sequence in Bouma's classification corresponds well with the lower part of Unit **4c** in our core. Bouma's "Td" corresponds to the upper part of the **4c** deposit, which shows parallel lamination. The "Tc" sequence from Bouma's classification cannot be identified in our cores as there is no evidence of cross-lamination or ripple structures. However, the Bouma "Tb" sequence can be correlated with Unit **4b.2** in the Lake Altaussee cores. Similarly, the homogeneous "Ta" sequence from Bouma is mirrored in our Unit **4a.2**. Another notable difference is that the Bouma sequence does not describe a clay/mud cap, which is present in our samples.

Figure 18.1 also compares the Altaussee deposit with the megaturbidite and backwash deposit described by Sabatier et al. (2022). As shown, most sections match well, such as the erosive contact with the coarse base, which corresponds to the base of **4c** in our cores. Similarly, the 'graded sand sequences with mud clasts' described by Sabatier et al. (2022) can be observed in some parts of the **4c** base, although not consistently across the lake. A correlation can also be made between the 'graded sands with grain size oscillation' described by Sabatier et al. (2022) and the transition from Unit **4c** to **4b.2**. Furthermore, 'homogeneous mud' is seen in Lithofacies **4b.1**, and the 'clay/mud cap' corresponds to Lithofacies **4a.2**.

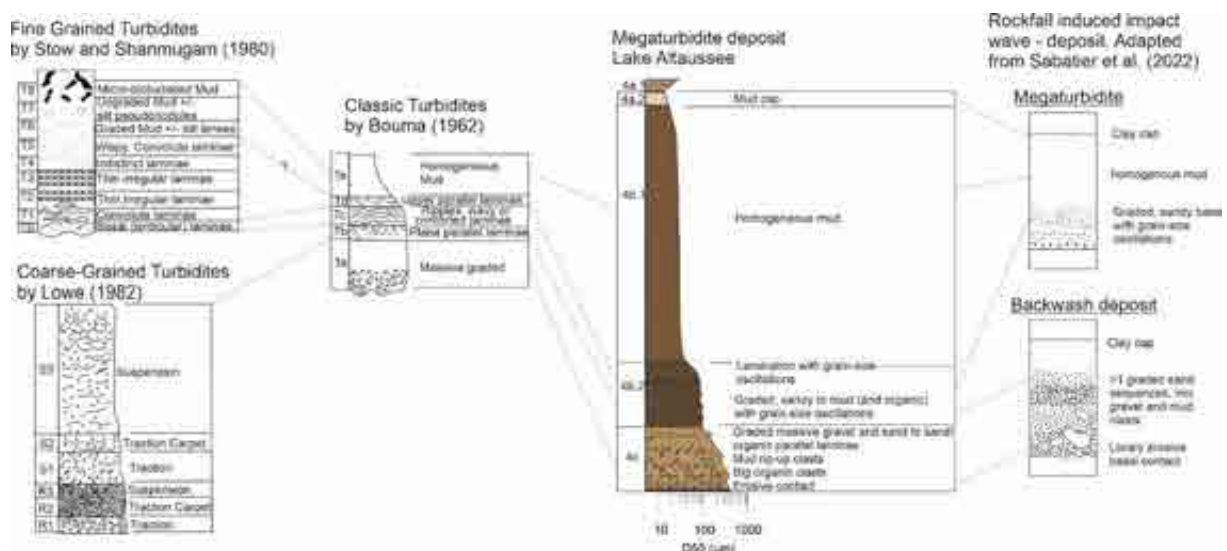


Figure 18.1: Illustration of the megaturbidite in Lake Altaussee and a correlation with existing turbidite classifications from Stow & Shanmugam (1980), Lowe (1982) and Bouma (1962) on the left; and a comparison with two deposits described in the paper by Sabatier et al. (2022) on the right.

As the sediment has many similarities with the description of a backwash deposit and a megaturbidite, further evidence for these processes can be investigated.

The morphology of the lake and its surroundings suggests a mass movement (more on this in Chapter 5.3). The blocks in the eastern part of the lake indicate that they entered the lake by a gravitational process. For the description of the megaturbidite it is already assumed that the blocks are related to the event, the exact reasons that support this assumption are described in the next Chapter 5.3.

The base of the megaturbidite appears similar in most sediment cores. It contains coarse material, larger stones, mud clasts and occasionally large organic pieces such as wood. A further subdivision of Lithofacies **4c** can be made on the basis of closer observation. The upper and lower parts of **4c** show some differences. The lower part - the first part of **4c** to be deposited - is coarse grained, chaotic and contains mud and gravel clasts. In contrast, the upper part of **4c** - deposited later - consists of finer grained, laminated sediment with alternating grain sizes. This shift in sediment characteristics suggests a change in sediment dynamics. The sediment in **4c** (especially the lower part) likely originates from lake external or coastal material, introduced by a mass movement, which also mixed up already-deposited lakebed sediment. This process is shown schematically in Figure 18.2-A. If the mass movement originated from the eastern or north-eastern areas of the lake, this should be supported by sedimentary evidence, such as more pronounced deposition near the source area. Indeed, the lower part of **4c** is not the same in all parts of the lake (Fig. 18.2). The lower part of Lithofacies **4c**, a mixture of mass movement material and megaturbidite deposits, varies depending on the location in the lake. In short cores from the eastern part of the lake, such as ALT20-07 (on top of the block), **4c** appears very coarse grained and poorly sorted, with several mud and gravel clasts. In contrast, cores from the deep basin (long core 1002-1-A, which reached this area) show less coarse material, probably because the basin is further from the source of the mass movement. However, core ALT20-15 from the western slope again contains very coarse material in the lower part of **4c**, although it is even further from the impact zone.

Examination of the size of the gravel clasts alongside the Hjulström diagram (A.3.2.) suggests that these clasts could not have travelled far due to their size. They could not have come from the northeastern coast and reached the plateau in the west, but were deposited simultaneously according to the stratigraphy. These clasts can be interpreted as backwash deposits from the western shoreline (Figure 18.2-B). Since it is assumed that these blocks propagated into the lake, they created an impact wave, which has affected both already-deposited lake bed material and the water body itself (See Chapter 5.3.) As described by Sabatier et al. (2022), an impact wave can lead to a backwash and further processes such as a seiche. The overlying sediment with fluctuating grain size layers seen throughout the lake could correspond to this next step - a seiching. The laminations in the sediment could have been caused by a seiche, or oscillation of the water body, as described in the papers by Vermassen et al. (2023), Beck (2009) and Sabatier et al. (2022). This process is observed in the upper part of Lithofacies **4c** and Lithofacies **4b.2** as shown in Figure 18.2-C. As a seiche causes the water body to

fluctuate, it has an erosive effect on the flanks and bed of the lake (Sabatier et al., 2022). Coarser material is introduced and finer material is deposited between the oscillations. This can lead to a grain size oscillation in a seiche deposit. Seiches often result in the deposition of a homogeneous layer on top of the silty/sandy lamination base, as noted by Vermassen et al. (2023) and Beck (2009). Once the water has calmed, the sediment falls out of suspension (shown in Fig 18.2-D). The large volume of sediment suspended during this process is reflected in the thickness of the homogeneous Lithofacies **4a.2** (Vermassen et al., 2023; Beck, 2009). Over time, only the finest particles remained in suspension and eventually settled to form Lithofacies **4a.2**, the mud cap.

Notably, a increase and subsequent decrease in organic content (LOI Data) occur within the turbidite. The organic values do not increase at the beginning of the event, but only within Lithofacies **4b.1**, where the water has calmed down and the sediment is very homogeneous. This is probably because the organic-rich lake sediment remobilised from the lake bed was resuspended and remained in suspension longer than the (partly newly introduced) clastic sediment. It can be seen that the organic content of the background sediment is generally higher than within the event layer. During the event, much clastic material (and terrestrial organic material) entered the lake, mixed with the existing lake bottom sediment and significantly reduced the organic content. Organic-rich material has a lower density than most clastic sediments, so it would take longer to settle out of the suspension cloud (Nigg et al., 2021). According to Nigg et al. (2021), an accumulation of fine-grained organic-rich sediment towards the top of the turbidite is indicative of a terrestrial origin of the sediment.

Contrary to the original assumption, Lithofacies **4a.1** is not deposited during the event, but shortly after. The grain size increases significantly again. A possible explanation for this lithofacies could be that the collapse of the rocks left a lot of clastic material on the lake shore and surrounding vegetation, which was carried into the lake during the next rainfall. However, this cannot be said with certainty, especially as it is unclear how much time has passed in these few millimetres.

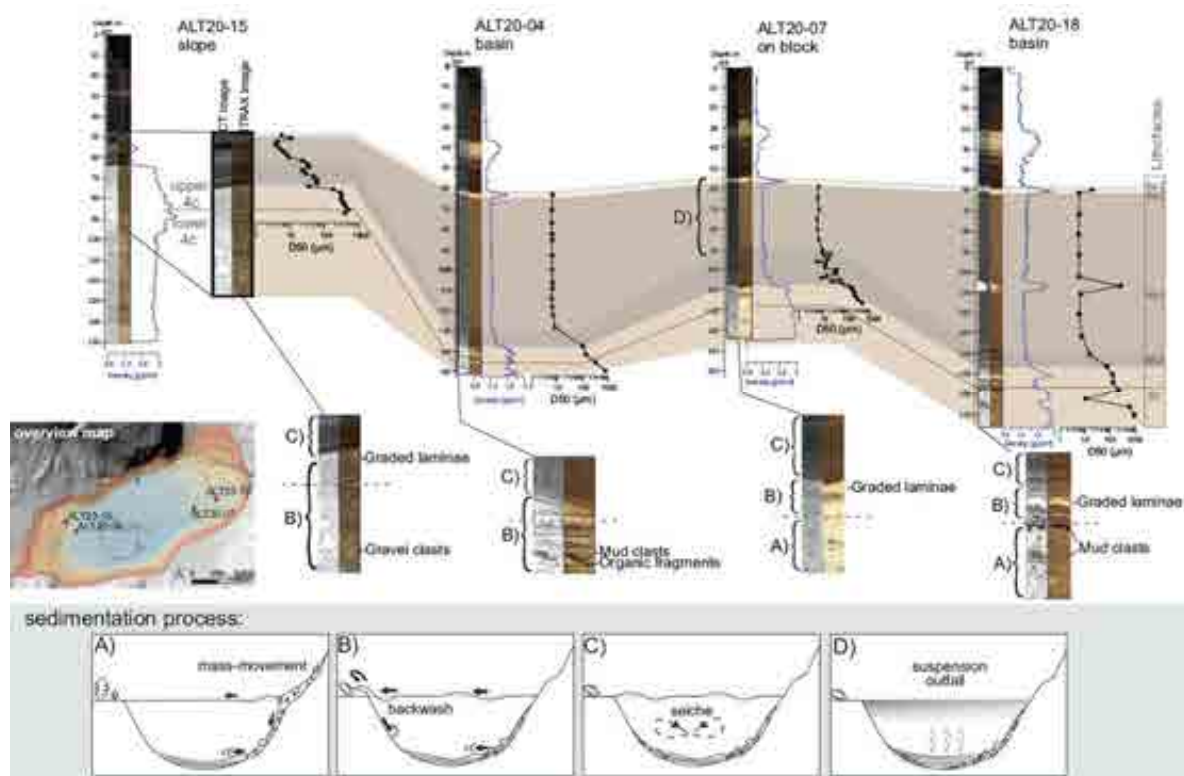


Figure 18.2: Various datasets of the megaturbidite, based on a selection of cores, are presented here. These include CT images, core photographs, density data and grain size (D50 in  $\mu\text{m}$ ). The grain size curves represent treated sediments. The lower section illustrates the conceptual model for the different processes by which the sediments were deposited, arranged in chronological order from left to right.

In order to describe this process accurately, it was necessary to rely on grain size data, but it should be noted that this is only clearly visible in the treated sediments. These differences are illustrated again in Figure 19. In core ALT20-07 the treated sediment lies on a diagonal line, as would be expected for a single pulse turbidite (from top right to bottom left). The coarse bottom **4c** lies on a line that gets finer as it goes down. The green dots (**4b.2**) show a change in the sediment that can also be seen in the core, clearly visible in cores ALT20-07 and ALT20-15 in Figure 19. The sediment shows some grain size oscillations, which are interpreted to be caused by seiche (as mentioned above). Subsequently, the yellow points (**4b.1**) all lie together, representing the homogeneous, uniform sediment of Lithofacies **4b.1**. In comparison, the untreated sediment for core ALT20-07 does not show a straight line of dots. Only at the coarse base of the turbidite where there is little organic material, does it follow a pattern. The figures for cores ALT20-15 and ALT20-18 are similar, but the sediment sequences are not as well preserved as in core ALT20-07. In ALT20-15 the turbidite units are deposited in very small amounts. An outlier or air bubble was measured there in **4b.1**. In core ALT20-18, it is also not a straight line in the treated sediment, as a mud clast was sampled in unit **4c**, which is an outlier. In Lithofacies **4b.1** the sand lens also forms an outlier that breaks the line.

It was possible to show that the chaotic evolution in the untreated sediment was due to the organic particles. Without the removal of the organic material, it would not have been possible to construct

such a detailed evolution of the grain size spectrum. This analysis shows that the yellow dots representing **4b.1** are indeed very homogeneous and that the laminated sediments of Unit **4b.2** show grain size oscillation. The overall linear progression of the turbidite indicates one pulse.

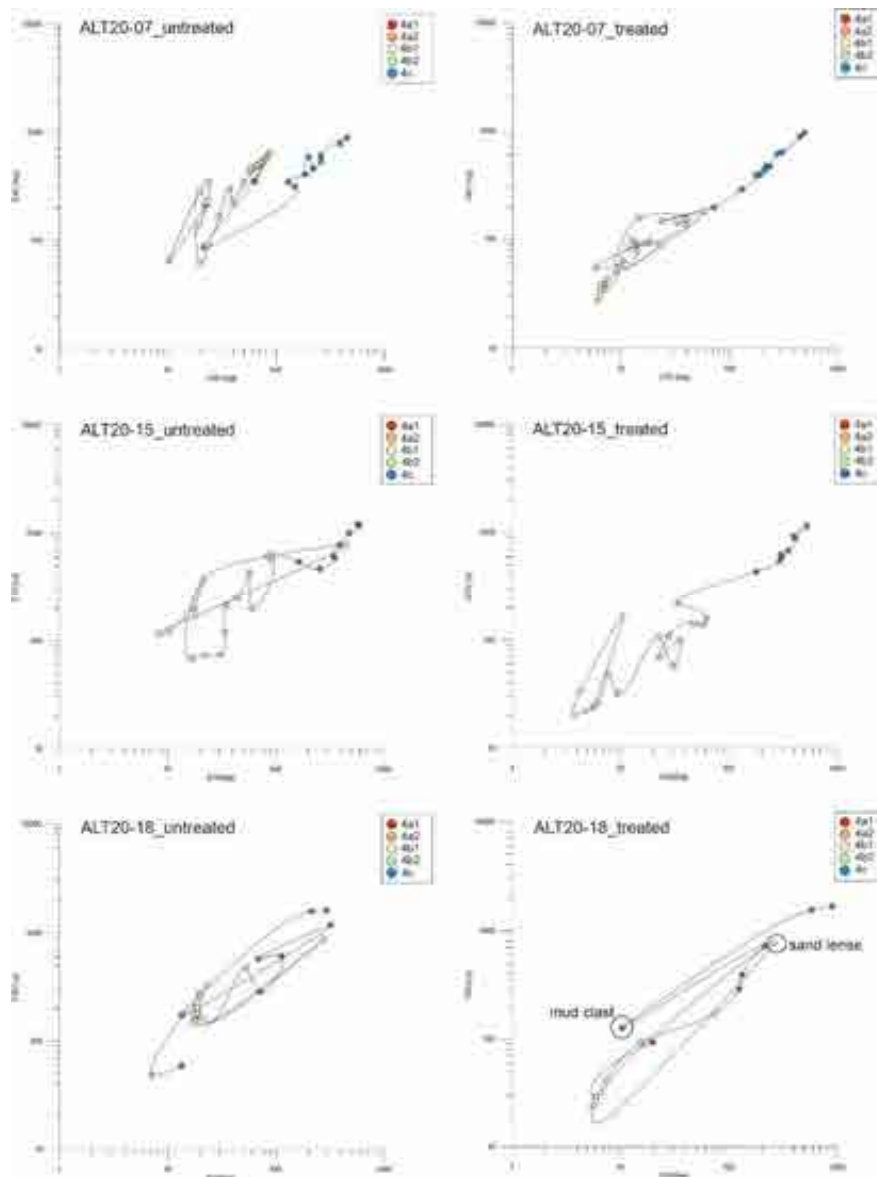


Figure 29: The comparisons of D50 ( $\mu\text{m}$ ) and D90 ( $\mu\text{m}$ ) values are shown here, based on samples from the event layer in cores ALT20-07, ALT20-15 and ALT20-18. On the left are the untreated sediment samples and on the right are the sediments treated with hydrogen peroxide.

### 5.3. Was the megaturbidite caused by one or more terrestrial mass movements that propagated into the lake?

Firstly, it should be noted that the grain size distribution of the event deposit indicates sediments typical for a short-term event, i.e., an "instantaneous" deposition compared to the slowly accumulating background sedimentation. During a flood event, the sediment inflow would not have an initial inflow peak, but would fluctuate over a longer period, with possible increases and decreases in grain size, as described by Vandekerckhove et al. (2020). The Augstbach is a small river that would require a large

input of sediment to produce a deposit several metres thick. However, there is no visible evidence of this. Furthermore, the thickest part of the event layer is in the deep basin and eastern part of the lake, areas further from the (potential) Augstbach inflow. A flood deposit would look more like the documented Augstbach Unit **3**, which is confirmed in the literature to have been deposited by the Augstbach. It is thickest in the western part and thins towards the east. The sediment composition is also different. The turbidite is rich in organic material, up to ~10%. The sediments of the Augstbach in Unit **3** have a maximum organic content of only 5%. It is therefore more likely that the turbidite consists of pre-existing background sediment that has been reworked by the impact of the blocks, which can explain the amount of organic material.

The morphology of the lake bed and surrounding area suggests that a mass movement took place. A strong indication of this is the presence of large blocks in the north-eastern part of the lake bed and along the shoreline to the east of the lake. Some of these blocks extend for tens of metres. These blocks indicate a gravitational process. Based on their distribution, it is possible to approximate their origin. However, it is not possible to verify which blocks came from which direction. There are at least two possible sources of these blocks, involving two areas close to the lake shore (A.4.1.). One is a cliff in the northern part of the lake, which rises prominently from the lake shore. Several blocks in front of this cliff may have originated here. Some smaller blocks in the eastern area lie directly in front of the Trisselwand, both on land and in the water and could have come from there, based on their location and size. These blocks are thought to be associated with the event that triggered the megaturbidite, as they are directly overlain by the megaturbidite and there is no evidence of older sediments on the blocks. The deposits of the megaturbidite extend throughout the deep undisturbed basin, and in a thinner form are also found on top of the blocks with all their units intact.

Grain size analyses were carried out to determine, among other things, whether there was one or more pulses (Fig. 19). The sediments of this event show a change in depositional dynamics. The sediment changes from a chaotic and coarse sediment to a finer sediment with fluctuating grain size layers and then to a homogeneous finer sediment ending in a mud cap. Overall, there is an upward fining trend that appears undisturbed. The sediment with oscillating grain size is attributed to a seiche and not to several pulses. Reasons for the assumption of a seiche have already been given in Chapter 5.2. and that it was deposited after a backwash deposit caused by an impact wave. Only in core ALT20-18 can a coarser roundish sand lens be observed within the homogeneous Lithofacies **4b.1**, visible in Fig. 12.3. However, as it only occurs in a single core between the blocks, it can't be considered as a second pulse, as the sediment could also come from the blocks, and it is not seen elsewhere. As there is no concrete evidence for a second pulse in the megaturbidite deposit, it can be assumed that this was a single event. To investigate the origin of the sand lens, further short cores could be taken from this location, around this block and in the vicinity of core location ALT20-18.

However, it cannot be definitively proven whether all the blocks were deposited at the same time or whether some were deposited earlier. There is also no evidence to support this, as no sediments older than the event were found on the blocks. It is also possible that some blocks were deposited earlier and that the sediment deposited on them was washed away by the impact of the second event. Whether there is evidence of an earlier event may be clarified by analysing the long cores.

Based on what we have observed, it is likely that this was a single event that resulted in several blocks being transported into the lake, probably from at least two different directions. This must have occurred simultaneously or within a very short time span of seconds to a few minutes (Van Dale et al., 2017), as there is no evidence in the sediment for multiple pulses in the turbidite. However, this question cannot be answered conclusively at this time. It may be possible to address this question more effectively with additional sediment cores from the eastern shoreline area, where the impact has occurred.

#### 5.4. Was the megaturbidite caused by a strong earthquake?

An earthquake could have triggered the mass movement into the lake, especially as there is evidence that material could have entered from two or more directions simultaneously. The geological map in Figure 4 shows several landslides and rockfall deposits around the lake and in the small valley to the north (Mandl et al., 2012). In addition, several confirmed and suspected faults are marked on the geological map near the lake (Mandl et al., 2012). These may also extend into the lake. The subaqueous craters lie along a line, as do the 'Liager', which are seasonal subaerial springs activated by heavy rainfall (Geyer et al., 2016). This may indicate that they lie along a fault line. Further south is the 'Toplitz fault', which runs along the Toplitzsee, Grundlsee and Bad Aussee; there is evidence of a vertical offset on this fault line (Slapansky & Ahl, 2012). In general, mass movements can occur more frequently on faults, but a fault directly on the lake would not necessarily be required to trigger such an event.

Mass movements can occur for a number of reasons. On the one hand, they can be influenced by preconditions such as steep slopes and the interaction of different geological units. On the other hand, there are triggers that can initiate mass movements, such as heavy rainfall events or earthquakes. In some cases, it's been documented that a combination of these has led to mass movement.

In the Salzkammergut region in particular, large mass movements such as landslides and rock falls can be explained by preconditioning factors. These occur due to the deformable Haselgebirge, which can deform under the load of the brittle carbonate platforms (Van Husen, 2012).

The Sandling landslide, one of the largest and most recent mass movements in this region, was caused by the interaction of deformable Haselgebirge and brittle rock formations (with a heavy rainfall event as the trigger). During this landslide in 1920, 200,000 m<sup>3</sup> of rock was set in motion and later triggered a debris flow that moved a total of 7 million m<sup>3</sup> of rock and soil (Lehmann, 1926). There was already a



landslide in this area in 1546 CE, which buried one of the oldest salt mines “Michlhallberg” in this region (Lehmann, 1926).

Furthermore, mass movements can be triggered by strong and long periods of rain, as described by several authors (Oswald et al., 2021; Swierczynski et al., 2013). It is well known that heavy precipitation was more frequent during colder periods, such as the Little Ice Age (LIA) and the mid-Holocene, leading to increased flooding (Swierczynski et al., 2013). However, sediment records from Lake Mondsee, which is close to Lake Altaussee, do not show a period of increased precipitation at the time of the mass movement 959-1195 years cal BP. It is possible that a combination of triggers was responsible. The rock may have been weakened and degraded by periods of precipitation, allowing a low-intensity earthquake to trigger a mass movement. Lauterbach et al. (2023) and Oswald et al. (2021) also describe how a rock can be weakened by another trigger before collapse occurs.

This brings up another trigger that can occur in the Alps: seismicity. Due to the north-south compression of the Alps, this can repeatedly cause small earthquakes in the Alpine region (Lenhardt, 2012). Lake Altaussee and its surroundings are located in a seismically low activity zone, classified as 'Zone 1' according to the map by Lenhardt (2012) in the Appendix (A.1.2.). In this zone, earthquakes are relatively rare. However, the area around Bad Ischl is known for mild earthquakes (Lenhardt, 2012). On average, this region experiences a noticeable small earthquake every two years, which does not cause any damage. According to Lenhardt (2012), earthquakes with magnitudes up to 3 and local intensities of IV-V occur occasionally in the areas of Bad Ischl, Hallstatt and Altaussee. According to Monecke et al. (2004) and Inouchi et al. (1996), a local intensity of at least VI to VII is required to trigger sediment deformation, turbidites and rockfalls. However, there are no records of such earthquake intensities in this area for at least the last 100 years (Grünthal et al., 2009).

It is also possible that the observed effects were not caused by a local earthquake, but by a more distant one whose surface effects are visible in this area. For example, as described by Daxer et al. (2022) at Lake Wörthersee, a distant earthquake - the 1976 Friuli earthquake - was thought to have triggered a turbidite. This phenomenon has been described not only at this lake but also at several others, as noted by Oswald et al. (2022) for Lake Achensee. It has been documented that a turbidite was deposited in Lake Achensee, triggered by a distant earthquake.

A look at lakes in the surrounding area also reveals some event deposits. In nearby Lake Hallstatt, Lauterbach et al. (2023) described three large events. Event 'E2' is particularly important for our study. This event layer was dated to  $1058 \pm 60$  cal BP ( $892 \pm 60$  CE). This overlaps strongly with the event deposit in Lake Altaussee, dated at 959 to 1195 cal BP (755-991 CE). Considering the potential error range, these two events could have been triggered by the same event. Lauterbach et al. (2023) described a megaturbidite about 145 cm thick that was also deposited after a subaerial mass movement. However, the evidence was not clear enough for the authors to determine a trigger.

Another nearby lake is Lake Mondsee, but no mass movement deposits or turbidites were found in this lake for this specific period. Lake Toplitzsee and Lake Grundlsee are in the immediate vicinity of Lake Altaussee, but no sedimentological data are available for these lakes.

Although this question cannot be fully answered, it can be assumed that the event was triggered by an earthquake, as several slopes at Lake Altaussee collapsed, with blocks propagating into the lake. Since a mass movement with a megaturbidite occurred not only at Lake Altaussee, but also at nearby Lake Hallstatt around the same time, it can be assumed that these events are related and may have the same trigger. It's possible that a weak local earthquake triggered the slope collapse, if heavy rainfall had already weakened the slopes. It could also be the result of a strong earthquake that occurred further away, as described by Oswald et al. (2022) for Lake Achensee. However, there is no clear evidence, nor can it be said with certainty, that it occurred simultaneously at both lakes. Considering the range of errors in the dated ages, it is possible that these events could have occurred several tens of years apart. To answer this question, several nearby lakes would have to be analysed for similar events.

## 5.5. Comparison of Lake Altaussee with Other Alpine Lake Studies

This section discusses how the sedimentary record of Lake Altaussee differs from other lake archives in the Alpine region and what similarities there may be. The last 1129 years of lake history are covered by the short cores. A large part of this sediment was deposited under the influence of natural hazards and human activities. The following geohazards and human influences have influenced the sediment dynamics within the lake:

- **Mass movements:** The major influence on the sediments of the short cores, was caused by the mass movement that entered the lake. As described above, mass movements are not uncommon in this area, especially in the Salzkammergut due to the geomechanical stratigraphy (Lenhardt, 2012). However, mass movements that have entered lakes and left their traces in the sediment can also be found throughout the Alpine region. The mass movement in Lake Altaussee is briefly compared with inner Alpine lakes in Switzerland, Lake Lucerne and Lake Oeschinen, to show that subaerial mass movements into mountain lakes are not rare in this setting. In 1601 CE, an earthquake of magnitude 6.2Mw occurred at Lake Lucerne, which triggered two subaerial mass movements and the failure of several subaqueous slopes - leading to a tsunami (Nigg et al., 2021; Schnellmann et al., 2006). This resulted in a mass flow deposit and a megaturbidite in the Chrüztrichter and Vitznau lake basins. The earthquake and its consequences resulted in a tsunami with backwash deposits and a seiche, which was reflected in the lake sediments (Schnellmann et

al., 2006). The process and the deposited sediments are very similar to the mass movement and megaturbidite in Lake Altaussee.

At Lake Oeschinen, another lake in the Swiss Alps, there are also some subaerial mass movements that have significantly affected the lake sediments and lake morphology. In their work, they emphasised that subaerial mass movements bring in terrestrial material and the role of impact energy (Knapp et al., 2018). At Lake Oeschinen, there have been several mass movements that have deposited an event layer described by Knapp et al. (2018). Some of these movements were triggered by earthquakes, as the lake is located in a seismically active zone. They were also able to show that several mass movements came from the same source. The authors suggest that about six events originated from two detachment scarps. Knapp et al. (2018) were able to show that some slope failures were prepared by earthquakes and then triggered by 'stress-relaxation processes'.

As described above, mass movements also occurred at Lake Hallstatt, which is close to Lake Altaussee. Several events occurred here, three of which were prominent. One event layer at the same time as the event layer at Lake Altaussee. Here, too, there was a mass transport deposit with an overlying turbidite (Lauterbach et al., 2022; Ortler et al., 2024). The origin of the mass movement there was terrestrial but, as in most cases, it is difficult to identify a trigger without historical records such as the 1601 CE Lake Lucerne earthquake.

- Subaquatic karst funnels: Another characteristic feature of Lake Altaussee are the subaquatic karst funnels, which mainly feed the lake with water. Although these are more in the background of this work and have not been described in detail, they are remarkable at the lake. They can occur in karst regions, but they are not an exception. Karst funnels with a maximum diameter of up to 150 metres can also be found in Lake Neuchâtel, Switzerland, as described by Wirth et al. (2020). The authors of this study were able to show that most of these karst funnels are connected to a karst system and can be an important part of a lake's hydrological cycle. The subaqueous karst funnels also play an important role in the water cycle of Lake Altaussee.

- Hydrological changes: A drastic change in the sedimentation rate can be seen in Lake Altaussee, caused by the redirection of the Augstbach (due to work on the salt mine). This is not the only lake where a hydrological change has occurred, affecting the dynamics of the lake. The work of Andric et al. (2020) on Lake Bohinj (Slovenia) showed that there were significant changes in the sedimentation rate. There was also a sudden and temporary increase in sedimentation rate in this lake. In the period between 2900 cal BP and 2100 cal BP the sedimentation rate increased, within this span the maximum peak was 3.2 mm/year (before 0.3-0.5 mm/year and after 0.9 mm/year). Andric et al. (2020) found several indications of increased input of terrestrial sediments

into the lake, suggesting a river relocation. It is not possible to identify a specific reason for this, as it could be due to a seismic event, a wetter climate or lake level fluctuations, and the area was already inhabited. Another reason for the increase in sedimentation rate could be increased soil erosion caused by deforestation for agriculture and mining.

## 6. Conclusion and Outlook

The following information about Lake Altaussee can be obtained by analysing the short cores:

- A megaturbidite was discovered in the sediment cores from Lake Altaussee, which was deposited between 959-1195 cal BP. This was caused by a mass movement into the lake. By interpreting the sedimentological data and comparing it with other studies, it could be concluded that the event was caused by a mass movement into the lake. Furthermore, it can be assumed from the available results that the blocks that fell into the lake came from two directions (presumably at the same time). The exact circumstances or triggers of this mass movement could not be clearly established, there are several possibilities such as earthquakes, heavy rain or spontaneous slope collapse.

Based on the high-resolution grain size data in combination with the CT data, a good reconstruction of the event chronology of the mass movement deposition could be obtained: The entry of mass transport material generates an impact wave, which leads to the formation of a backwash deposit. This is followed by seicheing—oscillating water movements that influence the sediment. As the water calms, the suspended material gradually settles to the bottom. It was also possible to show the influence of organic particles on the grain size analysis.

- Through sediment analyses and literature research, Lithofacies **3**, which differs significantly in sediment composition and dynamics, could be attributed to the temporary relocation of the Augstbach. This river was diverted into Lake Altaussee in the period ~581 - 769 cal BP (1181-1369 cal CE), resulting in an increased (clastic rich) sediment inflow. Literature records (Lammer, 1998; Geiswinkler, 2014) show that the stream was diverted away from the lake in 1316 CE due to work on the salt mine. However, no evidence was found that the river was initially led into the lake. As there is evidence of salt mining in Altaussee since 1147 CE (Lammer, 1998; Geiswinkler, 2014), it can also be assumed that the Augstbach was led into the lake by humans. This could have had various reasons for fishing or trade as rivers were used as transport routes. It could also have been naturally diverted by vegetation or sedimentation.
- The results show that human influences and natural hazards have strongly influenced the sediment dynamics at Lake Altaussee. It can be seen how sensitive the Alpine ecosystem is under the influence of natural hazards and human activity. The diversion of the river and the deforestation in the course of the mine show how anthropogenic influences can change the sediment dynamics inside the lake, as well as a mass movement into the lake.

Not all questions could be answered with certainty, such as whether the event was triggered by an earthquake or if previous mass movements had occurred in the lake. However, a clearer understanding of the lake's dynamics and its evolution over the centuries was achieved. To determine if an

earthquake may have been the trigger, studying other lakes in the region to identify similar events at the same time would be beneficial. Since a similar event was found in the nearby Lake Hallstatt, further investigation into whether evidence of the same event exists in the nearby lakes Grundlsee and Toplitzsee could help clarify the spatial extent of the event. To gain a better understanding of the lake's changes between the Late Glacial period and the event (959-1195 cal BP), additional studies of older sediments are needed. These could provide insights into prior events, potentially explored through long cores. Furthermore, investigating recent sediments could reveal how human activities and surrounding life have impacted the ecosystem, including long-term traces, such as microplastics, which may have lasting effects on the lake's flora and fauna.

## 7. References

Aigner, G. (2009): Badegewässerprofil, Altaussee See Süd. Erstellt vom Bundesministerium für Arbeit, Soziales, Gesundheit und Konsumentenschutz und Amt der Steiermärkischen Landesregierung.

Andrič, M., Sabatier, P., Rapuc, W., Ogrinc, N., Dolenc, M., Arnaud, F., Von Grafenstein, U., Šmuc, A. (2020). 6600 years of human and climate impacts on lake-catchment and vegetation in the Julian Alps (Lake Bohinj, Slovenia). *Quaternary Science Reviews*, 227, 106043.

Appleby, P. G. (2001). Chronostratigraphic techniques in recent sediments. Tracking environmental change using lake sediments: basin analysis, coring, and chronological techniques, 171-203.

Arias, P.A., N., Bellouin, E., Coppola, R.G., Jones, G., Krinner, J., Marotzke, V., Naik, M.D., Palmer, G.-K., Plattner, J., Rogelj, M., Rojas, J., Sillmann, T., Storelvmo, P.W., Thorne, B., Trewin, K., Achuta Rao, B. Adhikary, R.P. Allan, K. Armour, G., ... and K. Zickfeld, 2021: Technical Summary. In *Climate Change 2021: The Physical Science Basis. Contribution of Working Group I to the Sixth Assessment Report of the Intergovernmental Panel on Climate Change* [Masson-Delmotte, V., P. Zhai, A. Pirani, S.L. Connors, C. Péan, S. Berger, N. Caud, Y. Chen, L. Goldfarb, M.I. Gomis, M. Huang, K. ... and B. Zhou (eds.)]. Cambridge University Press, Cambridge, United Kingdom and New York, NY, USA, pp. 33–144.

Arnaud, F., Poulenard, J., Giguët-Covex, C., Wilhelm, B., Révillon, S., Jenny, J. P., Revel, M., Enters, D., Bajard, M., Fouinat, L., Doyen, E., Simonneau, A., Pignol, C., Chapron, E., Vannière, B., Sabatier, P. (2016). Erosion under climate and human pressures: An alpine lake sediment perspective. *Quaternary Science Reviews*, 152, 1-18.

Beck, C. (2009). Late Quaternary lacustrine paleo-seismic archives in north-western Alps: Examples of earthquake-origin assessment of sedimentary disturbances. *Earth-Science Reviews*, 96(4), 327-344.

Behm, M., Plan, L., Seebacher, R., Buchegger, G. (2016): „Kapitel: Dachstein S. 569-588“ in Spötl, C., Plan, L., Christen, E., Behm, M. (Hsg.) *Höhlen und Karst in Österreich* (Kataloge des Oberösterreichischen Landesmuseums - Neue Serie). Herausgeber: OÖ Landes-Kultur GmbH. ISBN-10: 3854743211.

Blaauw, M., & Christen, J. A. (2011). Flexible paleoclimate age-depth models using an autoregressive gamma process, *Bayesian Analysis* 6 (3) 457 – 474. <https://doi.org/10.1214/11-BA618>

Blöschl, G., Kiss, A., Viglione, A., Barriendos, M., Böhm, O., Brázdil, R., Coeur, D., Demarée, G., Llasat, M.C., Macdonald, N., Retsö, D., Roald, L., Schmocker-Fackel, P., Amorim, I., Bělinová, M., Benito, G., Bertolin, C., Camuffo, D., ... and Wetter, O., 2020. Current European flood-rich period exceptional compared with past 500 years. *Nature* 583, 560–566.

Blume, H. P., Stahr, K., & Leinweber, P. (2011). *Bodenkundliches Praktikum: Eine Einführung in pedologisches Arbeiten für Ökologen, Land-und Forstwirte, Geo-und Umweltwissenschaftler*. Spektrum Akademischer Verlag, Heidelberg, 110, 102.

Bouma, A.H., (1962). *Sedimentologie einiger Flysch-Lagerstätten: A Graphic Approach to Facies Interpretation*. Elsevier, Amsterdam, 168 S.

Bouma, A. H. (1987). Megaturbidite: An acceptable term? *Geo-Marine Letters*, 7(2), 63-67.

Brauer, A., Endres, C., & Negendank, J. F. (1999). Lateglacial calendar year chronology based on annually laminated sediments from Lake Meerfelder Maar, Germany. *Quaternary International*, 61(1), 17-25.

Brisset, E., Guiter, F., Miramont, C., Revel, M., Anthony, E. J., Delhon, C., Arnaud, F., Malet, E., De Beaulieu, J. L. (2015). Lateglacial/Holocene environmental changes in the Mediterranean Alps inferred from lacustrine sediments. *Quaternary Science Reviews*, 110, 49-71.

Burstein Hewitt, L. (2017): *Walter Munk - Part 2: At Home; His house is his hand-built castle*. La Jolla Light Press. Online Journal. Accessed on: 03.05.2023.

Costanza, R., Graumlich, L.J., Steffen, W., Crumley, C., Dearing, J., Hibbard, K.A., Leemans, R., Redman, C.L., Schimel, D., 2007. Sustainability or collapse: What can we learn from integrating the history of humans and the rest of nature? *Ambio* 36, 522–527.

Croudace, I. W., Rindby, A., & Rothwell, R. G. (2006). ITRAX: description and evaluation of a new multi-function X-ray core scanner. *Geological Society, London, Special Publications*, 267(1), 51-63.

Daxer, C., Ortler, M., Fabbri, S. C., Hilbe, M., Hajdas, I., Dubois, N., Peichl, T., Hammerl, C., Strasser, M., Moernaut, J. (2022). High-resolution calibration of seismically-induced lacustrine deposits with historical earthquake data in the Eastern Alps (Carinthia, Austria). *Quaternary Science Reviews*, 284, 107497.

Deheyn, D.D., Häuselmann, P., Burschil, T., Fabbri, S.C., Fiebig, M., Gasperl, W., Grabner, M., Haas, J.N., Holzinger, A., Kalss, H., Kofler, W., Kremer, C., Moernaut, J., Ortler, M., Permann, C., Schmalfuss,



C., Verlinden, C., Wagner, S., Weber, L.-M., Wenger, V., Wriessnig, K., Zafiu, C., Heine, E., n.d. Lake Altaussee Monitoring Programme: Comprehensive investigations of an inner alpine lake. in prep.

Festi, D., Brandner, D., Grabner, M., Knierzinger, W., Reschreiter, H., & Kowarik, K. (2021). 3500 years of environmental sustainability in the large-scale alpine mining district of Hallstatt, Austria. *Journal of Archaeological Science: Reports*, 35, 102670.

Geologische Bundesanstalt (1991-not published). IDNDR-Aktivitäten der Geologischen Bundesanstalt im Zeitraum von VII/1990 bis IX/1994: Ergebnisse aus dem Schwerpunkt 4: Seen des Salzkammergutes. Wien, Österreich: Geologische Bundesanstalt, S. 149-177.

Geotek (Hrsg.) (2021) Multi-Sensor Core Logger, Manual Version Januar 2021.

Geyer, E., Seebacher, R., Tenreiter, C., Knobloch, G. (2016): „Kapitel: Totes Gebirge S. 599-622“ in Spötl, C., Plan, L., Christan, E., Behm, M. (Hsg.) *Höhlen und Karst in Österreich* (Kataloge des Oberösterreichischen Landesmuseums - Neue Serie). Herausgeber: OÖ Landes-Kultur GmbH. ISBN-10: 3854743211.

Gilli, A., Anselmetti, F. S., Glur, L., & Wirth, S. B. (2013). Lake sediments as archives of recurrence rates and intensities of past flood events. *Dating Torrential Processes on Fans and Cones: Methods and Their Application for Hazard and Risk Assessment*, 225-242.

Grünthal, G., Wahlström, R., & Stromeyer, D. (2009). The unified catalogue of earthquakes in central, northern, and northwestern Europe (CENEC)—updated and expanded to the last millennium. *Journal of Seismology*, 13, 517-541.

Hajdas, I. (2009). Applications of radiocarbon dating method. *Radiocarbon*, Cambridge University Press 51(1), 79-90.

Heine, E. (2021). Altausseer See 3D –Bathymetrie und Objektkartierung mittels Fächerecholot und Unterwasserroboter. Universität für Bodenkultur Wien.

Heiri, O., Lotter, A. F., & Lemcke, G. (2001). Loss on ignition as a method for estimating organic and carbonate content in sediments: reproducibility and comparability of results. *Journal of paleolimnology*, 25, 101-110.

Hübl, J., Pürstinger, C. (2003): WLS Report 92: Dokumentation und Grundlagenerhebung zur Aufarbeitung der Hochwasserereignisse vom August 2002 im Bereich der WLV-Gebietsbauleitung Salzkammergut, im Auftrag der WLV Sektion Oberösterreich.

Inouchi, Y., Kinugasa, Y., Kumon, F., Nakano, S., Yasumatsu, S., & Shiki, T. (1996). Turbidites as records of intense palaeoearthquakes in Lake Biwa, Japan. *Sedimentary Geology*, 104(1-4), 117-125.

Kaushal, S., & Binford, M. W. (1999). Relationship between C: N ratios of lake sediments, organic matter sources, and historical deforestation in Lake Pleasant, Massachusetts, USA. *Journal of Paleolimnology*, 22, 439-442.

Knapp, S. (2018). Wiederkehrintervalle von Fels-und Bergstürzen abgeleitet aus sedimentologischen Untersuchungen (Öschinensee und Eibsee). In 18. Fachtagung Rutschungen.

Lamer, R. (1998): Das Altausseer Land, Geschichte und Kultur einer Landschaft. Verlag Styria ISBN-10: 3222126135.

Lauterbach, S., Brauer, A., Andersen, N., Danielopol, D. L., Dulski, P., Hüls, M., Milecka, K., Namiotko, T., Obremaska, M., Von Grafenstein, U., Declakes Participants. (2011). Environmental responses to Lateglacial climatic fluctuations recorded in the sediments of pre-Alpine Lake Mondsee (northeastern Alps). *Journal of Quaternary Science*, 26(3), 253-267.

Lauterbach, S., Strasser, M., Kowarik, K., Reschreiter, H., Mandl, G. W., Spötl, C., Plessen, B., Brauer, A. (2023). Large-scale mass movements recorded in the sediments of Lake Hallstatt (Austria)—evidence for recurrent natural hazards at a UNESCO World Heritage site. *Journal of Quaternary Science*, 38(2), 258-275.

Lehmann, O. (1926). Die verheerungen in der Sandlinggruppe (Salzkammergut). *Akad. Der Wiss.* In Wien, Denk, 100, 259-299.

Lenhardt, W. A. (2010): Erdbeben Gefährdung, Zoneneinteilung Österreichs entsprechend ÖNORM EN 1998-1; Österreichischer Geophysikalischer Dienst an der Zentralanstalt für Meteorologie und Geodynamik.

Lenhardt, W. A. (2012): "7. Seismotektonik/Erbeben" in Mandl, G. W., Van Husen, D., Lobitzer, H. (Hrsg). *Geologische Karte der Republik Österreich 1: 50 000 Erläuterungen zu Blatt 96 BAD ISCHL*. Eigentümer, Herausgeber und Verleger: Geologische Bundesanstalt.

Lobitzer, H. (2011). *Geologische Spaziergänge Ausseerland – Salzkammergut*. Geologische Bundesanstalt, Kammerhofmuseum Bad Ischl- Wien.

Lobitzer, H. (2012). „9. Mineralische Rohstoffe“ in Mandl, G. W., Van Husen, D., Lobitzer, H. (Hrsg). Geologische Karte der Republik Österreich 1: 50 000 Erläuterungen zu Blatt 96 BAD ISCHL. Eigentümer, Herausgeber und Verleger: Geologische Bundesanstalt.

Lobitzer, H., Mandl, G. W., Van Husen, D. (2012). „3. Erforschungsgeschichte“ in Mandl, G. W., Van Husen, D., Lobitzer, H. (Hrsg). Geologische Karte der Republik Österreich 1: 50 000 Erläuterungen zu Blatt 96 BAD ISCHL. Eigentümer, Herausgeber und Verleger: Geologische Bundesanstalt

Lowe, D. R. (1982). Sediment gravity flows; II, Depositional models with special reference to the deposits of high-density turbidity currents. *Journal of sedimentary research*, 52(1), 279-297.

Meiburg, E., & Kneller, B. (2010). Turbidity currents and their deposits. *Annual Review of Fluid Mechanics*, 42, 135-156.

Mandl, G. W. (2012a). „Kapitel 1. Geographischer Überblick“ in Mandl, G. W., Van Husen, D., Lobitzer, H. (Hrsg). Geologische Karte der Republik Österreich 1: 50 000 Erläuterungen zu Blatt 96 BAD ISCHL. Eigentümer, Herausgeber und Verleger: Geologische Bundesanstalt.

Mandl, G. W. (2012b). „Kapitel 4. Geologischer Bau“ in Mandl, G. W., Van Husen, D., Lobitzer, H. (Hrsg). Geologische Karte der Republik Österreich 1: 50 000 Erläuterungen zu Blatt 96 BAD ISCHL. Eigentümer, Herausgeber und Verleger: Geologische Bundesanstalt.

Mandl, G. W. (2012c). „Kapitel 5.1. Vom Sediment zum Gebirge“ in Mandl, G. W., Van Husen, D., Lobitzer, H. (Hrsg). Geologische Karte der Republik Österreich 1: 50 000 Erläuterungen zu Blatt 96 BAD ISCHL. Eigentümer, Herausgeber und Verleger: Geologische Bundesanstalt.

Mandl, G. W. & Lobitzer, H. (2012). „Kapitel 6.1. Oberperm bis Paläogen“ in Mandl, G. W., Van Husen, D., Lobitzer, H. (Hrsg). Geologische Karte der Republik Österreich 1: 50 000 Erläuterungen zu Blatt 96 BAD ISCHL. Eigentümer, Herausgeber und Verleger: Geologische Bundesanstalt.

Mandl, G. W. & Van Husen, D. (2012). „Kapitel 2. Geologischer Überblick“ in Mandl, G. W., Van Husen, D., Lobitzer, H. (Hrsg). Geologische Karte der Republik Österreich 1: 50 000 Erläuterungen zu Blatt 96 BAD ISCHL. Eigentümer, Herausgeber und Verleger: Geologische Bundesanstalt.

Monecke, K., Anselmetti, F. S., Becker, A., Sturm, M., & Giardini, D. (2004). The record of historic earthquakes in lake sediments of Central Switzerland. *Tectonophysics*, 394(1-2), 21-40.

Neuner, R. M. (2022). Analyse der Sedimentdynamik in der Nähe von Unterwasserquellen im Altaussee See (Salzkammergut). Bachelorarbeit, Institut für Geologie, Fakultät für Geo- und Atmosphärenwissenschaften, Leopold-Franzens-Universität Innsbruck.

Nigg, V., Bacigaluppi, P., Vetsch, D. F., Vogel, H., Kremer, K., & Anselmetti, F. S. (2021). Shallow-water tsunami deposits: Evidence from sediment cores and numerical wave propagation of the 1601 CE Lake Lucerne event. *Geochemistry, Geophysics, Geosystems*, 22(12), e2021GC009753.

Ortler, M., Brauer, A., Fabbri, S. C., Haas, J. N., Hajdas, I., Kowarik, K., ... & Strasser, M. (2024). Late Pleistocene to Holocene event stratigraphy of Lake Hallstatt (Salzkammergut, Austria): revealed by the Hipercorig drilling system and borehole logging. *Scientific Drilling*, 33(1), 1-19.

Oswald, P., Strasser, M., Hammerl, C., & Moernaut, J. (2021). Seismic control of large prehistoric rockslides in the Eastern Alps. *Nature communications*, 12(1), 1059.

Panalytical, Malvern. "Changing the Properties of Particles to Control Their Rheology."URL: <https://www.azom.com/article.aspx> (2015).

Passega, R. (1964). Grain size representation by CM patterns as a geologic tool. *Journal of Sedimentary Research*, 34(4), 830-847.

Pelzl, B., Pelzl, M. (2005): Die blaue Farbe des Planeten, Katalogbände zur Steirischen Landesausstellung 2005. ISBN: 3902216158, 9783902216151.

Reimer, P.J., Austin, W.E.N., Bard, E., Bayliss, A., Blackwell, P.G., Bronk Ramsey, C., Butzin, M., Cheng, H., Edwards, R.L., Friedrich, M., Grootes, P.M., Guilderson, T.P., Hajdas, I., Heaton, T.J., Hogg, G.A., Hughen, K. A.,... and Talamo, S. (2020). The IntCal20 Northern Hemisphere Radio-carbon Age Calibration Curve (0-55 cal kBP). by the Arizona Board of Regents on behalf of the University of Arizona. *Radiocarbon* - Vol 62, p 725–757. DOI:10.1017/RDC.2020.41.

Riedl, H. E., Friehs, B., Hochreiter, M., Ellinger, A. (2008). 1. Steirischer Seenbericht – Ergebnisse der limnologischen Untersuchungen von 1999-2007 unter Berücksichtigung früherer Veröffentlichungen. Fachabteilung 17C Referat Gewässeraufsicht der Steiermärkischen Landesregierung.

Rubensdotter, L., & Rosqvist, G. (2009). Influence of geomorphological setting, fluvial-, glaciofluvial-and mass-movement processes on sedimentation in alpine lakes. *The Holocene*, 19(4), 665-678.

Sabatier, P., Moernaut, J., Bertrand, S., Van Daele, M., Kremer, K., Chaumillon, E., & Arnaud, F. (2022). A review of event deposits in lake sediments. *Quaternary*, 5(3), 34.

Schmalfuss, C., Firla, G., Lüthgens, C., Neuhuber, S. M., Fiebig, M. (2022). Early results from the ICDP project DOVE (Drilling Overdeepened Alpine Valleys): Revisiting the Hole of Bad Aussee. Conference: PANGEO Austria 2022 At: Leoben, Austria.

Schnellmann, M., Anselmetti, F. S., Giardini, D., McKenzie, J. A., & Ward, S. N. (2002). Prehistoric earthquake history revealed by lacustrine slump deposits. *Geology*, 30(12), 1131-1134.

Schnurrenberger, D., Russell, J., & Kelts, K. (2003). Classification of lacustrine sediments based on sedimentary components. *Journal of Paleolimnology*, 29, 141-154.

Schubert, G. (2012). „Kapitel 10. Hydrogeologie“ in Mandl, G. W., Van Husen, D., Lobitzer, H. (Hrsg). *Geologische Karte der Republik Österreich 1: 50 000 Erläuterungen zu Blatt 96 BAD ISCHL*. Eigentümer, Herausgeber und Verleger: Geologische Bundesanstalt.

Schwingschlögl, R. (1986). *Photogeologie und Bruchtektonik des Totengebirgsplateaus*. Gesellschaft der Geologie-und Bergbaustudenten.

Shanmugam, G. (1997). The Bouma sequence and the turbidite mind set. *Earth-Science Reviews*, 42(4), 201-229.

Slapansky, P., & Ahl, A. (2012): „Kapitel 8. Geophysikalische Untersuchungen“ in Mandl, G. W., Van Husen, D., Lobitzer, H. (Hrsg). *Geologische Karte der Republik Österreich 1: 50 000 Erläuterungen zu Blatt 96 BAD ISCHL*. Eigentümer, Herausgeber und Verleger: Geologische Bundesanstalt.

Stow, D. A., & Shanmugam, G. (1980). Sequence of structures in fine-grained turbidites: comparison of recent deep-sea and ancient flysch sediments. *Sedimentary Geology*, 25(1-2), 23-42.

Strachwitz, M. Graf von Helmstatt: (2021). *Analyse der Sedimentdynamik im Altaussee See anhand von sechs Kurzkernen*. Bachelorarbeit, Institut für Geologie - Fakultät für Geo- und Atmosphärenwissenschaften, Franzens-Universität Innsbruck.

Strasser, M., Monecke, K., Schnellmann, M., & Anselmetti, F. S. (2013). Lake sediments as natural seismographs: A compiled record of Late Quaternary earthquakes in Central Switzerland and its implication for Alpine deformation. *Sedimentology*, 60(1), 319-341.

Tóth, Z., Spieß, V., & Jensen, J. (2014). Seismo-acoustic signatures of shallow free gas in the Bornholm Basin, Baltic Sea. *Continental Shelf Research*, 88, 228-239.

Van Daele, M., Cnudde, V., Duyck, P., Pino, M., Urrutia, R., & De Batist, M. (2014). Multidirectional, synchronously-triggered seismo-turbidites and debrites revealed by X-ray computed tomography (CT). *Sedimentology*, 61(4), 861-880.

Vandekerckhove, E., Van Daele, M., Praet, N., Cnudde, V., Haeussler, P. J., & De Batist, M. (2020). Flood-triggered versus earthquake-triggered turbidites: A sedimentological study in clastic lake sediments (Eklutna Lake, Alaska). *Sedimentology*, 67(1), 364-389.

Van Husen, D. (2012). „Kapitel 5.2. Landschaftsgestaltung durch die Eiszeit“ in Mandl, G. W., Van Husen, D., Lobitzer, H. (Hrsg). *Geologische Karte der Republik Österreich 1: 50 000 Erläuterungen zu Blatt 96 BAD ISCHL*. Eigentümer, Herausgeber und Verleger: Geologische Bundesanstalt.

Van Husen, D., & Mayer, M. (2007). The hole of Bad Aussee, an unexpected overdeepened area in NW Steiermark, Austria. *Austrian Journal of Earth Sciences*, 100, 128-136.

Wagner, S. (2021). *Altausseer See - Geomorphologische Kartierung des Seebodens und der Uferzone anhand von photogrammetrischen und Multibeamecholotaufnahmen*; Universität für Bodenkultur, Wien.

Wilhelm, B., Rapuc, W., Amann, B., Anselmetti, F. S., Arnaud, F., Blanchet, J., Brauer, A., Czymzik, M., Giguët-Covex, C., Gilli, A., Glur, L., Grosjean, M., Irmeler, R., Nicolle, M., Sabatier, P., Swierczynski, T., Wirth, S. B. (2022). Impact of warmer climate periods on flood hazard in the European Alps. *Nature geoscience*, 15(2), 118-123.

Wirth, S. B., Bouffard, D., & Zopfi, J. (2020). Lacustrine groundwater discharge through giant pockmarks (Lake Neuchatel, Switzerland). *Frontiers in Water*, 2, 13.

## 8. Appendix / Supplementary Data

### A.1.1. Tectonic overview map of the Bad Ischl map sheet

The tectonic features of the area around Lake Altaussee are shown. The lake is marked with a red circle on the map.



Figure A.1.1.: Tectonic maps from map sheet Geofast Bad Ischl 96 by Mandl et al. (2012).

### A.1.2. Earthquake hazard map for Austria

The Figure shows the earthquake hazard map for Austria, divided into hazard zones. In the Figure, the red star marks the region around Lake Altaussee. As can be seen, this region lies in hazard zone 1, with an effective horizontal ground acceleration of 0.35-0.50 ( $\text{m/s}^2$ ).



Figure A.1.2.: Earthquake hazard map for Austria by Lenhardt, W., (2012), the red star marks the region around Lake Altaussee.

### A.1.3. Map of the faults in this region

The map below shows the major faults in this region. Lake Altaussee is circled in red for reference.

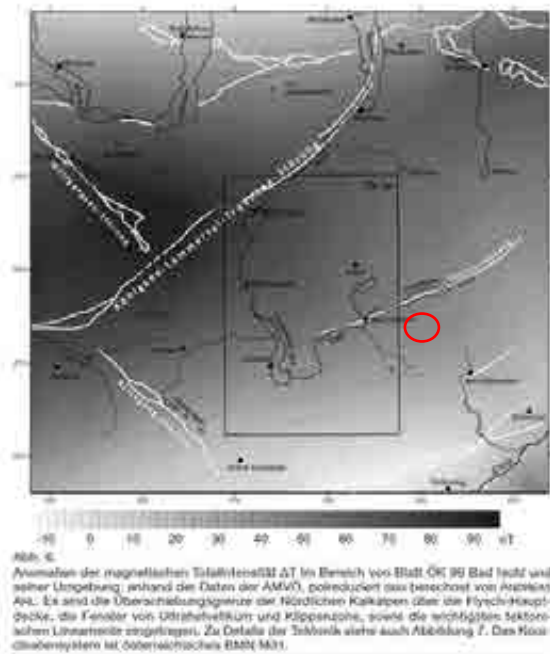


Figure A.1.3.: Figure from chapter 8. 'Geophysikalische Untersuchungen'. Modified from Slapansky P., und Ahl A. (2012). 'Erläuterung Kartenblatt Bad Ischl 96'.

### A.2.1. Short-cores coring campaign in 2020

The 22 short cores taken from Lake Altaussee in 2020 are shown. Not all cores were used and mentioned within this thesis. For example, the cores that were taken near the crater were not included here, neither was core ALT20-21, as it was taken near the shore for testing purposes.

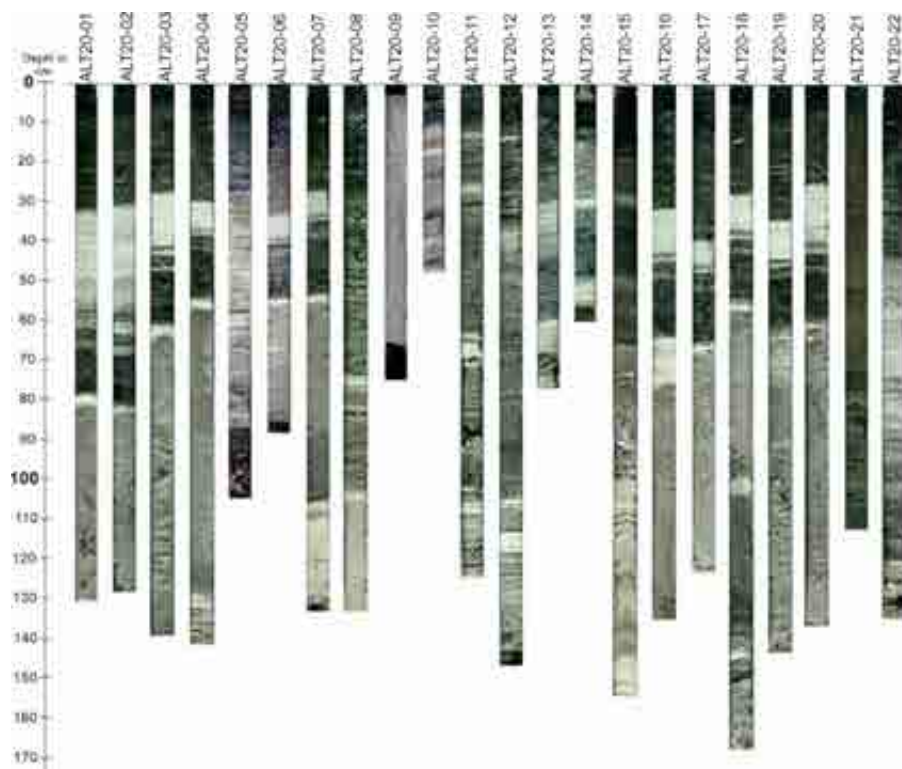


Figure A.2.1.: The cores ALT20-01 to ALT20-22 which were taken during the core campaign in September 2020.



### A.2.2. XRF- Core Scanning

The Itrax Core Scanner combines Roentgen fluorescence analysis, X-ray imaging and optical imaging to provide detailed geochemical information where all chemical elements are determined simultaneously.

At the heart of the instrument sits an optical camera, a laser scanner to determine topography, a roentgen fluorescence detector, an X-ray tube, a beamformer, and an X-ray camera (Croudace et al., 2006). Due to the operation of the X-ray source of the ITRAX core scanner, the radiographic images show only an approximately 2-cm-wide section of the total width of the core.

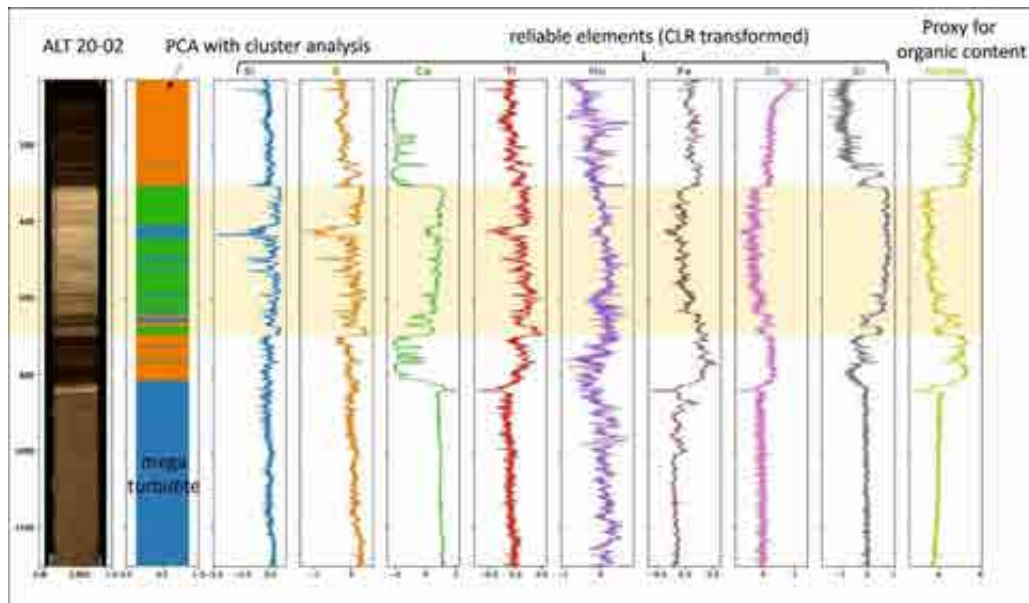


Figure A.2.2.: XRF example on the core ALT20-02. Illustration by Marcel Ortler.

### A.2.3. Calibration curve of $^{14}\text{C}$ data

The figure below shows the calibration curves of the relevant  $^{14}\text{C}$  samples used for the age model. All samples were taken from the core ALT20-02.

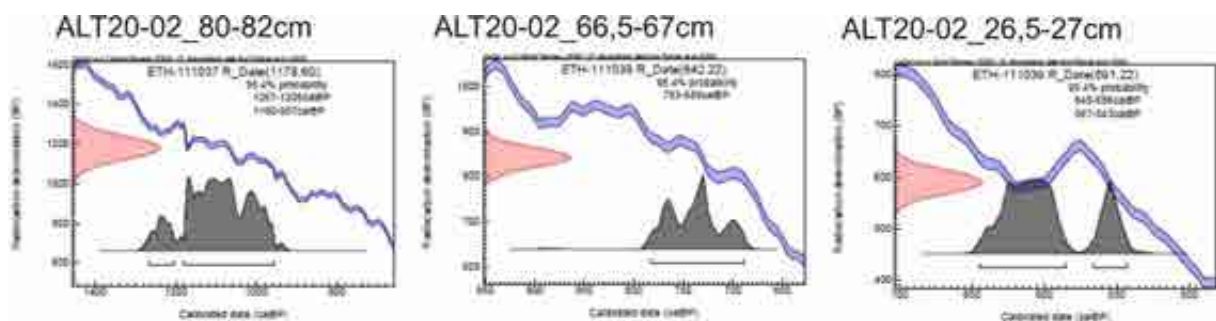


Figure A.2.3.: Calibration's curve of  $^{14}\text{C}$  samples

### A.3.1. Sample table LOI measurement

Table A.3.1.: The table of samples used for the LOI measurement is visualised.

Sample ID	Lithofacies	Organic Content in %
ALT20-06_8,5-9,0cm	1a	21,64
ALT20-06_11,5-12cm	1b	19,05
ALT20-06_16,5-17cm	2a	16,37
ALT20-06_21-21,5cm	2a	16,70
ALT20-06_29-29,5cm	2a	14,16
ALT20-06_35-35,5cm	3	5,05
ALT20-06_39-39,5cm	3	3,83
ALT20-06_46,5-47cm	2b	12,95
ALT20-06_52-52,5cm	2b	15,31
ALT20-06_56-56,5cm	4a.2	3,54
ALT20-06_60-60,5cm	4b.1	9,95
ALT20-06_64-64,5cm	4b.1	10,49
ALT20-06_68-68,5cm	4b.1	9,38
ALT20-06_72-72,5cm	4b.1	7,98
ALT20-06_76-76,5cm	4b.1	6,69
ALT20-06_80-80,5cm	4b.2	5,67
ALT20-06_84-84,5cm	4b.2	5,80
ALT20-13_75-75,5cm	4c	3,24

### A.3.2. Hjulström Diagram

To find out whether the larger clasts of lithofacies 4c of the ALT20-15 slope core could have travelled a long distance, the clasts were plotted in a Hjulström diagram. This shows that the clasts are too large to be transported across the entire lake.

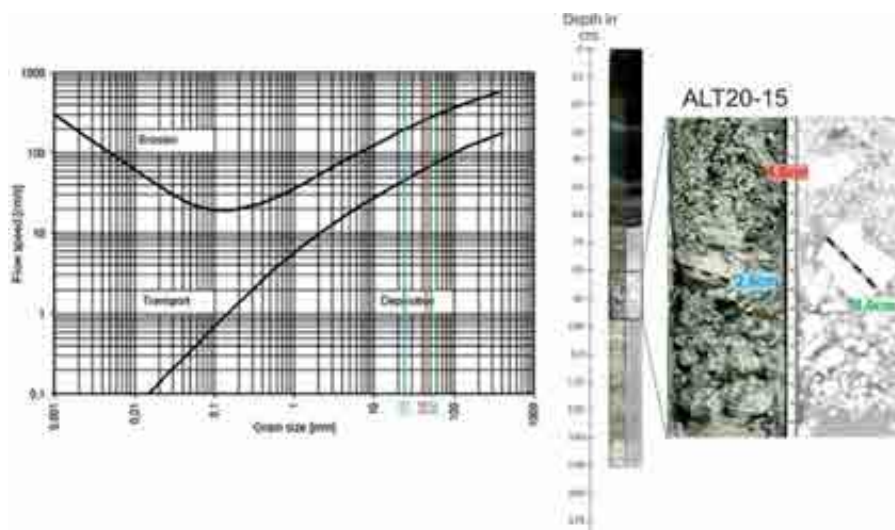


Figure A.3.2.: Hjulström Diagram of lithofacies 4c from core ALT20-15.

### A.3.3. List of smear slide images

In the table below, the core names and core depths of the smear slides are listed. These smear slides are shown in Figure 13. to show the difference between treated and untreated sediment.

Furthermore, the smear slides of the lithofacies are shown, which are not part of the event location.

Unit	untreated - picture	treated - picture
1b	ALT20-04 09.5cm	ALT20-17 12.5cm
2a	ALT20-14 22cm	ALT20-04 27cm
3	ALT20-04 41cm	ALT20-05 49cm
2b	ALT20-04 54cm	ALT20-04 52cm
4a.1	ALT20-07 59.5cm	ALT20-18a 59cm
4a.2	ALT20-04 62cm	ALT20-07 59cm
4b.1	ALT20-04 88cm	ALT20-07 75cm
4b.2	ALT20-04 130cm	ALT20-07 98cm
4c	ALT20-04 157cm	ALT20-07 112cm









	untreated	treated with H <sub>2</sub> O <sub>2</sub>	grainsize & organic
1b			- D50= 30µm D90= 250µm ~19% organic
2a			- D50= 30µm D90= 369µm ~14-17,7% organic
3			- D50= 9µm D90= 62µm ~4-5% organic
2b			- D50= 24µm D90= 280µm ~13-15% organic

Figure A.3.3.: Origin of the sediment used for smear slides Figure 13.

### A.3.4. Differences D50(µm) treated and untreated

In the following figure, the treated and untreated lines are overlaid for comparison. The lines are the D50(µm) values of the ALT20-15 and ALT20-18 cores.

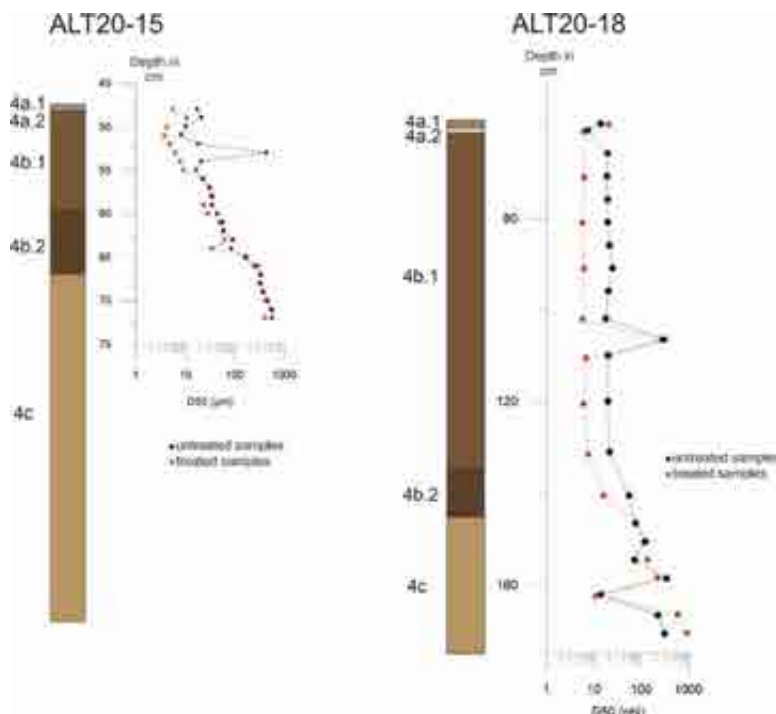


Figure A.3.4.: The D50 values are shown to illustrate the difference between the treated and untreated condition of the cores ALT20-15 and ALT20-18.

#### A.4.1. Origin of the Blocks

This figure shows the distribution of the blocks in the lake basin. Also shown are the two walls from where the material for the terrestrial mass movement may have entered the lake - which is discussed in chapter 5.3.

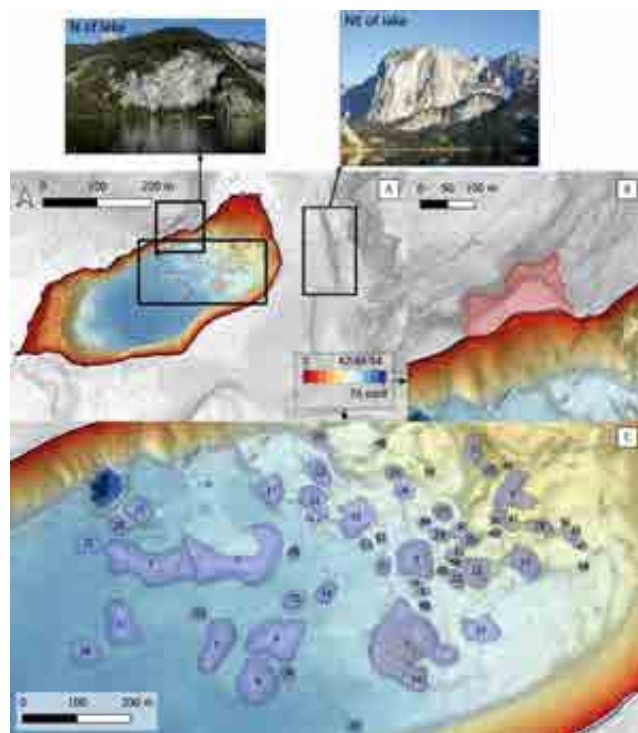


Figure A.4.1.: A: overview of the lake with blocks in the basin and the locations of the potential block origin highlighted. B: A closer look at the northern wall. C: A detailed view of the distribution of blocks in the central basin. Photos of the northern and north-eastern walls are shown in the upper part of the figure. Modified after Marcel Ortler, 2024.